Assessing adsorption of heavy metals from urban stormwater runoff in the Bluebloqs biofiltration system

Pim Versteeg
April 2020

TU Delft

Field Factors

April 2020

Cover photo: Bluebloqs demo in winter, Aartselaar (M. Snoek, 2019)

April 2020

Assessing adsorption of heavy metals from urban stormwater runoff in the Bluebloqs biofiltration system

By
Pim Versteeg

for the degree of
Master of Science in Civil Engineering

Date of submission: 9-04-2020
Date of defence: 15-04-2020

Graduation Committee

Dr. B.M. van Breukelen	Delft University of Technology Sanitary Engineering
Prof.dr.ir. L.C. Rietveld	Delft University of Technology Sanitary Engineering
Prof.dr. P.J. Stuijfzand	Delft University of Technology Geo-Engineering
K. Peña, MSc. M.Arch,	Field Factors

Sanitary Engineering section, Department of Water Management
Faculty of Civil Engineering and Geosciences
Delft University of Technology

ABSTRACT

Pressure on fresh water resources has led to water scarcity and increasing demand for alternative water resources, such as rainwater. Nevertheless, heavy metal contamination is a limiting factor for re-use of urban stormwater. This research focusses on the adsorption of heavy metal contaminants by biofiltration systems, specifically on the Bluebloqs Biofilter, to fulfil the water quality requirements for infiltration. The effect of various physical and chemical conditions on HM adsorption were assessed.

A field experiment was built in the summer of 2019 and operated during 5 months. A range of low to high heavy metal concentrations was synthetically dosed to functional prototype of the Bluebloqs Biofilter, with the aim to characterise both the removal efficiency as well as geochemical processes in the filter media.

Results showed that due to saturation of the filter media, Cd and Zn concentrations in the effluent rose above the Dutch infiltration standards after 74 bed volumes. Ni, Cd and Zn were most susceptible for bed saturation as average concentrations over biofilter depth increased by operation. Highest removal of all heavy metals happened in the top 5 cm of the filter bed.

A surface complexation sorption model was developed in PHREEQC to evaluate adsorption of Cd, Cu, Ni and Zn. The model was established by calibration on batch adsorption experiment data of the same heavy metals. With this modelling tool, various physical and chemical conditions in stormwater could be easily simulated and extrapolated, as well as characteristics of filter media that could be modified. Surface complexation modelling showed a reasonable fit compared to the Freundlich isotherm.

The order of adsorption to the filter media was Cu>Cd>Zn>Ni. Batch simulations showed that by raising solution pH, adsorption of each HM was increased for both quartz sand and iron oxide coated sand. For pH 7.0, the partition coefficient for iron oxide coated sand was 1.34, 16.8, 19.9 and 23.9 for Ni, Cd, Cu and Zn respectively. For pH 8.0, the partition coefficient rose to 12.9, $2.15*10^{3}$, 282 and 698 in the same order. In the case of quartz sand and pH 7.0, partition coefficient was found $4.7*10^{-2}$, 1.18, 1.41 and 14.8 for Ni, Zn, Cd and Cu respectively. When increased to pH 8.0, partition coefficients rose to 0.7, 34.0, 228 and 201 in the same order.
To a lower extent, increase of ionic strength of the solution had a negative effect on the adsorption of Cu and Cd. By increasing the Zn and Cu proportion by a factor 5.0 in the influent stormwater, adsorption of Ni and Cd was negatively affected, but only for unrealistic high concentrations.

One dimensional transport simulations were performed for the average stormwater compositions found at the field experiment. Ni showed first breakthrough in the filter due to lower affinity, followed by Zn, Cd and Cu. Increase of the pH from 7.0 to 8.0 delayed breakthrough by a factor 9.2, 15.8, 25.9 and 135.1 for Cu, Ni, Zn and Cd respectively, despite the type of media used in simulations. By changing the 20% of the top layer of the total filter length from quartz sand to iron oxide coated sand in the model, the adsorption capacity increased and delayed the breakthrough of heavy metals by a factor ±2.36 at all pH conditions.

Comparison of the established sorption model with field experiment data showed underestimation of Ni adsorption, while Cd and Cu were overestimated. Zn adsorption showed the most similarity between model results and field data. The model cannot provide an accurate prediction on HM adsorption, but it can be used to compare in between HMs.

For the first mature system of the Bluebloqs biofilter, operational in Spangen, Rotterdam since the summer of 2018, the first exceedance of the Zn for the infiltration standards was predicted after 410 bed volumes, due to saturation of filter media. This resulted in elevated Zn concentration in the effluent. Further improvement of the sorption model could be established by additional batch adsorption experiments to obtain more trustworthy results.

Keywords

Urban stormwater management, biofiltration systems, heavy metals, adsorption, surface complexation, PHREEQC

PREFACE

This document presents the Master Thesis of Pim Versteeg, his final work for the Master Civil Engineering, with specialisation in Water Management at the Delft University of Technology. The content of this thesis is created by Pim Versteeg, under the guidance of dr. Boris van Breukelen.

This thesis is also written for Field Factors, in order to provide design guidelines to optimise the performance of the Bluebloqs biofilter. By this research, a little piece of the ‘black box’ puzzle was solved to better understand the biofiltration system in search of an ideal design to re-use every single raindrop.

The report is composed of a dual assignment: a field experiment and the development of a PHREEQC surface complexation sorption model. The field experiment is part of the EIT Climate-KIC Bluebloqs Demonstrator project. A demonstrator of the Bluebloqs Biofilter was built at the Aquafin campus in Aartselaar, Belgium. The aim of this demo is to research the potential implementation of the Bluebloqs Circular Water System in Flemish context, where yet no infiltration standards on heavy metals are constructed.

The sorption model is developed to predict adsorption of heavy metals when environmental conditions and the type of filter media are changed. By the use of this model, the removal efficiency of heavy metals can be anticipated, allowing for improvements in the design of biofiltration systems.

P. Versteeg
Delft, April 2020

April 2020

ACKNOWLEDGEMENT

This thesis project has been a journey from May 2019 through April 2020. It has been a year of hard work, which I could not have done without the help of a bunch of people.

Thanks to the team of Field Factors. Mirthe, Kieran, Wilrik, Thomas and Joshua helped me a lot throughout the last year. I was lucky to be part of this enthusiastic team. The presentations, great lunches together, and games of table tennis were a lot of fun. Field factors is a great office and their vision and energy helped me writing this thesis with that energy.

Special thanks to the members of my graduation committee. Thanks to Pieter Stuijfzand and Luuk Rietveld for their guidance with expertise and experience. Your feedback helped me to zoom in to the right focus and to zoom out to keep perspective, to ensure the practical relevance.

Thanks to Karina Peña as my company supervisor from Field Factors. Thanks for taking the time and show your interest and in the meanwhile, brought a beautiful new person to the world. You are very strong and really an inspirational person to me.

Many thanks to Boris van Breukelen for your support on daily basis. Your enthusiasm about what we could model with PHREEQC motivated me, it feels that we have developed something that can be useful and relevant. Thanks for all the time the door to your office was open for help with minor and major questions.

A thank you to Jacintha. Shared dreams and shared adventures brought us here. Together we suffered through high school, university and thesis. It must be that we are indeed soulmates. And now, we are at our graduation as #teamciviel.

Lastly, a thank you to my mum, dad, brother and sister. For being able to use the car to visit the demo in Belgium. For making sure that I could focus on this project and not to worry about other things. Thank you for being patient with me.

LIST OF CONTENTS

LIST OF FIGURES

LIST OF ABBREVIATIONS

ASR	Aquifer storage and recovery
BB	Bluebloqs biofilter
BV	Bed volume
CKIC	Climate-KIC
EC	Electrical Conductivity
IOCS	Iron-oxide coated sand
FCS	Fresh coarse sand
FFS	Fresh filter sand
HFO	Hydrous ferric oxide
HM	Heavy metal
PAH	Polycyclic aromatic hydrocarbons
pH_{pzc}	pH point of zero charge
PV	Pore volume
RE	Removal efficiency
SCM	Surface complexation model
SSF	Slow sand filter
UCS	Used coarse sand
UFS	Used filter sand
UWB	Urban Water Buffer
VSFW	Vertical subsurface flow wetland

GLOSSARY OF TERMS

Adsorption: Accumulation of molecules at the surface of a solid or liquid.

Equilibrium: State when net rate of sorption is zero, adsorption and desorption are equivalent.

Rainwater: Umbrella term for precipitation, in all forms including thaw water, before runoff dissolution processes have taken place.

Solute: Dissolved fraction of contaminant molecules in a solution.

(Ad)Sorbate: Molecules in the bulk phase being adsorbed and complexed with sorbent surface.

(Ad)Sorbent: Medium (solid or liquid) which adsorbs the sorbates.

(Ad)Sorptive : Free molecule/ion in bulk phase which can potentially be adsorbed.

NOMENCLATURE

A	surface area	$[m^2]$
C_e	equilibrium concentration	$[g\ L^{-1}]$
c_i	molar concentration of ion	$[mol\ L^{-1}]$
C_i	initial concentration	$[g\ L^{-1}]$
C_o	concentration out	$[g\ L^{-1}]$
C_s	solid concentration	$[g\ L^{-1}]$
D	dispersion coefficient	$[m^2\ s^{-1}]$
F	Faraday constant	$[C\ mol^{-1}]$
f_n	amplification factor of zinc concentration	[-]
f_u	amplification factor of copper concentration	[-]
G_{ad}	adsorption Gibbs free energy	[J]
G_{coul}	coulombic term Gibbs free energy	[J]
G_{intr}	intrinsic term Gibbs free energy	[J]
H_{ad}	enthalpy of adsorption	$[J\ mol^{-1}]$
I	ionic strength	$[mol\ L^{-1}]$
K_{ad}	adsorption constant	[-]
K_d	distribution coefficient	$[L\ g^{-1}]$
K_F	Freundlich constant	$[L\ g^{-1}]$
K_L	Langmuir constant	$[L\ g^{-1}]$
n	heterogeneity factor	[-]
q	electric charge	[C]
q_e	sorption capacity at equilibrium	$[\mu g\ g^{-1}]$
R_g	gas constant	$[J\ K^{-1}\ mol^{-1}]$
R	retardation	[-]
$\equiv S$	surface sorbent media	[-]
S	sorbed concentration per mass sorbent	$[g\ g^{-1}]$
S_{ad}	entropy of adsorption	$[J\ K\ mol^{-1}]$
S_m	maximum sorbed concentration per mass sorbent	$[g\ g^{-1}]$
t	time	[s]
T	temperature	[K]
V	volume	$[m^2]$
v_p	pore water velocity	$[m\ s^{-1}]$
v_w	water velocity	$[m\ s^{-1}]$
x	distance	[m]
X	Sorptive	[-]
z	elementary charge	[C]
z_i	ion charge number	[C]
z_e	background valence electrolyte	[C]
ε_0	permittivity of a vacuum	[-]
ε_r	relative dielectric constant of water	[-]
κ	Debye length	$[m^{-1}]$
σ	surface charge density	$[C\ m^{-2}]$
ψ	potential	[V]
ψ_0	surface potential	[V]

1. Introduction

1.1. THE URBAN WATER CRISIS

One of the main challenges is extreme water scarcity for more than half of the world's population by the end of the 21st century (Hejazi *et al.*, 2014). Within urban areas the demand on water increases with the growing population, economic growth and extension of urban areas (Oki, 2006). However, water resources are limited and become more stressed, inevitably encountering water shortages in the future. This leads to a direct water crisis and demands for a more sustainable living (Kummu *et al.*, 2016).

Water quality is directly related to the water crisis, when polluted water is de facto unusable and unsafe (Rijsberman, 2006). As long as techniques for water desalination are prohibitively expensive and energy consuming, society remains dependent on its fresh water resources. Functions of the fresh water use in urban areas vary and require different water quality standards. I.e. drinking water has strict quality standards and should fulfil many requirements in terms of maximum allowable concentrations of constituents (RIVM, 2011). However, other urban water uses, non-potable water applications, may not require drinking water quality. Non-potable applications can vary from irrigation, flushing, washing or groundwater replenishment. In the Netherlands, many of these applications are currently fulfilled with drinking water. Alternative water resources could however feasible, by using rainwater or greywater (Zhang *et al.*, 2010).

Climate change is adding a new challenge to urban water management. With an increase of intensities of rain events, and on the other hand longer periods of droughts, the hydrological changes in cities are becoming more severe and its consequences unprecedented (Hoegh-Guldberg *et al.*, 2015)(Figure 1-1). Urban environments are characterised with paved surfaces, where no rainwater can infiltrate to the ground and therefore a lack of water retention. For stormwater, sewer system infrastructure was built to transport excess water. When the capacity of sewerage systems cannot cope with the great volume of rainfall, they overflow discharge to surface waters or even streets may flood streets. Costs of the damage due to urban floods can rise too enormous amounts (Jonkman *et al.*, 2004) (CNT, 2014).

On the other hand, due to higher temperatures and incoming solar radiation, the risk of dry spells in summer periods may happen more frequently (KNMI, 2018). Drought and water shortage, have a direct economic effect on sectors such as agriculture, transport, water utilities, built environment, nature and more. For the Dutch agricultural sector, the economic damage of the dry year of 2018 is estimated in the range of 375 million to 1.9 billion euros (ECORYS, 2019).

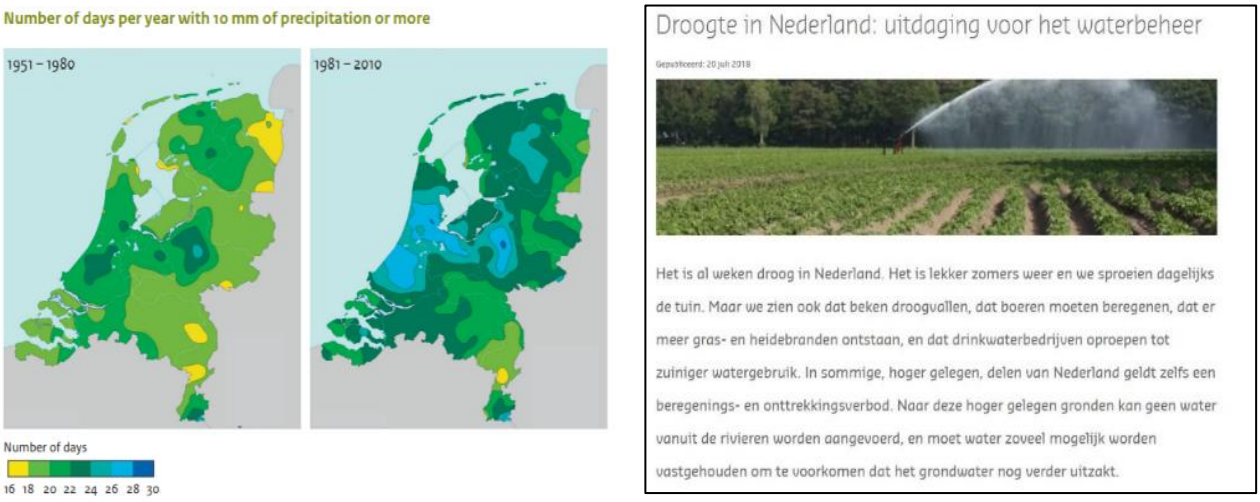

Figure 1-1 How climate change challenges the Dutch water management. Left: Increase of days with high precipitation intensities in the Netherlands (KNMI, 2011) *Right: Drought captivated the Netherlands in the summer of 2018* (Deltares, 2018)

1.2. SHIFT TOWARDS CIRCULAR WATER SYSTEMS

Clean water is not an endless resource. Urbanisation and climate change effects demand for a new approach for the urban water system. Traditionally, waste water and stormwater are considered as waste products and depend on an extended pipeline system. Circular water systems consider these streams as a valuable resource and by recovery and re-use, a closed loop water cycle can be created (van Hattum *et al.*, 2016). Fortunately, there comes more awareness for the need to move towards a sustainable circular economy (WBCSD, 2020).

Due to health challenges in cities in the prior century, wastewater was piped out with large drainage infrastructure to treatment plants or water bodies out of the urban settings (Jenssen and Pandey, 2012). Today, many of these centralised water systems are still used in our cities. Decentralised water systems are infrastructure systems that have closer proximity of water collection and re-use or disposal (Eckelberry, 2016). Hereby, costs of long pipeline infrastructure and centralised water systems are avoided. Water reclamation, grey water recycling and rainwater harvesting are all examples of decentralised processes (Leigh and Lee, 2019).

The Urban Waterbuffer (UWB) is a concept to create retention and storage of stormwater in urban areas while improving the water supply. The adaptability of cities to cope with droughts and floods can be tackled by introducing UWBs as a sustainable and circular solution for urban water management (Zuurbier *et al.*, 2019). Stormwater becomes available for the non-potable water functions. Hereby, the drinking water can be used for potable water functions and it reduces the flow of stormwater to surface waters and water treatment plants (Figure 1-2).

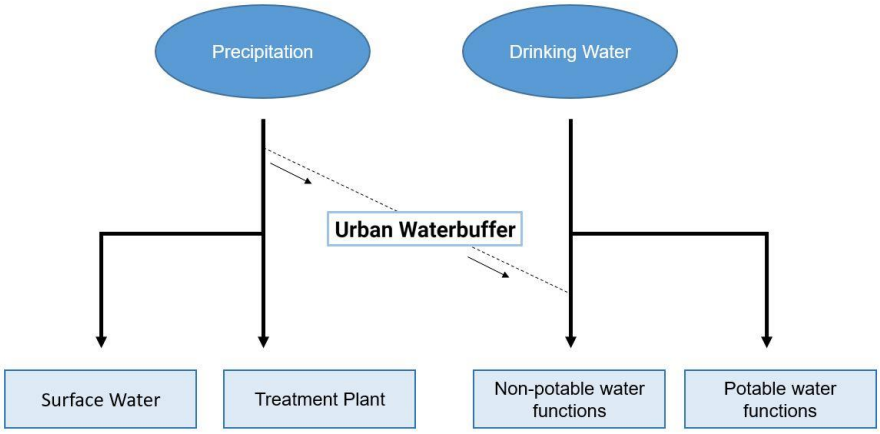

Figure 1-2 The Urban Waterbuffer harvests stormwater for non-potable water functions.

Bluebloqs Circular Water System

Bluebloqs is a nature-based technology to collect, treat, store and distribute stormwater in urban environments, applicable on local scale (Field Factors, 2019). This concept implements a new fresh water source with rainwater as its basis and introduces a decentralized water supply.

The aim is to remove stormwater runoff pollutants by a biofiltration system, the so-called Bluebloqs Biofilter (BB) (Field Factors, The Netherlands). After the biofiltration step, water is infiltrated to the subsurface via infiltration wells, also known as aquifer storage and recovery (ASR). The stored water can be pumped from the aquifer for local non-potable water functions.

By decentralising the water system and integrating the Bluebloqs technology, the municipal water system could benefit on:

- limiting (pluvial) urban flooding by catching urban stormwater runoff;
- saving on drinking water, by providing an alternative water resource;
- becoming resilient to drought, by storing surplus water in wet periods;
- disburdening of the sewerage system by reducing discharge;
- mitigating heat stress, by retaining water in the city.

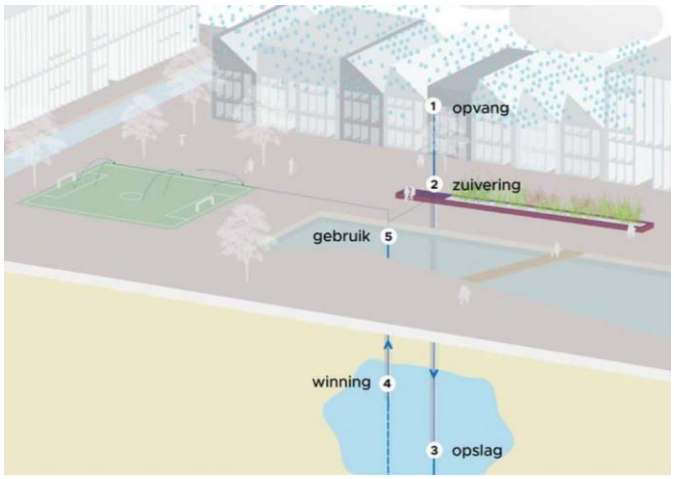

Figure 1-3 Rainwater cycle and implementing treatment and infiltrating steps with the Bluebloqs system (Field Factors, 2018)

The first full-scale pilot application of the Bluebloqs system (BB1.0) has been implemented in the project Urban Waterbuffer Spangen, in Rotterdam, the Netherlands. By the application of the Bluebloqs technology water is collected, treated and stored on neighbourhood level. Aquifer recharge is applied to the brackish groundwater and creates a new resource for augmented freshwater supply. Freshwater abstraction is applied in a later stage when there is a raised water demand for irrigation of the Sparta football stadium, irrigation of the biofilter or for cooling purposes (Field Factors, 2019).

1.3. THE LIMITS TO STORMWATER RE-USE

Before a raindrop precipitates from a cloud, it is relatively clean. But in an urban environment, anthropogenic activities result in pollution of rainwater. Composition of rainwater changes by factors along its pathway, which already starts with atmospheric pollution. On the earth's surface, it is affected by urban settings, with various materials and surface characteristics. These factors deteriorate the water composition, decrease the water quality and thus limit the re-use of rainwater (Zhang *et al.*, 1999).

For longer periods of drought, it can be expected that the first flush contains greater amounts of sediment in runoff water (Blecken *et al.*, 2009b). Or when heavy rainfall is expected, a different composition might be observed and consequently affect some of the physical parameters in the water (i.e. pH, temperature, oxygen content). Climatic conditions will negatively impact the rainwater composition in the future (Haque *et al.*, 2016).

Re-use of harvested rainwater can introduce risks by poor water quality (Eriksson *et al.*, 2007). Heavy metals (HMs) are well-known pollutants that end up in urban runoff by building materials and traffic, and deteriorate the stormwater quality. HMs introduce human health risks already by low concentrations and increase toxicity and cause environmental pollution by accumulation (Bradl, 2004) (Walsh *et al.*, 2016). Without proper treatment, HMs are a main concern in receiving water bodies when concentrations are not within water requirements for groundwater infiltration (Søberg *et al*. 2014).

The Bluebloqs biofiltration technology has to treat stormwater runoff to meet quality regulations for deep infiltration under these conditions, for the Netherlands composed in the Dutch Infiltrations standards (Appendix I). Quality standards are composed to prevent soil pollution by accumulation of toxic compounds of the infiltrated water and protect a clean aquifer. The challenge for re-use of stormwater runoff is to provide adequate water quality under variation of climatic conditions and for varying water composition and contamination.

1.4. PROBLEM STATEMENT

The Bluebloqs demo in Spangen has been operational since September 2018. Monitored data of target pollutants show that the treatment performance of the BB works and improves since the start of operation, according to the biofilter effluent concentrations (Zuurbier and van Dooren, 2019). Within the catchment area a wide variety of urban activities take place that influence the water system, leading to various influent HM concentrations. Especially zinc and iron levels are remarkably high at this location.

The treated stormwater of the Spangen demo fulfils the Dutch infiltration standards for HM concentrations and other critical parameters, so it is permitted to infiltrate and store water. However, different urban stormwater runoff compositions will be encountered for new projects of the Bluebloqs system at different locations. With only one full-scale system up to now, there is a need to have insight on how the biofilter performs if location-specific and climatic conditions are so particular. The function of the BB is to guarantee the necessary water quality by removing HMs under various conditions, when the goal is to re-use every water droplet.

A substantial amount of dissolved HMs is removed by adsorption on the filter media in biofiltration units (Søberg *et al*. 2014). Most studies concern efficiency on entire biofiltration systems, but how the removal mechanism of HMs fundamentally works in the filter media, remains fairly unknown. To improve the performance of the BB, there is a need to quantify the effects of different climatic conditions on adsorption. To avoid the risk to not meet infiltration standards, it is critical to determine what the limits of the BB system are to guarantee an acceptable water quality for aquifer recharge and water re-use, specifically for HMs. If a deviation in stormwater composition or changes of physical and chemical conditions occur, the subsequent effect on adsorption capacities of the filter media have to be determined.

Traditionally, *Freundlich* and *Langmuir* adsorption isotherms are commonly used for various HM adsorption modelling for specific sorbent media. However, these analytical models are only useful under fixed physical and chemical conditions and lack the ability to predict the dependency of different climatic conditions (Jeppu and Clement, 2012). Surface complexation models (SCMs) are numerical approaches that are able to extrapolate adsorption to other environmental conditions (Dzombak and Morel, 1990). However, SCMs are complex to do by hand, time-consuming and not yet applied to entire biofiltration systems (Jeppu and Clement, 2012). There is a need for a simple adsorption model to simulate and extrapolate adsorption capacities of filter media when stormwater compositions and climatic conditions change.

1.5. SCOPE

This study focusses on the removal of HM pollution from urban stormwater runoff using biofiltration techniques. The Bluebloqs Biofiltration system, comprised by a combination of slow sand filter (SSF) with vertical subsurface flow wetland (VSFW), serves as a case study.

The study focusses on chemical adsorption as the main treatment mechanism of dissolved HMs by filter media. Other water treatment processes are however interrelated to chemical sorption and therefore addressed. The adsorption mechanism for removal of HMs is assessed and explained by surface complexation modelling and specifically the diffuse double layer model. Quartz sand and iron oxide coated quartz sand, in the filter layer and top layer respectively, are evaluated on adsorption capacity.

Contamination of urban stormwater runoff is focussed on urban pollution sources, including residential, commercial, transport and recreational functions. Arsenic, cadmium, chromium, copper, lead, nickel and zinc are HMs taken in account for urban stormwater analysis. Adsorption modelling is limited to cadmium, copper, nickel and zinc. Chemical conditions are limited to the change in pH value of water solutions, change of ionic strength and change zinc and copper proportions of HM concentrations in urban stormwater runoff.

The treatment performance is assessed in relation to the legal water quality standards in The Netherlands and are listed in *Infiltratiebesluit Bodembescherming* (Dutch infiltration standards in Appendix I) (VROM, 2009). The geographical scope limits to climatic conditions of north western Europe. Specifically Köppen Marine West Coast (“Cfb”) climate zone, The Netherlands and Belgium, where the case studies are located. Average yearly temperature are at 10 °C, and yearly rainfall of approximately 800 mm (KMI, 2019)(ClimateData, 2019) (Weatherbase, 2019).

Research Objectives

The main objective of this research is to get insights onto the treatment performance of HMs in biofiltration systems in order to identify the conditions and limitations that influence the adsorption process under diverging tempo-spatial conditions and environmental circumstances.

This is derived to three specific objectives in this research:

1) To assess the heavy metal removal performance of the Bluebloqs biofilter with various stormwater compositions under various climatic conditions.

2) To define a predictive working mechanism on the sorption of heavy metal of various media.

3) To determine technical design guidelines for heavy metal removal by the Bluebloqs biofilter with various heavy metal concentrations and under various conditions.

Research Questions

To realise the abovementioned objectives, research questions are composed.

- *To what extent does variation in chemical and physical conditions in stormwater have an effect on the removal efficiency of heavy metals in the filter media?*

- *How can the adsorption of heavy metal pollutants in the filter media be described and modelled?*

- *How can the adsorption process in the filter media be improved for the removal of heavy metals under a variation of chemical and physical conditions?*

1.6. METHODOLOGICAL APPROACH AND OUTLINE OF THIS RESEARCH

The necessity of removal of HMs from stormwater is described in this introduction chapter. Specifically, the main objective is to understand the adsorption process by different filter media and different conditions. Research questions are formulated to guide the research.

Chapter 2 describes the background theory of this research. The processes of how HMs end up in urban stormwater, treatment processes and adsorption fundamentals are extensively described. This shows how a practical case study relates to fundamental research.

Chapter 3 describes how data is gathered by a field experiment and an adsorption model. A recently built field demo at Aartselaar is used to analyse the processes in outdoor conditions and the dosage of a range of HM concentrations. For prediction of the adsorption mechanism in other conditions, a surface-complexation adsorption tool is developed in PHREEQC. Furthermore, this adsorption model is used to identify the development of the adsorption processes in a one dimensional system and development of a biofiltration system.

The results of the field demo and the adsorption model are addressed in chapter 4. The interpretation of the results is then discussed in this section. Data derived from both methods is compared to validate and understand the adsorption processes of HMs, and also how it can differentiate from model to practice. Also, application of the adsorption modelling tool to design a biofiltration system or to evaluate the performance of an operational biofiltration system is highlighted, complemented with a simulation example for a real case.

The conclusions of this study are presented in chapter 5. Recommendations for improvement of the applied methods and for further research are elaborated in chapter 6.

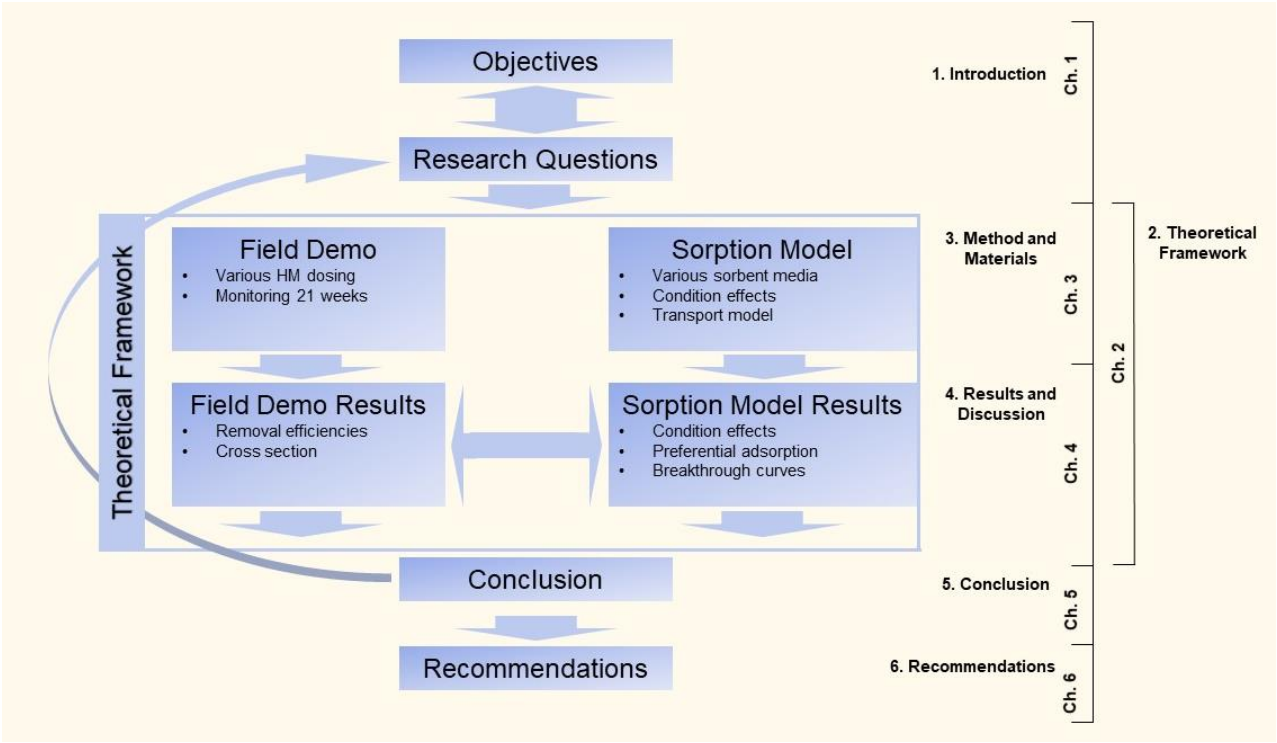

Figure 1-4 Methodological Framework and outline of this research

2. THEORETICAL FRAMEWORK

2.1. URBAN HYDROLOGY AND RAINWATER COLLECTION

Urban climate deviates in many ways from the surrounding rural context. This is expressed in urban hydrology, by more precipitation and higher storm intensities in urban areas. And also in different environmental conditions, like an increase of dust particles, lower humidity, less incoming radiation and higher temperatures. Whereas in rural environment, lower winter minima and summer maxima temperatures and higher humidity are observed. (Landsberg, 1981). Due to the ongoing urbanization, these conditions have to be more often integrated in the water assignments on local and regional scale.

An overview of the urban water cycle fluxes, is depicted in Figure 2-1. Specific percentages of fluxes in this figure are rather location specific, but these are roughly assumed in this ratio for Dutch and Flemish cities (Van de Ven, 2017). A big portion of water volume enters the city by precipitation. In the Netherlands and Belgium rainwater runoff from buildings and roads flows short distances over the paved surface to be collected in gulley pots to enter the stormwater sewer system. This happens with the vast majority of the precipitation volume that falls in paved areas. However, also a portion of the precipitation is retained and subsequently infiltrates in the subsurface. Another portion of the precipitation evaporates from paved areas (Brolsma and Molenaar, 2015).

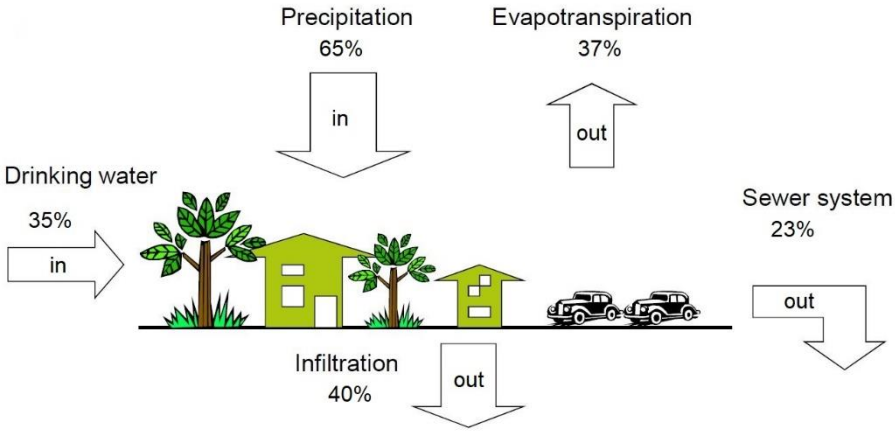

Figure 2-1 A rough estimation of the urban water fluxes for Dutch cities (Van de Ven, 2017)*. 65% of the water volume that flows into the city is precipitation, 35% of the volume is drinking water. Water that leaves the city is 40% infiltrated, 37% evapotranspiration and 23% of the water volume leaves the city by a sewer system.*

The water that collected in the stormwater sewer system is transported to the waste water treatment plant. Wastewater collection in the Netherlands has shifted at many sites from combined sewer system to a separate sewer system. The waste water from households is collected in a separate sewer, disconnected from the storm water sewer. If the capacity of the sewer system is exceeded, the surface water is no longer polluted by household waste water at combined sewer overflow locations. With drainage exceedance in a stormwater sewer, the excess water is discharged via a separate sewer overflow. Nevertheless, this overflow discharge also deteriorates the surface water quality (Istanbulluoglu, 2018) (Brown, Keath and Wong, 2009). Of course, it is desired to have this as minimum as possible.

With proper design the stormwater is conducted to the waste water treatment plant. Often the stormwater is treated and household waste water are treated by the same treatment plant. Due to increasing water scarcity (earlier mentioned in 1.1), stormwater should not be treated as a waste product, but as a valuable resource.

2.2. STORMWATER RUNOFF CONTAMINATION

Rainwater composition varies with place and time and is influenced by many (anthropogenic) pollution sources (earlier mentioned 1.3). The water matrix can already change by air pollution and greenhouse gases before it falls on the surface. Contamination of the water passing through the atmosphere makes that rainwater is not pure water (Chandra Mouli, Venkata Mohan and Reddy, 2005)(Kulshrestha *et al.*, 1999).

Due to industrial growth, anthropogenic emissions of sulphur dioxide and nitrogen oxides increase and cause acid rain events more frequently (NASA, 2011)(Bhargava, 2013). Toxic contaminants, including HMs, pesticides, polycyclic aromatic hydrocarbons (PAH) and even pharmaceuticals, have increased in urban water cycles by urbanisation (McGrane, 2016).

Variation in urban typology contributes to the runoff water quality (Yong and Chen, 2002). Even on a smaller scale, construction materials used within a catchment area can heavily influence the runoff quality, leading to HM particles and dissolved fractions (Burkhardt *et al.*, 2011). Precipitation runs off over paved areas, which further pollutes the rainwater by uptake of HMs, oil, grease and other organic pollutants. This process changes the water composition, strongly dependent on the area characteristics, or in other words the function of the surface (Deletic, 1998). The runoff water can already be quite polluted before it enters the sewer system (Figure 2-2).

Additionally, quantitative impacts on the urban water cycle are the increase of precipitation, increase of rainfall intensity and the longer periods of drought (Schijven and de Roda Husman, 2005). Due to different storm intensities or duration of dry spells, the build-up and wash-off of sediments in the stormwater can lead to a large bandwidth of concentrations in the stormwater (Wijesiri *et al.*, 2016).

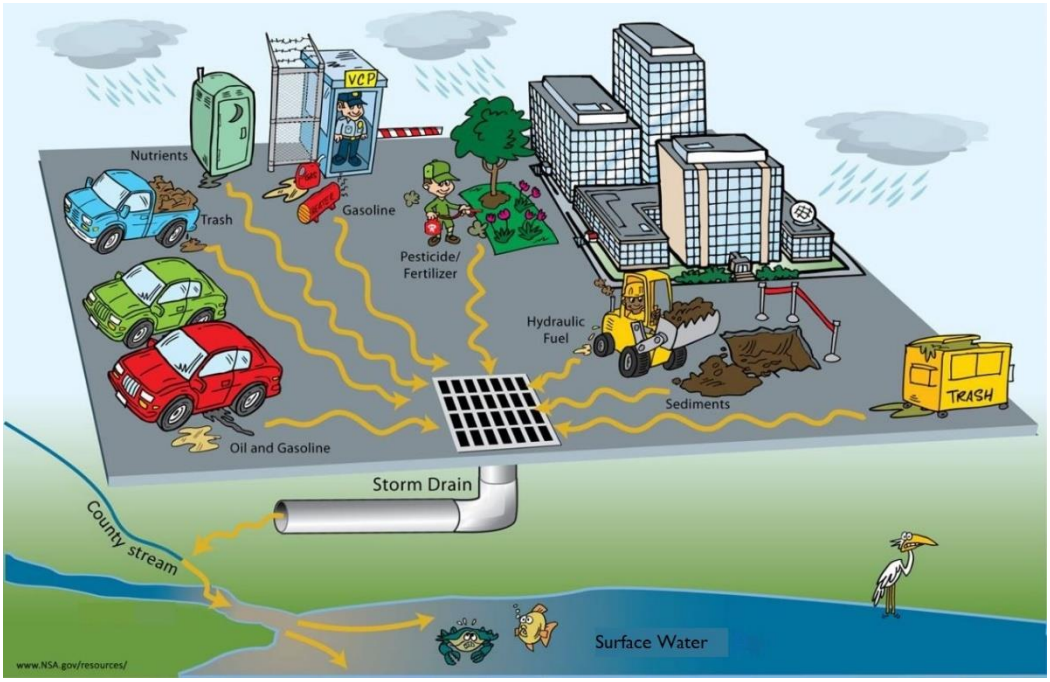

Figure 2-2 Overview of contamination sources by runoff processes in an urban environment (Adapted and adjusted from Chesterfield County, 2019)

2.2.1. Heavy metals

HMs end up in the stormwater in urban environments, and are detected particle-bound to suspended solids and in dissolved forms. The distribution of particle bound or dissolved varies for each HM (Figure 2-3). Most common HMs detected in urban stormwater are lead, copper, zinc, nickel and cadmium (Boogaard *et al.*, 2005). Some of the most frequent pollution sources related to HM pollution are listed in Table 2-1.

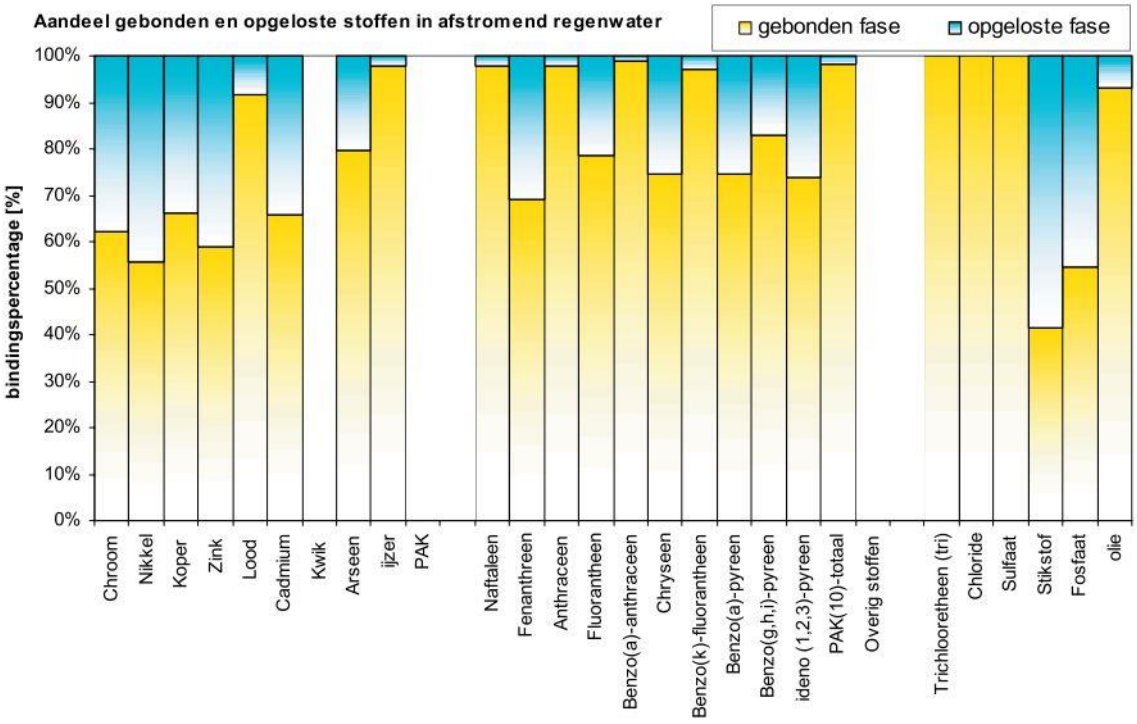

Figure 2-3 Fraction of particle bound contamination (yellow) and dissolved contamination (blue) in runoff water (Boogaard *et al.*, 2005).

The persistency of HMs, reactiveness and toxicity at low concentrations makes it subject to enhanced surveillance. Elevated levels can cause harmful conditions to humans and the ecosystem. HMs are nonbiodegradable and have to be removed either physically or chemically (Gall *et al.*, 2015).

Arsenic

Arsenic (As) is not often mentioned in stormwater studies, but more often for ground water resources. Nevertheless it is relevant due to its serious health risks, like skin cancer and skin pigmentation (USEPA, 2000) and it can still end up in stormwater by paint and for some specific industries (Liu *et al.*, 2019). As has an atomic mass of 74.9216 g mol^{-1}. As readily forms covalent bonds with non-metals and most common oxidation states are found arsenite (+3) and arsenate (+5).

Cadmium

Cadmium (Cd) sources include mostly wet deposition, but also brake pads, corrosion and other industrial emissions. Highest concentrations originate from traffic areas, while runoff from roofs show a significantly lower concentration. Cd is detected mainly in densely urbanised areas (Duncan, 1999). A Cd atom has an atomic mass of 112.41 g mol^{-1}, mainly found in the Cd^{2+}-form and a relatively volatile species.

Chromium

Chromium (Cr) sources are mostly plating materials and corrosion of cars (Cederkvist *et al.*, 2013). It exists as Cr(III) and Cr(VI), the last one is strongly oxidative, highly mobile and has potential toxic effects. On the contrary, Cr(III) is stable with soil complexes. Cr has an atomic mass of 52.0 g mol^{-1}.

Copper

Copper (Cu) sources mainly include brake wear, dry depositions and building material. Cu is an essential trace element in our diet and naturally present. It is often used in building material. However, an overexposure of can cause gastrointestinal stress and anaemia to human health (ATSDR, 2004). A Cu atom has an atomic mass of 63.5 g mol^{-1}.

Table 2-1 Overview of origin of HM pollution sources and consequences of high exposure

Heavy metals detected in stormwater runoff	Sources in urban areas	High exposure consequences	Reference
Arsenic As	Chromated copper arsenate	Skin damage	Liu *et al.*, 2019
Cadmium Cd	Wet deposition, dry deposition, automobile brakes	Muscle pain, lung damage	Davis *et al.* 2001
Chromium Cr	Automotive steel, plating material	Respiratory tract	Macnamara and Derry, 2017
Copper Cu	Automobile brakes, dry deposition, buildings	Nausea, stomach cramps	Davis *et al.,* 2001
Lead Pb	Dry deposition, wet deposition, buildings	Kidney damage, high blood pressure	Davis *et al.,* 2001
Nickel Ni	Diesel fuel, asphalt paving, waste incineration	Skin rash, lung functioning	Boogaard *et al.*, 2014
Zinc Zn	Car tires, buildings, automobile brakes	Respiratory distress, low blood pressure	Davis *et al.*, 2001

Lead

Lead (Pb) is significant pollutant due to its toxicity and persistency, although it is often used in many common applications. Biggest sources of Pb in stormwater runoff are dry and wet deposition, but also from materials of buildings. For example in lead painting and building materials. Pb is mostly particle bound in stormwater (Boogaard *et al.*, 2014). A Pb atom has an atomic mass of 207.2 g mol^{-1}.

Nickel

Nickel (Ni) in stormwater runoff is not often detected in high concentrations. Ni is naturally occurring, but also used in stainless steel and , but also from the combustion of diesel and gasoline. Exposure to Ni can affect human health on lungs or skin irritation. A Ni atom has an atomic mass of 58.7 g mol^{-1}.

Zinc

Zinc (Zn) in stormwater predominantly originates from tire wear and roofing material. Especially in catchment areas with zinc roofing, elevated concentrations appear in the stormwater runoff. Zn is an essential element in our diet and relatively harmless to other HMs, however overexposure can cause interference of the uptake of Cu. A Zn atom has an atomic mass of 65.38 g mol^{-1}.

2.2.2. Iron and manganese

Iron (Fe) and manganese (Mn) are also metals, yet more frequently found in various water cycles. Although both elements can be listed as HMs based on its density, it is addressed separately due to lower toxicity, often higher concentration levels and more frequent presence in nature. Both are not considered to be a pollutant itself, but Fe and Mn can even be media to fix other pollutants like HMs (Contin *et al.*, 2007). A high content of Fe can however cause clogging in a filter and is particle bound to suspended solids .

Fe and Mn are naturally present in the Earth's crust and often present in groundwater resources (BC Ground Water Association, 2007). Elevated Fe concentration can hereby originate from groundwater leakage to the sewer system or by dissolution of building materials containing iron. In the Spangen pilot, mentioned below in 2.3.3, Fe and Mn are detected in the influent water due to the leakage of groundwater into the separate sewer.

Also, Fe is commonly used within building materials like steel and even for decorative purpose. Mn is found naturally in rocks and sediment, anthropogenic sources for Mn are automobile parts or industrial waste (USGS, 2014).

2.2.3. Other contaminants

Other contaminants can also be found in stormwater. Although these are not extensively addressed in this report, these contaminants are relevant when assessing water quality related to rainwater re-use.

- **Primary nutrients:** Mostly referred to as forms of nitrogen (N), phosphorus (P) and potassium (K). These are required in large quantities by plants. Nutrients end up in stormwater by fertilisers, faecal matter of animals or

other waste sources (Glibert *et al.*, 2005). Mainly N and P are associated with stormwater pollution. An excessive concentration of nutrients can lead to eutrophication and algae blooming in surface waters or within biofilters, disrupting ecosystems (Tekerlekopoulou, Pavlou and Vayenas, 2013). However, nutrients are also needed in moderate concentrations for plant and bacterial growth.

- **Dry deposition**: During dry weather conditions particulate matter and aerosols in the atmosphere can settle on the surface. If a dry spell has occurred the pollution load can be much higher as the water catches the settled deposition. Pollution can attach to dust particles, which are washed off with the rain event (Van de Ven, 2016).
- **Wet deposition**: Is the phenomena when absorption of pollution occurs in the droplets of precipitation. Gases and particulate matter in the atmosphere are transferred to the rainwater and it often acidifies the water.
- **Polycyclic aromatic hydrocarbons (PAH)**: Consist of solely carbon and hydrogen atoms and are composed in aromatic rings (US Environmental Protection Agency, 2013). PAH exist in more than 100 forms, of which 16 (ΣPAH_{16}) PAHs end up in stormwater runoff via human and natural processes, generally reflecting combustion sources like gasoline and crude oil (Abdel-Shafy and Mansour, 2016). Additionally, the atmospheric deposition corresponds to stormwater runoff compositions. Runoff and atmospheric deposition are the primary mechanisms of the PAH contaminating the water. Excessive exposure may cause lung cancer as most significant health effect (Abdel-Shafy and Mansour, 2016).
- **Mineral oils**: Higher alkanes, with nine or more carbon atoms, which originate from mineral sources by shops, garages or cars. Mineral oils interfere with biological life and are hard to degrade.
- **Pesticides:** Mixtures of substances used to control harmful organisms, pests, while protecting the crops (Nicolopoulou-Stamati *et al.*, 2016). Pesticides are intensely used in urban areas for weed and vermin control in (public) gardens and agricultural practice (Pimentel, 1995). Overexposure to pesticides can have toxic effects to human health (e.g. cancer, asthma) and health of the environment and biodiversity (Geiger *et al.*, 2010).
- **Salts:** Also events like spreading road salt for de-icing increase the sodium and chlorine concentrations. Or even leakage of lead, iron, aluminium and phosphorus when non-purified rock salt is used (HowStuffWorks, 2019). During snowfall events, pollutants can also accumulate in snow, leading to a different water matrix for snowmelt water (Brezonik and Stadelmann, 2002).
- **Pathogens:** Pathogens can strictly limit the use of stormwater and are found in a large variety (Sidhu *et al.*, 2012). The most abundant forms in stormwater are *E. Coli* and *fecal coliform* and indicate presence of harmful pathogens with a significant risk, causing serious health effects and illnesses (Page *et al.*, 2010). Improper disposal of pet waste and soil waste can get pathogens in stormwater.

2.3. BIOFILTRATION SYSTEMS

Stormwater biofiltration systems have the aim to remove the aforementioned pollutants that contaminate the stormwater runoff. Contamination of water can disrupt the ecosystem or human health by direct re-use. Stormwater treatment systems should fulfil the required water quality criteria.

Biofiltration technologies are more frequently used in stormwater management. Biofilters are a low energy treatment technology, which consist of filter media with an active biological layer (Hatt *et al.*, 2009). Biofilters are traditionally included in drinking water treatment, for its high organic removal and have been used and studied for centuries (Saladrich Català, 2019). By its high retention and treatment capacity, biofilters can also be used for stormwater treatment (Hatt *et al.*, 2009).

In the last decades, various biofiltration treatment technologies have been developed specifically for urban stormwater. Treatment wetland systems, biofiltration swales, detention ponds or the Bluebloqs Biofilter are examples of technologies implemented on field scale, and they differentiate in design and operation (Whitacre, 2014). Ultimately, the similarity between these systems is the simultaneous treatment processes when water flows along vegetation and media (Saladrich Català, 2019).

2.3.1. Bluebloqs Biofilter design

The Bluebloqs Biofilter (BB1.0) exists of a porous media and vegetation on top, depicted in Figure 2-4. The filter material retains and delays the water flow, supports the vegetation and treats the stormwater runoff. The porous media consists of four different sand layers. The top, transition and drainage layer consist of quartz sand (Kremer, 2014). One can compare the media similar to the treatment by a slow sand filter. The sand media is separated from the surrounding soil and groundwater by a geotextile and a polyethylene protective membrane.

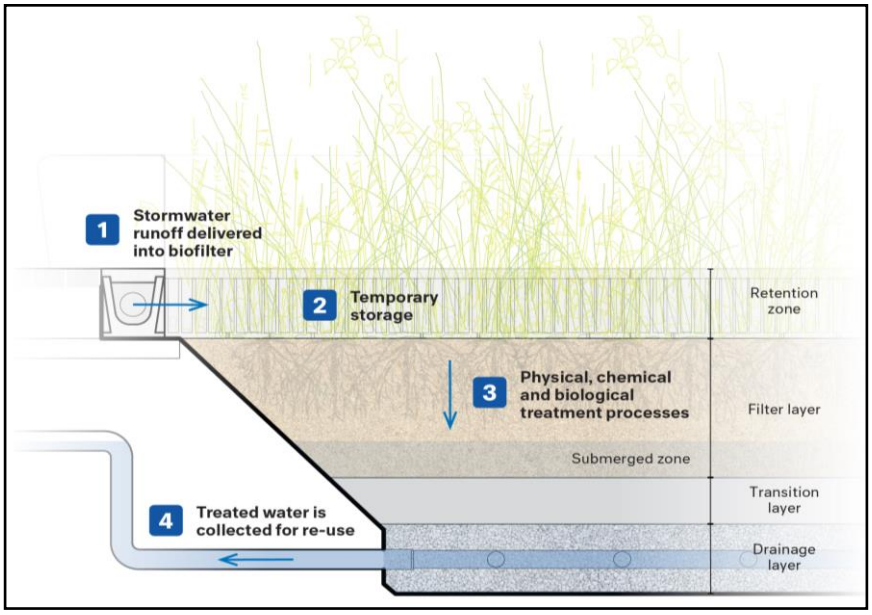

Figure 2-4 Schematic design of the Bluebloqs Biofilter (BB1.0) (Field Factors, 2018)

Filter media

The filter, transition and drainage layer have increased grains size respectively, which is related to its function (Table 2-2). The consistency of quartz sand is 98.6 m% SiO_2 , 0.33 m% Fe_2O_3, 0.46 m% Al_2O_3, 0.48 m% K_2O and the rest is other compounds. The bulk density is 1.5-1.6 g cm^{-3} (Kremer, 2015). The top layer consists of iron-oxide coated sand (IOCS), which is a by-product of drinking water companies (AquamineralsBV, 2019). The porosity of the filter bed is 25-35 % when compacted and not compacted (Saladrich Català, 2019).

Table 2-2 Media configuration of layers in Bluebloqs biofilter (BB.01)

Layer	Media Classification (NEN 5104)	Mineral	Grain size (mm)	Layer depth (cm)
Top Layer		Quartz sand with iron depositions	2-8 mm	±1
Filter Layer	Medium sand – Coarse sand	Quartz sand	0.4 - 0.8	60
Transition Layer	Coarse sand – Very coarse sand	Quartz sand	0.8 - 1.25	20
Drainage Layer	Very coarse sand	Quartz sand	< 1.8	30

Iron-oxide coated sand (IOCS) or Fe-coated sand is quartz sand with any form of iron oxide minerals precipitated onto the outer layer of quartz sand. Iron-oxides have been found in many phases, resulting from various aqueous processes, pH- and redox conditions (Fernández-Remolar, 2014). The different forms have a variability of mineral structures of which goethite, hematite and magnetite are best known crystalline forms. IOCS has more pores and a higher specific surface area than regular mineral quartz sand and hereby a higher adsorption capacity, explained in section 2.5. IOCS used in this research, is a by-product from rapid sand filters in drinking water treatment plants and given a new purpose in the BB.

Vegetative layer

Vegetation of the BB1.0 consists of wetland plants (*macrophytes*), as these plants can cope with a large amount of water to survive. This vegetative layer performs similar to a VSFW, with oxygen in the upper layer of the soil matrix and providing nutrient and organic material absorption via the roots (Tilley *et al.*, 2014). *Calamagrostis acutiflora, Carex nigra, Carex Testacea, Iris sibirica, Lythrum salicaria, Mentha aquatica* and *Panicum virgatum* are initially planted.

Figure 2-5 Left: Vegetation in the Bluebloqs demo in Spangen, after one year of installation, July 2019. Right: New species nest in the Bluebloqs biofilter in Aartselaar, October 2019 (Versteeg, 2019)

2.3.2. Bluebloqs Biofilter operation

Water flows in downward vertical direction from the vegetative layer through the sand layer under gravitational force. During the operation the water level rises above soil layer and creates a ponding layer, which mimics a natural wetland (Figure 2-6).

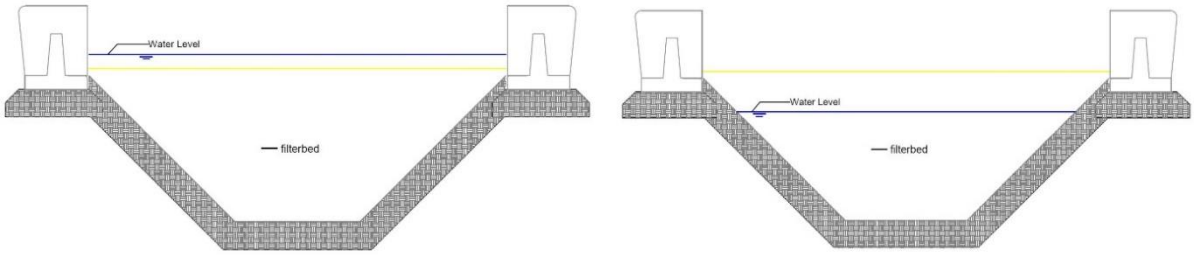

Figure 2-6 Left: Water level during operation of the BB ponds 10 cm above filter bed. Right: Water level 30 cm under filter bed level in non-operational conditions and maintains the submerged zone.

Water level in the biofilter is regulated by a nearly placed sump. The water level in the sump is designed to be as high as the water level in the biofilter, as both locations are under atmospheric conditions and connected. To control the water level, a pump in the sump is operated to drain the water to the infiltration well.

During dry periods, when the system is not in operation, a submerged zone is created by controlling the water level at the drainage tank at approximately 30 cm below top layer. At top layer aerobic conditions are generated for nitrification, also partly from roots of vegetation (Blecken *et al.*, 2009a). The submerged zone with anaerobic/anoxic conditions is maintained to enhance denitrification (Payne *et al.*, 2015). Furthermore, the submerged zone can lead to a small pH increase (Blecken *et al.*, 2009a).

2.3.3. The first Bluebloqs system: Pilot Spangen, Rotterdam

In 2018 the first full-scale application of the Bluebloqs system was implemented in the pilot project Urban Waterbuffer Spangen, in Rotterdam, The Netherlands. Stormwater runoff from a total surface area of approximately 46,000 m^2, including roofs, streets, a public square, parking lot and a football stadium, is collected in a separated stormwater sewerage (Figure 2-7).

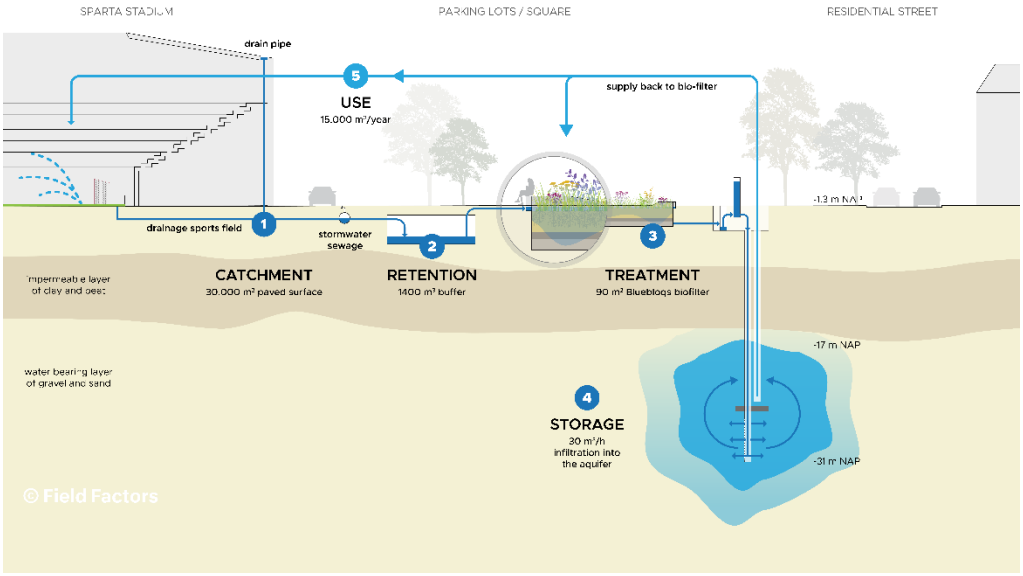

Figure 2-7 Schematic cross-section of the Bluebloqs system in pilot Spangen, Rotterdam (Field Factors, 2018)

The sewer is connected to a 1400 m^3 underground retention basin, using the Rigofill® inspect blocks system (Fränkische Rohrwerke, 2016a). This retention buffer disburdens the sewer system in periods of heavy rainfall. The velocity of the water flow decreases within this basin. Under a lowered flow, with a maximum discharge of 30 $m^3\ h^{-1}$, the water flows through a pipeline passing a SediPoint® system (Fränkische Rohrwerke, 2016b), a sedimentation shaft. Coarser particles, litter, oil and other non-aqueous phases are removed by this system under sedimentation.

Water flows to the BB, with a maximum discharge of 30 $m^3\ h^{-1}$. Water enters the filter media from distribution channels placed along the filter bed. The surface area of the biofilter is 90 m^2, so a maximum water velocity of 0.33 $m^3\ h^{-1}\ m^{-2}$ is created. Water ponds on top of the filter and flows vertically through the filter bed and the root zone of vegetation, simulating slow sand filtration under gravitational forces and vertical flow constructed wetlands.

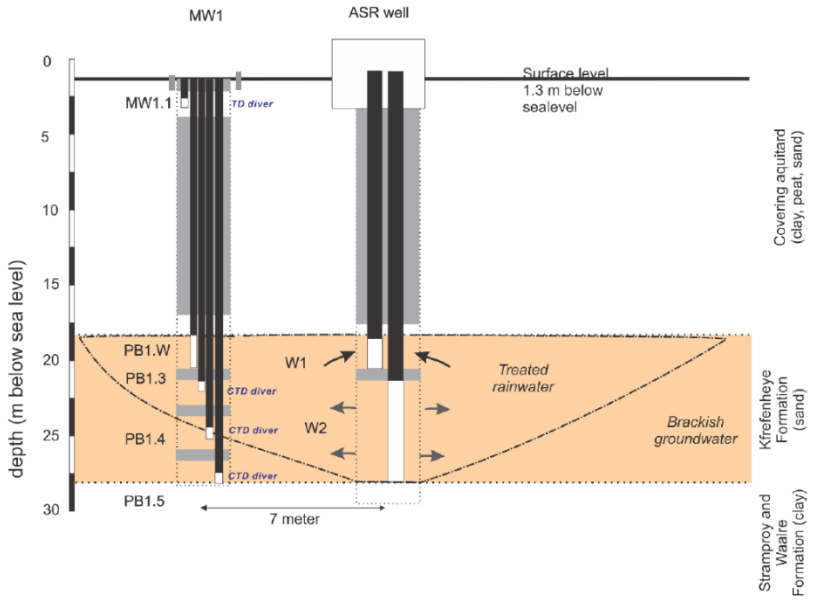

Figure 2-8 Cross section of the ASR wells and monitoring at Spangen demo (Zuurbier et al., 2019).

Filtered water is collected at the bottom of the biofilter in a drainage pipe (Ø400 mm) and pumped into a standpipe (Ø500 mm). Figure 2-8 shows how the water is infiltrated in a sand aquifer under gravitational forces 26 m below ground level. Water is infiltrated by a first well (W2) to create a fresh water aquifer storage. The density difference between fresh and brackish water creates an artificial freshwater aquifer. As freshwater is lower in density it floats upwards. Freshwater is recovered by a second well (W1) at 16.25 m depth, so above the infiltration well. The extracted water is then used for the irrigation of the artificial grass in the Sparta football stadium, for the biofiltration irrigation or other water features.

2.4. BIOFILTER TREATMENT PROCESSES

Water treatment processes can be either physical, chemical, biological or a combination of those. Each of these processes has an effect on specific target pollutants and its properties (Saladrich Català, 2019). Vegetation and the top filter layer is assumed to be where most of the water treatment processes take place. By water passing vertically downwards through the filter matrix, numerous treatment processes occur (Table 2-3).

Table 2-3 Overview of biological, chemical, physical or a combination of the processes in a biofilter (Saladrich Català, 2019)

Science	Process	Description
Physical	Sedimentation	Gravity to remove suspended solids from water.
	Mechanical filtration	Particles too large to follow tortuous channels.
	Physical straining	Particles too large to fit between grains.
	Physisorption	(weak) Van der Waals forces of substrate to adsorbate molecules.
Biological	Plant uptake	Mineral nutrients (macro/micro) uptake through plant roots.
	Nitrification	Bacterial oxidation of ammonium or ammonia to nitrate.
	Denitrification	Bacterial reduction of nitrate to dinitrogen gas.
	Die-off	Die-off of microorganisms.
	Biodegradation	Breakdown of organic matter by microorganisms.
Chemical	Precipitation	Solid formation from a solution by (super)saturation.
	Chemisorption	Valence forces or chemical bonds of substrate on adsorbate molecules, from aqueous state to solid state.
Combined	Fixation	Nitrogen fixed and converted to ammonium.

These processes occur at various locations in the biofilter and sometimes only under specific conditions. For example, gross of nitrification processes will occur under aerobic conditions, which is above the submerged zone. While denitrification typically takes place under anoxic conditions (Metcalf and Eddy, 2003).

In this study, the main focus of research lies on the removal of HMs by adsorption process. It is expected that this mainly occurs in the top layer and filter layer within the biofilter. However, other treatment processes can take place in parallel or followed by adsorption and are relevant for understanding the overall BB performance.

Chemical precipitation

Precipitation is the chemical process in which dissolved ionic components in water react and forms to solid phase. In traditional water treatment this is used to remove metallic cations. Precipitation can be promoted by addition of compounds that destabilise the ions and neutralises charge, i.e. by dosage of iron and aluminium salts. Coagulation is often induced by dosing opposite charge particles, and particles enmeshed into larger solids. Precipitate, the solid form, is then removed by physical processes like filtration or sedimentation, when size and mass increase. Iron oxide-coated sand enhances oxidation of soluble iron Fe^{2+} to Fe^{3+}, of which the latter oxidation state is faster to precipitate to $Fe(OH)_3$ (Devi *et al.*, 2014).

Mechanical filtration

The removal of particulate material and suspended solids in the BB is mainly by physical processes. The filter media is supported by the transition layer and due to the small grains, small tortuous channels are created. Larger particles are trapped when the channels are smaller than the flocs size. Mostly, this step takes place in the top layer of the filter layer (Saladrich Català, 2019). As HMs are largely particulate-bound (see Figure 2-3), it is expected that the highest removal is also at the top layer (Hatt, Deletic and Fletcher, 2007).

Plant uptake

Plant uptake can contribute to a significant break down of organic matter and uses up available nitrogen, phosphate and carbon dioxide. For example, constructed wetlands are often used as post treatment of waste water treatment plants (Langergraber, 2005). Also metals, such as iron, molybdenum, nickel, copper, zinc and manganese are known as essential micronutrients and absorbed by plants (Peralta-Videa *et al.*, 2009). Carbonates in the soil can inhibit the transferring of HMs from soil to plants (Wang *et al.*, 2015).

Microbiological activity

Purification in biofiltration systems is by microbiological activity in a biological (Schmutzdecke) layer. This complex biological layer consists of protozoa, bacteria and other microorganisms that purify the water and is located in the top layer of sand filters. Trapped particles, carbon species other and impurities are degraded on this layer (Ranjan and Prem, 2018). The Schmutzdecke development on biofiltration systems depends on presence of substrate and oxygen (Graham and Collins, 2014). Maturation of the Schmutzdecke can range from several weeks up to several months (Hendricks, 2006). Microbiological activity can cause a pH drop by the production of CO_2 (Muhammad *et al.*, 1997).

2.5. ADSORPTION

2.5.1. Fundamentals of adsorption

Adsorption is a phenomenon between two chemical phases. A so-called adsorbate, in gas (g), aqueous (aq) or liquid (l) mobile phase, accumulates to the surface of a solid (s) phase, increasing in concentration (Ali and Gupta, 2007). The adsorbate is forced onto the sorbent, the solid phase. This force can be physical sorption, which arise by van der Waals forces, meaning intermolecular attraction or repulsion (Derouane and Chang, 2000). However, a greater force is induced by chemisorption: electrostatic Coulomb forces when sorbent surface and the adsorbate have an opposite electrical charge. Chemisorption creates an ionic/chemical bond and is often significantly stronger than physical sorption in water treatment processes (Karge and Weitkamp, 2008). Chemical adsorption is considered a chemical reaction.

Adsorption is an active treatment method to improve water quality, by adhesion of contaminants onto sorbent material. Often materials with a high surface area are used, like activated carbon, to link the solutes to the surface and enhance the formation of the chemical bond (Al-Anbar, 2011).

Diffuse double layer

The electrical diffuse double-layer model (DDL) describes the structure of surfaces in liquids. The electrical potential of the surface varies and influences the attraction, based on the Gouy-Chapman principle. DDL is described by introducing the primary layer and diffuse layer, between three planes with associated potentials. Figure 2-10 describes and visualises the DDL and how the potential evolves. In the first layer the ions are adsorbed and fixed, with opposite charge of the surface. Adsorbed particles are only a few nanometres from the surface. The second layer is the diffuse layer, where ions move are influenced by electrical potential and retain some freedom of movement. Potential is balanced by counter ions up to the slipping plane at zeta potential.

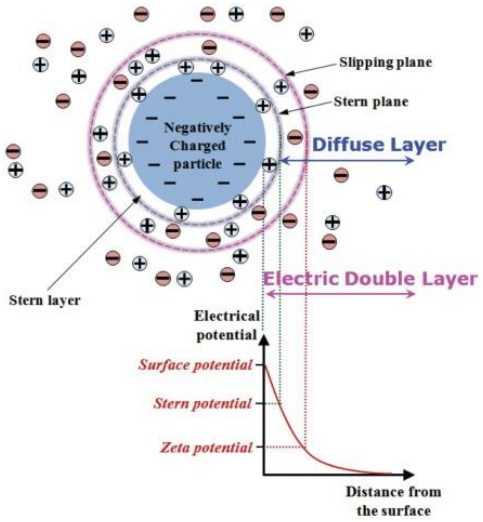

Figure 2-9 Schematic illustration of the double diffuse layer model. Negatively charged particles may represent sorbent media, which attracts positively charged particles surrounding the media and created the Stern layer.

The Stern layer can be subdivided in the inner sphere and outer sphere. Adsorbed particles in the inner sphere share an electron between the sorbate and the surface, called an inner-sphere complex. Inner sphere complexes are directly bound to the surface. Outer-sphere complexes the sorbate and surface remain separate entities and the hydrogen sphere of the sorbate stands (Payne *et al.*, 2013).

DDL is a commonly used approach to describe the potential development and surface structure in liquids, but also constant capacitance models and triple layer models with a variety of parameters are used. In this report, the scope is limited to DDL models.

Surface potential

Sorptive material is positively or negatively charged, respectively cationic sorptives and anionic sorptives, or is neutral with as much positive as negative surface functions. Electrons can however be not evenly distributed on the surface, and so nonpolar (Young and Weber, 2018). The charge of a particle can be expressed by the surface charge density by:

$$\sigma = \frac{q}{A}$$

where σ = charge density [C m^{-2}] , q = electric charge [C] and A = surface area [m^2]. The point of zero charge for quartz sand lies at 3.0, so in neutral conditions (pH = 7.0 ± 0.5), quartz sand media surface has a negative charge (Cao *et al.*, 2010) (Tschapek and Wasowski, 1986).

DDL shows that the electrical potential decreases exponentially over distance from the surface. The Grahame equation combines that to the charge density and becomes:

$$\sigma = (8RT\varepsilon_r\varepsilon_0 I)^{1/2}\sinh\left(\frac{z_e\psi_0 F}{2R_g T}\right)$$

where z_e is the valence of a background electrolyte [C], Ψ_0 is the potential at the surface [V], F is the Faraday constant [C mol^{-1}], T is temperature [K], R_g is the gas constant[J K^{-1} mol^{-1}], I is ionic strength of the solution in contact with the surface [mol L^{-1}], ε_r is the relative dielectric constant of water [-], and ε_0 is the permittivity of a vacuum [-] (Lennard-Jones, 2014). The potential decreases with distance from the surface:

$$\psi(x) = \psi_0 e^{-\kappa x}$$

where κ= Debye length [m^{-1}] and Ψ = potential at distance x from the surface [V]. The Debye length is considered the thickness of the diffuse layer. The layer varies by ionic strength. When I is high, the Debye length is compressed (Badawy and Alkhalik, 2009):

$$\kappa^{-1} = (3.94 * 10^{-24} \varepsilon_r \left(\frac{T}{I}\right))^{0.5}$$

With T = temperature [K], I = ionic strength [mol L^{-1}] and ε_r = relative dielectric constant of water[-].

Charge of sorbent media and sorptives is not constant, but can change with different physical and chemical conditions. Variable charge surfaces exhibit acid-base properties (Payne *et al.*, 2013). Also, presence of organic ligands in stormwater can form complexes with HMs, lowering the surface charge (Khaodhiar *et al.*, 2000) (Stietiya, 2010). Some effects were identified and elaborated.

Effect of pH on surface charge

Adsorption is a process strongly dependent on the pH of the contact solution. In general, a lower pH has a negative effect on the metal or cation adsorption capacity, while a higher pH shows better adsorption results (Abbar *et al.*, 2017). The pH of the contact solution affects the surface charge of the media, by formation of OH-groups or O^--groups in the inner sphere.
An acidic solution, with low pH, contains more H^+ and deprotonation of the surface is unlikely to occur. A high pH, contains less H^+ ions and protonation of the surface happens easier and result in more O^- groups.
With a pH below the pH point of zero charge (pH_{pzc}) of the media protonation of hydroxyl groups happens, so more OH-groups on the surface. Whereas, when the pH increases above pH_{pzc} of a specific media, deprotonation occurs and more O^--groups are at the surface (Figure 2-10). The pH at which the surface has net no charge is the *point of zero charge* (pH_{pzc}). Surfaces of the inner spheres are thus charged as a function of pH, therefore it depends which and how strong compounds attract and repulse by ionic forces (Li *et al.*, 2016).

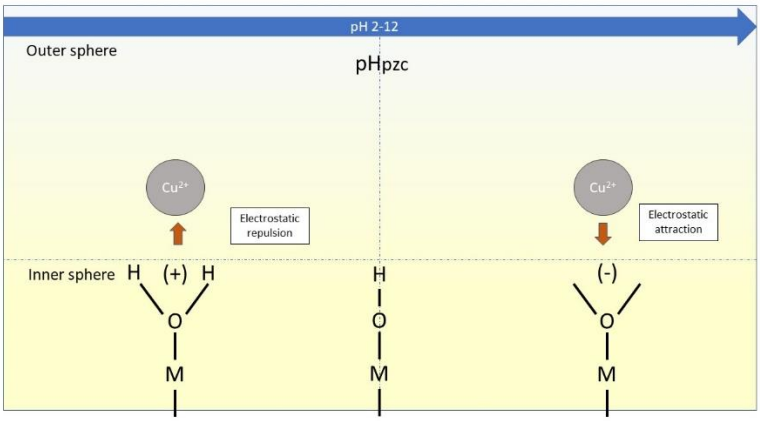

Figure 2-10 Protonation of metal-oxide adsorbents and effects on cation adsorption. Adapted and edited from Li et al. (2016)

Effect of ionic strength on adsorption

Also of some importance is the ionic strength effect on adsorption in the liquid-solid interface. Ionic strength is determined by the total amount of dissolved ions multiplied by the charge of the ions in the solution:

$$I = \frac{1}{2}\sum_{i=1}^{n} c_i {z_i}^2$$

with c_i =molar concentration of ion I [M] and z_i = valence number of dissolved ion. A high ionic strength in the water suppresses the diffuse layer of the sorbent media. This decreases the distance of electrostatic repulsive forces (Speed, 2016). The classical ionic strength effect is described that by an increasing ionic strength, the ion uptake decrease, which is related to the outer sphere adsorption. It originates from the explanation that a higher ionic strength increases the competition for a surface functional group. This is caused by outer sphere complexation or decreasing the activity by formation of aqueous complexes. (Hayes and Leckie, 1987) (Badawy and Alkhalik, 2009). However, also promotive effects and insensitivity of adsorption to increasing ionic strength are reported by Lützenkirchen (1997).

2.5.2. Sorption modelling

It is well known that adsorption is influenced by pH of the solution, the PH_{pzc} of sorbent material, the ionic strength I of the solution and the charge of the sorbate. Sorption processes can be examined with multiple empirical relations and isotherms. Most known forms to describe the (ad)sorption in aqueous solutions is by K_d-linear modelling or non-linear *Langmuir* and *Freundlich* isotherm. These analytical models are most often used to interpret experimental data.

Linear adsorption isotherm

Net migration between the solid and water interface can be described by a mass-based partition coefficient K_d and describes the ratio of sorbed phase and in-solution phase (Vandergraaf, Ticknor and Melnyk, 1992). This linear adsorption is also referred to as *Henry's* law isotherm:

$$K_d = \frac{S}{C} = \frac{mass\ sorbate\ /\ volume\ (sorbed\ concentration)}{mass\ of\ solute\ /\ volume(dissolved\ concentration)}\ [\frac{kg\ L^{-1}}{kg\ L^{-1}}]$$

It describes the mobility of an adsorbate and distribution to liquid or adsorbed phase. K_d term is valid for a particular adsorbent and fixed background chemical conditions.

K_d-value linear isotherm modelling assumes that adsorption is a linear process by the assumption that K_d has constant distribution, meaning a higher initial solute concentration still considers the same ratio of adsorbed concentration and dissolved concentration. However, this model has it shortfalls as available sorption sites and surface charge evolves during the adsorption process. Linearity is therefore not often considered accurate for high concentrations.

Freundlich isotherm

Freundlich sorption isotherm is used for non-linear regression to give better representation, with the assumption of a heterogeneous surface and exponential distribution of active sites. This isotherm is constructed empirically by:

$$S = K_F C^{1/n}$$

with n as heterogeneity factor related to the solutes, K_F is the Freundlich constant [L g^{-1}] and C is the solute concentration [g L^{-1}]. Larger n indicates the distribution of active sites. The above formula can be rewritten to a linear *Freundlich* model to:

$$\log(S) = logK_F + nlog(C)$$

By creating plot figures with logarithmic scale on each axis, a straight line will form. The slope of this line represents the n-value, while the log K_F value represents the value that crosses the y-axis.

Langmuir isotherm

Langmuir sorption assumes adsorption uniformly on the active sites of the surface layer as a one step process. The unoccupied sites are then available for adsorption and are occupied when solutes are sorbed. *Langmuir* isotherm is based on the theory that at maximum coverage a monomolecular layer is created, so there is no stacking of sorbed molecules. It gives:

$$S = \frac{S_m K_L C}{1 + K_L C}$$

with S_m is the maximum sorbed concentration per mass sorbent [g g^{-1}], K_L is the Langmuir constant [L g^{-1}], S is the sorbed concentration per sorbent [g g^{-1}] and C is the dissolved concentration [g L^{-1}].

Surface complexation models

The surface complexation model is described as formation of bonds between metals and ligands at the water-solid interface, similar to the formation of aqueous complexes in solution, described in 2.5.1 (Dzombak and Morel, 1990). This modelling incorporates chemical bonding of solute species with active surface material and the electrostatic interaction.

Adsorption can be expressed in a chemical equilibrium based on mass and charge balance:

$$\equiv SOH + X^z \rightarrow \equiv SOX^{z-1} + H^+, \qquad \frac{[\equiv SOX^{z-1}][H^+]}{[\equiv SOH][X^z]} = K_{ad}$$

where X is the sorptive, z is valence of charge and ≡S is a representation sorbent media active surface. The surface shares an electron with the sorbate and the chemical bond is formed. A proton is replaced and released. For chemical equilibria, the K_{ad} stability constant expresses the equilibrium state (rate reaction forward equals rate reverse reaction). The K_{ad} value describes the relationship of the species, similar to aqueous complexes.

2.5.3. Surface complexation modelling

In this research, surface complexation models were applied as method to incorporate the effects of environmental conditions, since it can be easily extrapolated to chemical conditions outside of investigated ranges. This mechanistic sorption model is less often used as the abovementioned K_d-linear modelling or non-linear *Langmuir* and *Freundlich* isotherm models, but it can provide more details on the adsorption processes in competitive (multiple-metal) systems.

The DDL approach suggests that one proton is released for each HM ion adsorbed to the surface. In the above chemical equilibrium, *X* can be replaced by other sorbate cations in the solution, specifically the HMs mentioned in section 2.2.1. Active sorption surfaces are often distinguished in strong and weak sites. Weak binding sites are associated with moderate to high cation concentrations and strong sites for lower cation concentrations For both types of site a reaction and associated K_{ad} stability constant is determined. One site binds to one sorbate in the abovementioned equilibria, although sorbates can bind to more than one site called multidentate adsorption.

Surface complexation reactions can be described by thermodynamics. The tendency of a sorbate to adsorb to a surface is expressed as an adsorption coefficient. The free energy of adsorption is described by:

$$\Delta G_{ad} = \Delta G_{intr} + \Delta G_{coul}$$

with ΔG_{ad} is Gibbs free energy of adsorption [J], with ΔG_{intr} is intrinsic complexation term [J] and with ΔG_{coul} is coulombic term [J]. The coulombic free energy represent the electrostatic force, given by:

$$\Delta G_{coul} = F \Delta z \psi_0$$

Where Δz is the change of valence of the surface species by adsorption reaction and F the Faraday constant [C mol^{-1}]. This term shows the relation to the potential of the sorbent at the surface. The relation between adsorption Gibbs free energy and K_{ad} is a s follows:

$$\Delta G_{ad} = -R_g T ln K_{ad}$$

The K_{ad} value then becomes:

$$K_{ad} = e^{-\Delta G_{ad}/R_g T} = e^{-\Delta G_{intr}/R_g T} e^{-\Delta G_{coul}/R_g T}$$

with T is temperature [K] and R_g is the gas constant[J K^{-1} mol^{-1}]. By knowing the ψ_0, which changes by chemical conditions of the environment and can be calculated with σ (section 2.5.1), the thermodynamic equilibrium of the complexation reactions can be determined (Lennard-Jones, 2014).

$$\Delta G_{ad} = \Delta H_{ad} - T\Delta S_{ad}$$

with ΔG_{ad} is Gibbs free energy of adsorption [J], ΔH_{ad} is enthalpy of the adsorption [J mol^{-1}], T is temperature [K] and ΔS_{ad} is the change entropy [J K mol^{-1}]. A negative Gibbs free energy indicates a spontaneous nature of the reaction. For metal adsorption, this most often the case, although it depends on the adsorbent-adsorbate combination (Sahmoune, 2019)(Kumar, 2011)(Al-Anbar, 2011). For chemisorption, the degree of freedom decreases and so the entropy decreases. The degree of adsorption increases with decreasing temperature.

By knowing the K_{ad} constant for a surface complexation reaction, under constant temperature, pressure and solution composition, the Gibbs free energy for the adsorption reactions can be thermodynamically be determined.

Hydrous ferric oxide as active sorption site

In practice, the surface can be any type of material, but active sorption sites are often introduced with metallic surfaces and more specifically hydrous ferric oxide (HFO). HFO is the primary iron oxide surface due to its large surface area and number of binding sites that catalyses the sorption force. This is also seen by the principle of dosage of iron salts as coagulants for metal sorption in conventional water treatment plants (Streat, Hellgardt and Newton, 2008). Surface complexation focusses on the complexation reaction of the adsorbate-adsorbent interaction, so active HFOs on the surface react with solutes.

HFOs are amorphous iron oxides in solid form by hydrolysis-precipitation processes of ferric salts (Dzombak and Morel, 1990). HFOs general representation is by $Fe_2O_3 \cdot nH_2O$ stoichiometry formula, where *n* varies from 1 to 3. However, the type of coated iron oxide depends on the physical and chemical environment during the precipitation process (Lo, Jeng and Lai, 1997). For example, hematite, goethite and ferrihydrite are natural mineral forms of hydrous ferric oxides with different structures, stability and characteristics (Streat, Hellgardt and Newton, 2008).. The pH_{pzc} for HFOs is range of 7.9 -8.2 (Dzombak and Morel, 1990), so in neutral pH conditions protonation of hydroxyl groups happens.

2.6. RETARDATION AND BREAKTHROUGH BY ADSORPTION

When water flows through porous media, adsorption slows down the transport of contaminants. By the adsorption reaction, the rate of movement of an adsorbed contaminant is retarded. Chemical retardation describes the slowing transport of contaminants, relative to the water transport(Volz, 2017). It represents the residence time until breakthrough occurs. Adsorption on media retards the passing of contaminants through the biofilter.

$$R\frac{\partial c}{\partial t} = D\frac{\partial^2 c}{\partial x^2} - v_p\frac{\partial c}{\partial x}$$

where R = retardation [-], D = dispersion coefficient [m^2 s^{-1}], c = concentration of contaminant [g L^{-1}], x = distance [m], t = time [s] and v_p = pore water velocity [m s^{-1}]. When a linear downward flow is assumed in the BB, retardation is:

$$R = 1 + K_d$$

with K_d = dimensionless partition coefficient, abovementioned in section 2.5.2. For SCMs, the complexation on the surface is the adsorbed fraction. K_d shows that higher adsorption values, so less remains in solution phase, results in a greater retardation of contaminants. The velocity of the contaminant in the media is determined by

$$v_c = \frac{v_w}{R}$$

with v_c = contaminant velocity [m s^{-1}] and v_w = water velocity [m s^{-1}]. Figure 2-11 shows the effect of K_d on the retardation of contaminant transport in porous media. A high K_d value resembles high adsorption capacity by the

porous media, a large fraction of the contaminants are removed from the solution. A low K_d value resembles lesser adsorption capacity by the media and more contaminants remain in solution and end up relatively faster in the effluent water, when a continuous flow is assumed.

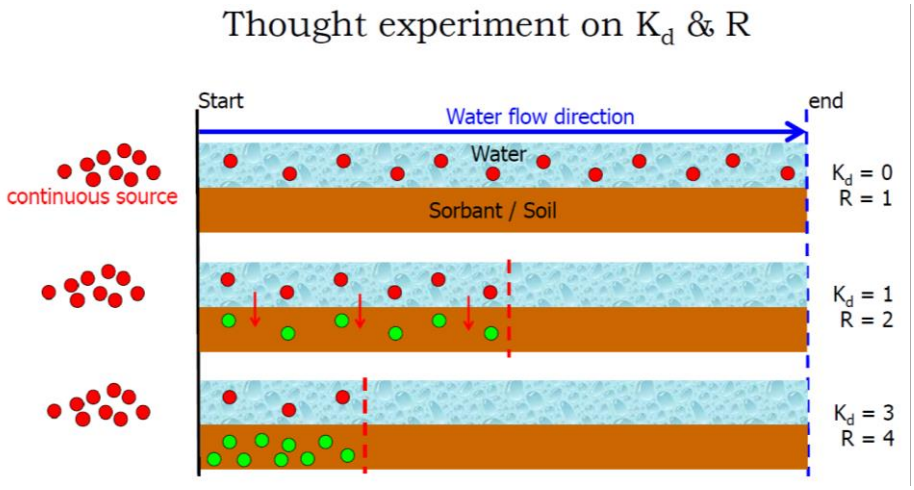

Figure 2-11 Schematic retardation process on contaminant transport. Adapted and edited from Van Breukelen, 2017

Breakthrough curve

A breakthrough curve for a fixed bed, in this case the BB, describes the course of sorptive concentration in the effluent at the outlet. Initially, the pollutants from a continuous feed are sorbed by the porous media and no concentrations are measured at the effluent. When the process continues at some point the pollutant will end up in the effluent, the breakthrough point. The breakthrough capacity is mass of the sorbate that is adsorbed by sorbents up to the breakthrough point. Further continuation of this process will cause saturation of the sorbent media and effluent concentrations will increase. After a certain period of operation, adsorption stops occurring and the bed is exhausted (Figure 2-12)(Patel, 2019). This is what is called the exhaustion point or complete breakthrough, when metals are no longer adsorbed by the filter media.

Delaying the breakthrough point and increasing the breakthrough capacity will result in longer operation of the biofilter, while maintenance and regeneration is postponed. An increased R value means a higher adsorption capacity of the bed and a delayed breakthrough point, what is desired for biofiltration systems.

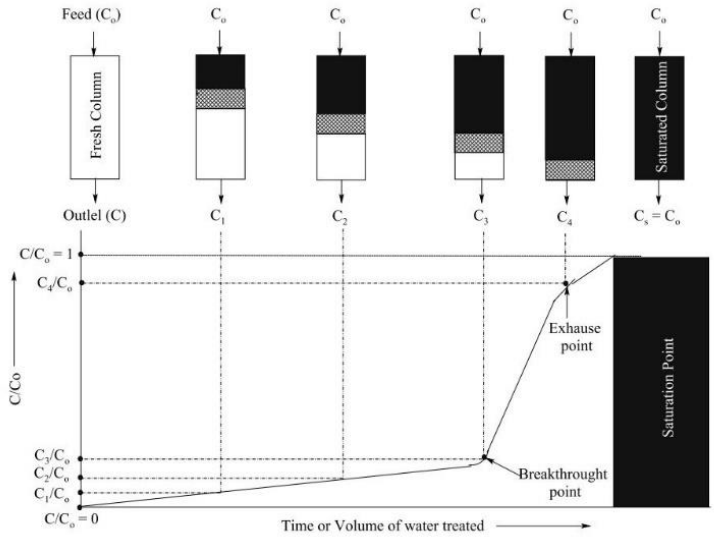

Figure 2-12 Representation of a breakthrough curve by the movement of a contaminant in a fixed filter bed. Adapted and edited from Patel, 2019.

3. MATERIALS AND METHODS

To identify sorption processes of HMs to filter media, both a field experiment was conducted and a sorption model was constructed. The field experiment was focussed on various concentrations of HMs that could occur in urban stormwater runoff and to analyse the development of the BB. The sorption model was developed to predict various conditions and the effect on HM adsorption by the BB.
From comparability of both methods, it could also emphasize differences between model settings and real world settings and it can assess the actual importance of theoretical modelling in field experiments.

3.1. FIELD EXPERIMENT: BLUEBLOQS BIOFILTER DEMO AARTSELAAR

As part of the EIT Climate-KIC Bluebloqs Demonstrator project, a small-scale operational prototype, i.e. a demonstrator, of the BB was built at the Aquafin campus in Aartselaar, Belgium, with the aim to research the possibilities to apply this technology as a sustainable water management solution in Flanders.

With the knowledge gained through the monitoring of the first system in the UWB Spangen, the treatment performance of the BB was optimised and adapted to the Flemish context. This demonstration site was used as a field experiment in this research.

The aim of the demo at the Bluebloqs demo in Aartselaar is to assess the possibilities to implement the BB as a sustainable water management measure in the Flemish context, where yet no infiltration standards on HMs are elaborated. It is however possible to compare water quality to *'Milieukwaliteitsnormen en milieukwantiteitscriteria voor grondwater',* the regulations on environmental quality and quantity standards for groundwater in Flanders.

The Bluebloqs demonstrator in Aartselaar was built in the end of June 2019 and was operated for 6 months. By creating artificially controlled pollutant dosages, the efficiency of the biofilter was researched. Compositions for the feed water were composed with a range of concentrations of HMs and nutrients frequently detected in urban stormwater runoff. Feed water was a combination of collected roof water and augmented with tap water.

3.1.1. Study area

The demo was built on the terrain of the waste water treatment plant of Aquafin, Boomsesteenseweg in Aartselaar, Flanders Belgium. Aartselaar is situated in the mid-north of Belgium in the province of Antwerp. The city of Antwerp is 7 kilometres north of the project location. Directly east of the project location lies a solid waste incineration plant (ISVAG) and a national highway lies on 300 metres of distance. This is relevant as these may be pollution sources by atmospheric deposition.

Runoff from a roof surface of approximately 250 m^2 of the research hall was collected. Water from the highest roof was conducted to the lower roof, over which the water was collected on the southern edge under a small slope.

Figure 3-1 Location of the Aartselaar demo (51°08'51.1"N 4°22'32.1E). Roof water catchment highlighted in red (left). During the field experiments, the demo was operated without concrete edges up to November 2019 (right) (Versteeg, 2019).

3.1.2. Demonstrator set-up

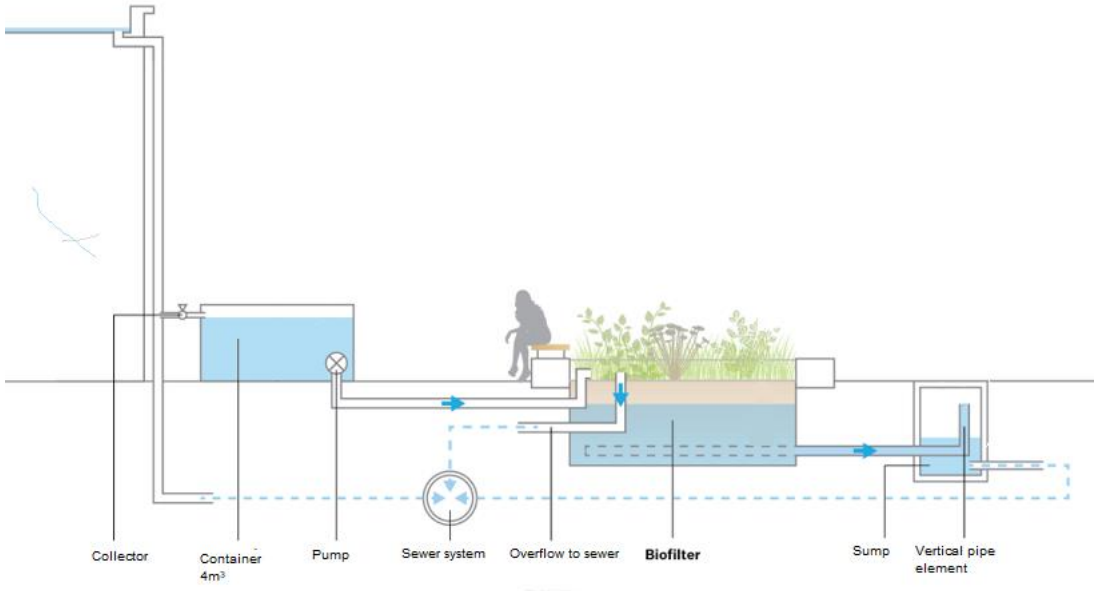

Figure 3-2 Aartselaar demonstrator set-up.

The biofilter has a surface area of 9 m^2 (3 x 3 m) and a depth of 1.1m. The sides of the filter layer are under a slope of 45°, leaving a base surface of 0.64 m^2 (0.8 x 0.8 m). This forms a total bed volume of 4 m^3. Depth and characteristics of the layers are similar to those of the Spangen pilot, mentioned in Table 2-2.
The vegetative layer consists of *Calamagrostis acutiflora, Carex nigra, Carex Testacea, Iris sibirica, Lythrum salicaria* and *Panicum virgatum*, similar to the same plants of those of the Spangen pilot, see section 2.3, with the exception of mint (Mentha Aquatica).

ic material absorption via the roots (Tilley *et al.*, 2014). *Calamagrostis acutiflora, Carex nigra, Carex Testacea, Iris sibirica, Lythrum salicaria, Mentha aquatica* and *Panicum virgatum* are initially planted.

Influent water was collected in a storage tank. To utilise rainwater, a connection is made with a nearby roof surface of ±250 m^2. The downspout was closed off and directly connected to fill a PVC storage tank. The storage tank was filled to 4m^3. Additionally, tap water was dosed to compensate for the lack of stormwater volume, dependent on the rainwater volume.

A peristaltic pump (Bredel 25) emptied the storage tank at the bottom to feed the biofilter. The flow could be regulated between 0.5-2 m^3 h^{-1}. For this research, flow velocity was set to 0.5 m^3 h^{-1}, each feed had a duration of 8 hours. The pump was connected to a hose (Ø 32 mm), that fed the inlet system of the biofilter. Operational water level (10 cm above filter bed) was established after approximately 90 minutes.

In parallel, a 1L bottle with the synthetic stormwater feed was also connected to the inlet system. Placed on a magnetic stirrer, the bottle emptied also within 8 hours. The tube was connected as T-piece to the hose. The chemicals were assumed to mix with the water that emptied from the storage tank and considered as influent water.

The influent was fed onto the biofilter by three sprinkler distribution pipes, elevated ± 20 cm above the filter bed. By small holes in the pipes the water distributed while it made contact with the air to enhance water aeration (Figure 3-3).

Figure 3-3 Left: Final design of the BB with concrete edges. Water was distributed onto the BB by three sprinkler pipes (Versteeg, 2019) Right: During operation the water level rises and mimics a wetland. Demo Aartselaar 19th of September 2019 (Versteeg, 2019)

The drained water was collected by a PVC pipe (Ø 110) with slots, placed in the drainage layer. Collected water flows into the drainage well (Ø 800, h: 1.5 m). The water level in the biofilter is controlled within the drain well, using the principle of level controlled drainage. When the system was operated, the water level was set to pond on top of the filter bed, 10 cm above filter bed level, by adjusting the water level in the drainage tank with a vertical pipe element. During times of no operation, the water level was set to 30 cm below the filter bed level.

The drainage well was emptied to the municipal sewer system. Water higher than 10 cm above filter level overflowed to a PVC pipe (Ø 90 mm) directly to sewer system.

The system was dimensioned based on the hydraulic characteristics of the filter media. The emptying time of the 4 m^3 storage tank was set for the Aartselaar demo at 8 hours, as well as the 1L chemical feed bottle. This resulted to a 0.5 m^3 h^{-1} flow. A minimum biofilter surface area of 9 m^2 was necessary to guarantee stability and placement and spacing of drainage pipes, so a 0.056 m^3 h^{-1} m^2 specific flow was obtained in the top layer and linear velocity increased with depth.

Table 3-1 Dimensions and characteristics of the field demo biofilter.

Specifics Bluebloqs Aartselaar Demo		
Length Upper Base	L1 (m)	3.0
Width Upper Base	W1 (m)	3.0
Upper Base Area	A1 (m^2)	9.0
Length Lower Base	L2 (m)	0.90
Width Lower Base	W2 (m)	0.90
Lower Base Area	A2 (m^2)	0.81
Height	H (m)	1.1
Height Filter Layer	h1 (m)	0.60
Height Transition Layer	h2 (m)	0.20
Height Drainage Layer	h3 (m)	0.30
Volume frustum	V (m^3)	4.6
Volume cube	V (m^3)	0.89
Porosity filter layer (assumed)	P	0.35

3.1.3. Filter media

Filter media for this demo was similar to the media used in the BB1.0 in Spangen (Table 2-2). The same layer dimensions and configurations were used. The pH of quartz sand was in range 5-8 (Kremer, 2014). The only difference was IOCS addition since the start of operation and some of the quartz sand from Spangen was taken to enhance inoculation of some bacteria.

Initial leaching from filter media

Fresh and used filter media was tested on initially present components (Table 3-2). This was observed from a similar batch experiment study for the same filter media (Spekreijse, 2019).
All filter media (5g) were acid washed in a 50 mL 10% HNO_3 solution in a 125 mL PE cup and shaken for 24hrs at 125 rpm on a rotary shaker. Hereafter, eluents were measured on the ICP-MS to determine the leached metals of each sorbent. The ICP-MS analysis is later discussed in section 3.1.7.

Table 3-2 Filter media for leaching test.

Material	**Supplier**	**Diameter**	**Origin**
Fresh fine filter sand (FFS)	Kremer	0.4 – 0.8 mm	Supplier
Used fine filter sand (UFS)	Kremer	0.4 – 0.8 mm	Spangen demo
Fresh coarse sand (FCS)	Kremer	0.8 – 1.25 mm	Supplier
Used coarse sand (UCS)	Kremer	0.8 – 1.25 mm	Spangen demo
Fe-coated sand (IOCS)	Aquaminerals	< 8 mm	Supplier

3.1.4. Influent water

Stormwater from the roof of research hall at the Aquafin campus was collected as feed water. Tap water was used for the feed when there was not sufficient stormwater collected for a run, if less than 4 m^3.

Tap water composition

Median composition of tap water composition was retrieved from Pipda (Vlaamse Milieumaatschappij, 2019). Except for Zn and Cu, no background values of HMs were found in the tap water.

Table 3-3 Median concentrations of tap water used at Aartselaar (Pipda 12). Zero values were excluded from this table.

Component	Unit	Median	Component	Unit	Median
EC	µS cm^{-1}	394.1	Al	µg L^{-1}	5.0
B	mg L^{-1}	0.1	pH	-	7.9
Cu	µg L^{-1}	1.0	Fe	µg L^{-1}	5.0
F	mg L^{-1}	0.1	SO_4	mg L^{-1}	61.7
NO_3	mg L^{-1}	1.4	Na	mg L^{-1}	13.5
Cl	mg L^{-1}	28.3	Mg	mg L^{-1}	5.6
Ca	mg L^{-1}	60.6	Zn	µg L^{-1}	3.6

Roof water composition

Stormwater from the roof in the Aartselaar demo was collected six times in October and November 2020 and shown in boxplots for HMs, Fe and Mn in Figure 3-4. Zn was found in the highest concentrations, followed by Pb, Cu and Ni respectively. Cd was found in lower concentrations in stormwater runoff.

Zn median value was at 58.0 µg L^{-1}, with one sample which exceeded the Zn Dutch infiltration limit with 74.5 µg L^{-1}. Pb median value was at 16.3 µg L^{-1} and three times exceeded the infiltration standard. Cu, Ni, As and Cd never exceeded the Dutch infiltration standards and were found in lower median values of 7.3, 1.3, 1.4 and 0.4, respectively. The roof material was unknown.

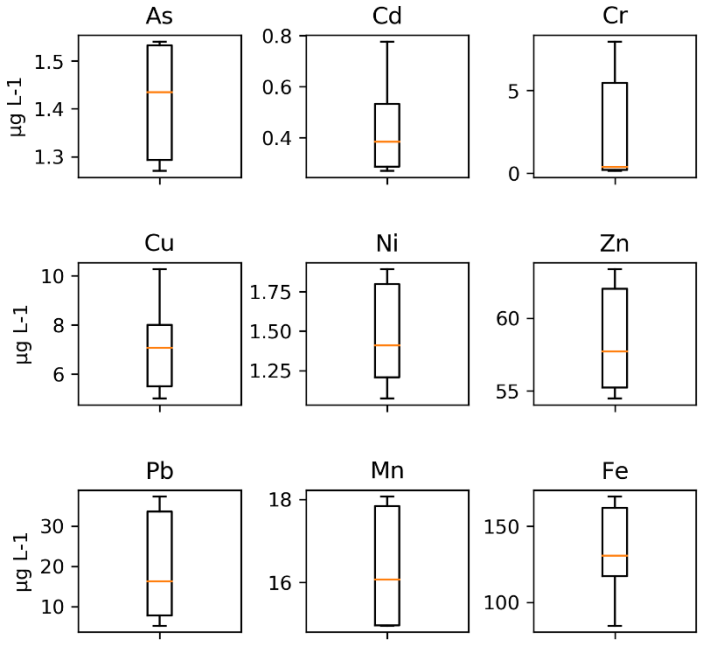

Figure 3-4 Box and whisker plots of Aartselaar demo roof water for HMs for six sampling rounds, excluding outlier data. Median values: 1.4 µg As L^{-1}, 0.4 µg Cd L^{-1}, 0.4 µg Cr L^{-1}, 7.3 µg Cu L^{-1}, 1.3 µg Ni L^{-1}, 58.0 µg Zn L^{-1}, 16.3 µg Pb L^{-1}, 16.1 µg Mn L^{-1} and 127.2 µg Fe L^{-1}.

3.1.5. Stormwater composition

Based on STOWA Dutch stormwater database (STOWA, 2007), Duncan stormwater quality statistical review (1999), influent concentrations at UWB Spangen and a first roof water sample at Aartselaar, a bandwidth of the various HM concentrations in stormwater was composed (Table 3-4). Literature showed Cd, Cr, Cu, Ni, Pb and Zn as major HMs in stormwater runoff. Aforementioned and also from mentioned references, compositions of stormwater varied a lot throughout the year and for each study case.

Figure 3-5 Chemical mixture on mixing plate, emptied parallel to the volume of water in the storage tank (Versteeg, 2019).

Heavy metals

Table 3-4 Stormwater runoff concentrations of heavy metal species found in databases, literature and relevant sampling sites

Median Stormwater values [µg L^{-1}]	**Dutch Drinking water Standards VROM (2011)**	**Dutch Infiltration Standards VROM (2009)**	**STOWA Stormwater Commercial (Lemmen and Boogaard, 2007)**	**STOWA Stormwater Residential (Lemmen and Boogaard, 2007)**	**Duncan, 1999**		**UWB Spangen (Zuurbier and van Dooren, 2019)**	**Aquafin Campus in November 2018**
Description			Roads and roofs	Roads and roofs	High urban - roofs	High urban - roads	Separate sewer system	Roof water sample
Cd	5.0	0.4	0.8	0.15	0.67	2.5	1.0	2.0
Cr	50	2.0	7.5	1.1	n.d.	15.0	n.d.	2.6
Cu	2000	15	11.0	11.0	15.0	76.0	5.0	47.4
Ni	20	15	6.8	3.6	n.d.	45.0	5.0	6.9
Pb	10	15	8.0	6.0	37.5	343	5.0	61.9
Zn	3000	65	150.0	250.0	335	469.9	160	404.7

- STOWA Stormwater Database of the Netherlands of roads and roofs of commercial areas (Lemmen and Boogaard, 2007)
- STOWA Stormwater Database of the Netherlands of roads and roofs of residential areas (Lemmen and Boogaard, 2007)
- Stormwater database of highly urban areas (Duncan, 1999)
- 8 samples of influent water of BB.01 Spangen taken from September 2018 to April 2019
- Single sample value of Aquafin roof water at Aartselaar campus of November 2018

The high variety in HM concentrations depended on the location, land use and point of collection. A clear influent composition was not easily constructed. Zinc was the metal with highest median concentrations for each reference. At the UWB Spangen, Zn was detected in elevated concentrations in the influent (and even sometimes in the effluent). Aartselaar campus sample showed even a value of 404.7 µg L^{-1}, which was water collected from the roof. Cd was often the lowest of the major HM groups, followed by Cr and Ni. According to Duncan (1999), the elevated Pb concentrations were mostly seen at the road samples and related to vehicle related pollution sources.

Cu and Zn deserved particular attention by their higher presence and wide variation in urban environments. From the Göbel, Dierkes and Coldewey (2007) research it was found that the building material of the roof had a major influence on the HM loading. Runoff stormwater from zinc roofs showed an Zn concentration increased by a factor 16 compared to runoff from different roof material. Also copper roofs showed an increase of Cu concentration by a factor 17.

3.1.6. Synthetic stormwater feeds

Synthetic stormwater feeds were based on proportion found in section 3.1.5. Cr was excluded from this experiment. For the purpose of this research, the influent water was varied to high, medium, low or no concentrations of synthetic stormwater feed. Each of these concentrations, numbered with capital letters, was dosed in periods of three weeks (Table 3-6), twice a week. The high concentration feed was dosed less frequent to prevent overexposure and bed deterioration. By a variation of the concentrations, which is expected to occur also under real conditions, the effects of these variations were studied.

Table 3-5 HM concentrations dosed during research period of 21 weeks with 7 different cycles. Feeds were dosed twice a week in 8h cycles for low and med cycles, and a lower frequency for high concentration cycles.

Heavy Metal [µg L^{-1}]	**Composition**						
	A	**B**	**C**	**D**	**E**	**F**	**G**
Weeks	0-3	4-6	7-9	10-12	13-15	16-18	19-21
Frequency / week	2	2	2	2/3	2	2	2/3
Cadmium (Cd)	-	2	4	8	2	4	8
Copper (Cu)	-	25	50	100	25	50	100
Nickel (Ni)	-	15	30	60	15	30	60
Lead (Pb)	-	75	150	300	75	150	300
Zinc (Zn)	-	250	500	1000	250	500	1000

Table 3-6 Nutrient and iron and manganese concentrations dosed during research period of 21 weeks with 7 different cycles. Feeds were dosed twice a week for low and med cycles. For high concentration cycles, feeds were dosed twice in the third week after two weeks of no operation.

Macrochemistry [mg L^{-1}]	**Composition**						
	A	**B**	**C**	**D**	**E**	**F**	**G**
Weeks	0-3	4-6	7-9	10-12	13-15	16-18	19-21
Frequency / week	2	2	2	2/3	2	2	2/3
Ammonium (NH_4)	-	1.2	2.4	4.8	1.2	2.4	4.8
Nitrate (NO_3)	-	0.4	0.8	1.6	0.4	0.8	1.6
Phosphate (PO_4)	-	0.05	0.1	0.2	0.05	0.1	0.2
Iron (Fe)	-	-	-	-	0.25	0.5	1
Manganese (Mn)	-	-	-	-	0.125	0.25	0.5

With addition and mixing of HMs and nutrients to the batch volume, a synthetic stormwater feed was created. Table 3-7 shows the solid chemicals that were dosed, dissolved and mixed in a 1L glass jar.

Table 3-7 Properties of chemicals dosed to influent water, used to represent HM contamination in stormwater runoff.

Material	Formula	Molecular weight [g mol^{-1}]	Grade
Heavy metals			
Cadmium Nitrate - tetrahydrate > 99.99%	$Cd(NO_3)_2 \cdot 4H_2O$	308.9	Alfa Aesar
Copper (II) Sulfate >99.0%	$CuSO_4$	159.6	Analar Normapur
Lead (II) Nitrate >99.0%	$Pb(NO_3)_2$	331.2	Analar Normapur
Zinc Chloride	$ZnCl_2$	136.3	Emsure
Nickel Chloride hydrate >99.95%	$Cl_2Ni \cdot H_2O$	147.6	Puratronic
Other metals			
Iron (III) Chloride	$FeCl_3 \cdot nH_2O$	162.2	Sigma Aldrich
Manganese Chloride	$MnCl_2$	125.8	Merck
Macro nutrients			
Potassium dihydrogen phosphate	KH_2PO_4	136.0	Merck
Potassium nitrate	KNO_3	101.1	Sigma Aldrich
Ammonium chloride	NH_4Cl	53.5	Sigma Aldrich

Adjustments of the PH values were performed with nitric acid HNO_3 69% (Rotipuhran) to create an acidic solution and keep HMs in solution.

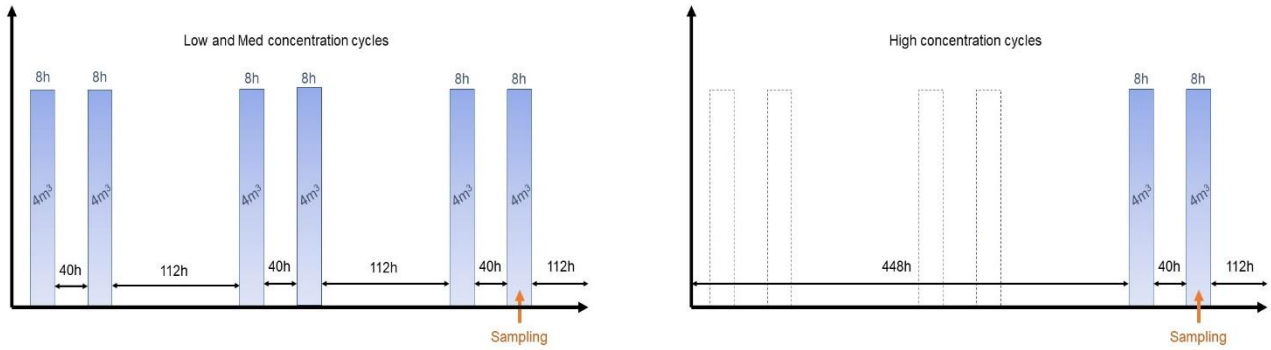

Figure 3-6 Operation schedule of the Aartselaar Demo by low and med concentration feeds (left) and by high concentration feed with two weeks of non-operation (right).

Operation

The system was operated twice per week, for 21 weeks (Table 3-8). A higher frequency was not possible due to limited personnel's capacity at location. In each cycle, the system was fed during 8 hours, a total water volume of $4m^3$, either tap water, runoff water or a mix of both. It created a 0.5 $m^3\ h^{-1}\ m^2$ flow, which was slightly higher than the emptying rate at Spangen pilot (section 2.3.3).

Each feed cycle represented one bed volume (BV), as $4m^3$ was dosed for $4m^3$ filter bed. Porosity was assumed 0.35, that resulted in approximately 3 times greater pore volume (PV) per run.

$$BV = \frac{Water\ volume\ passed\ [m^3]}{Filter\ bed\ volume\ [m^3]}, PV = \frac{BV}{0.35}$$

Table 3-8 Operational schedule for Aartselaar demo

Feeding schedule for Aartselaar Demo									
Date	Phase	Conc.	Feeding					Flow [m3/h]	Operation time [h]
			mon	tue	wed	thu	fri		
08-07	Build	-							
15-07									
22-07	A	x0		4m3		4m3		0.5	8
29-07				4m3		4m3		0.5	8
05-08				4m3		4m3		0.5	8
12-08	B	x0.5		4m3		4m3		0.5	8
19-08				4m3		4m3		0.5	8
26-08				4m3		4m3		0.5	8
02-09	C	x1		4m3		4m3		0.5	8
09-09				4m3		4m3		0.5	8
16-09				4m3		4m3		0.5	8
23-09	D	x2	dry	dry	dry	dry	dry		
30-09			dry	dry	dry	dry	dry		
07-10				4m3		4m3		0.5	8
14-10	E	x0.5		4m3		4m3		0.5	8
21-10				4m3		4m3		0.5	8
28-10				4m3		4m3		0.5	8
04-11	F	x1		4m3		4m3		0.5	8
11-11				4m3		4m3		0.5	8
18-11				4m3		4m3		0.5	8
25-11	G	x2	dry	dry	dry	dry	dry		
02-12			dry	dry	dry	dry	dry		
09-12				4m3		4m3		0.5	8

3.1.7. Water sampling and analyses

At the end of each feed cycle, water samples were collected (Figure 3-6). Influent samples were taken before water passing the biofilter, when the system was in operation at least 90 minutes and water ponded on top of the filter. Effluent samples were collected after passing the biofilter, in the drainage tank, at least 4 hours after start of the operation, to flush all standing water. Influent concentration (C_i) and effluent concentration (C_o) were used to determine the treatment efficiency of the BB. The metal removal efficiency (RE) was calculated with:

$$Removal\ Efficiency\ [\%] = \frac{C_i - C_o}{C_i} * 100$$

The influent was collected at the distributor before it was sprayed onto the bed. The effluent sample was collected in the drainage tank in the standing pipe, the first location to catch the water after passing the filter bed (Figure 3-7).

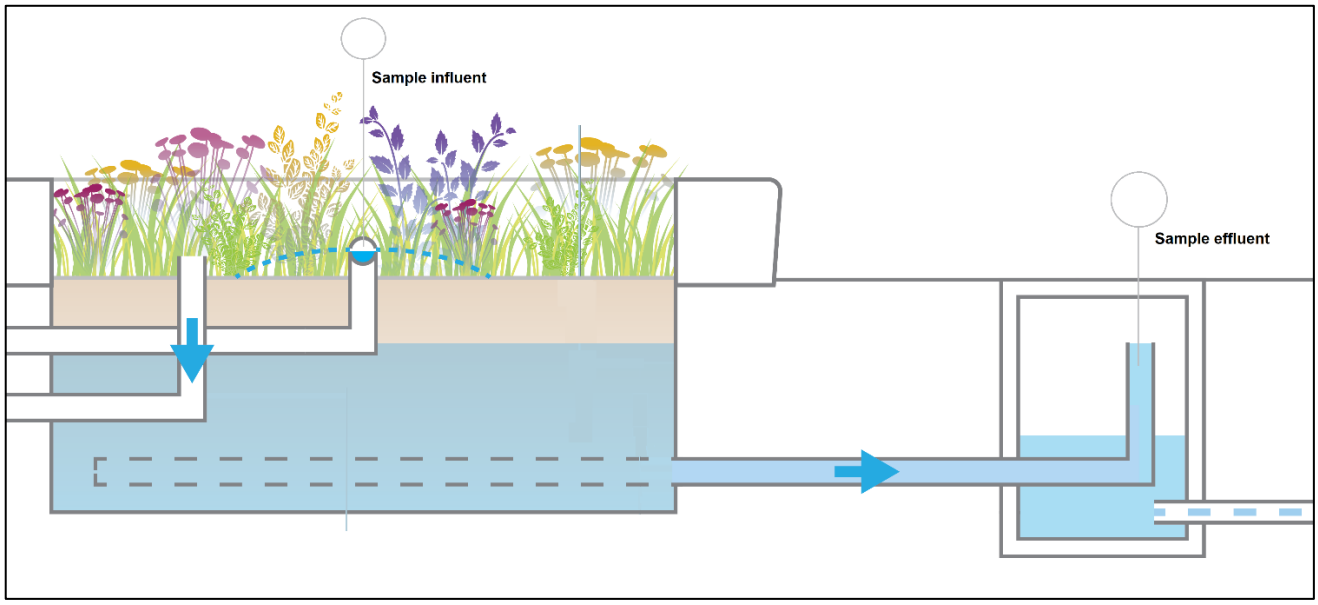

Figure 3-7 Sampling location influent and effluent at the Aartselaar demo.

To gain insight into hydrochemical gradients in the biofilter, water samples were taken from multiple depth levels by a so-called minifilter, Figure 3-8, based on van Breukelen and Griffioen (2004). Two minifilters were placed at time of installation of the biofilter. Water at 5, 10, 20, 40, 55 and 70 cm depth in the filter bed was abstracted by this minifilter. At each of these depth a horizontally placed syringe, filled with aquarium mineral wool and packed with filter sock, abstracted water at this layer. The syringes were connected to an electricity tube (13Ømm) with 3D-print connection parts. The electricity tube was a total length of 100 cm, placed at 80 cm depth from top layer. Rauclair-E PVC tubes (Ø3mm) were used to abstract water via the syringes.

A 50 mL syringe was used on the tubes to collect the water. The first and second collections were discarded to avoid analysing standing water in the syringe and tube. The third dose was 0.45 µm filtered and collected in 15 mL bottles. For sampling round E both filtered and unfiltered samples were collected, to identify fractioning of dissolved and particulate forms of HM. Filtered represented the dissolved fraction, unfiltered the total content.

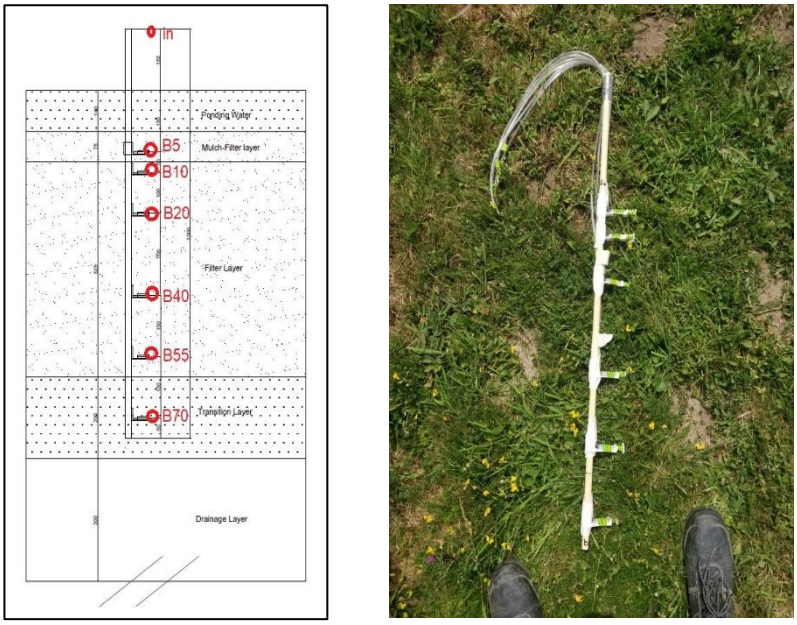

Figure 3-8 Left: Cross section of minifilter in filter bed. Right: construction of a minifilter.

In-situ measurements

The water was tested at each sampling point in-situ on pH, DO, EC and temperature (T). DO was measured by a Greisinger G1610 DO-meter hand device. pH was measured by a Greisinger GMH5500 pH-meter hand device. EC and T were measured by a GMH3400 EC-meter hand device. Each meter was calibrated before a sampling round. DO was calibrated in saturated air, EC was calibrated with 1413 µS cm^{-1} conductivity solution, pH was calibrated with pH 4, pH 7 and pH 10 buffer solutions.

Ion chromatography

A main matrix of the water composition was determined by Ion Chromatography (IC)(Methrohm 818 anion system and Methrohm 883 cation system) in the WaterLab of the TU Delft. Samples of the field demo were filtered by 0.45 µm and stored at 4 °C. Samples were tested on cations (K, Na, NH_4, Ca and Mg) and anions (F, Cl, Br, NO_2, NO_3, PO_4 and SO_4). Calibration curves were fitted on standards of 100, 50, 10 and 1 ppm.

Inductively coupled plasma mass spectrometer

The HMs in the water matrix were measured by the Inductively Coupled Plasma Mass Spectrometer (ICP-MS)(Analytik Jena PlasmaQuant MS) at the WaterLab of the TU Delft. Samples of the field demo were filtered by 0.45 µm, acidified with 1:100 69% HNO_3 (Rotipuhran) and stored at 4 °C. Samples were tested on Fe, Mn, Zn, Pb, Cu, Cd, Ni, As. Samples were diluted by purified water to stay under the 100 µg L^{-1} (ppm) upper detection limit.

External water quality data

Additional water quality analysis on the biofilter samples was sourced out to the lab of Aquafin to analyse on DOC, microbiology and suspended solids. Samples of the influent and effluent were collected in 1L glass jars, stored and collected the day after. Analysis followed within the same week.

3.2. SORPTION MODEL: PHREEQC

To better understand the adsorption processes in the BB and effect of chemical and physical conditions, PHREEQC (version 3) was used to simulate the adsorption by various media. For this method the WATEQ4F.dat (Ball and Nordstrom, 1991) was used as main database.

Surface Complexation in PHREEQC incorporates the Dzombak and Morel (1990) DDL models that explicitly calculates the protonation of hydroxyl groups and aqueous species (Borkovec and Westall, 1983), and also non-electrostatic surface-complexation model (Nair, Karimzadeh and Merkel, 2014). SCMs were elaborated earlier at section 2.5.3.

Intermezzo: introducing PHREEQC

PHREEQC (Parkhurst and Appelo, 1999), or pH-REdox-EQuilibrium, is a software package to model (geo)hydrological chemistry in aqueous solutions, developed by the United States Geological Survey. The computer program is written in C++, with version 3 as the latest version. Notepad++ was used for writing, editing and running PHREEQC3, and freely distributed online (Appelo, 2017).

PHREEQC calculates reactions and equilibria based on a database on thermodynamic reactions and data, based on mass balance law and electrical charge balance. Reactions are registered in databases, which have thermodynamic data/stability constants (log K_{ad} values) from researches of the last 30 years. Databases consist of aqueous speciation, surface speciation, ion-exchange relationships and rate reactions in geochemistry. By the relationships and conditions, simulations of chemical processes and physical transport are assessed.

The simplest form of a reaction in PHREEQC can be conceptualised by a well-mixed solution with reactants in a beaker which then will react and calculated to equilibrium. SOLUTION keyword determines the chemical composition of the water. SURFACE specifies a sorbent material and reacts with a SOLUTION composition.

3.2.1. Sorption modelling approach

Sorption modelling was performed with batch and one dimensional transport simulations. The sorption model was first calibrated to Genç-Fuhrman *et al.* (2007) data in batch mode, by adjusting the characteristics of sorption sites and stability constants for complexation reactions. Then, this calibrated model was assessed in batch mode on pH effect, ionic strength effect and influent proportions of HMs, for both quartz sand and IOCS.
Furthermore, the model was used for one dimensional modelling, to represent sorption processes of water transport in filter media. Roof water at Aartselaar, representing an average inflow composition to the BB at the field experiment, was simulated with different pH conditions and different media configurations. Also, synthetic feeds to the BB (section 3.1) were simulated to show the effects of various concentrations and to compare and validate results to the field experiment. Lastly, the transport sorption model was assessed on the operational biofilter at Spangen pilot, to define the current state and predict when infiltration standards cannot be met.

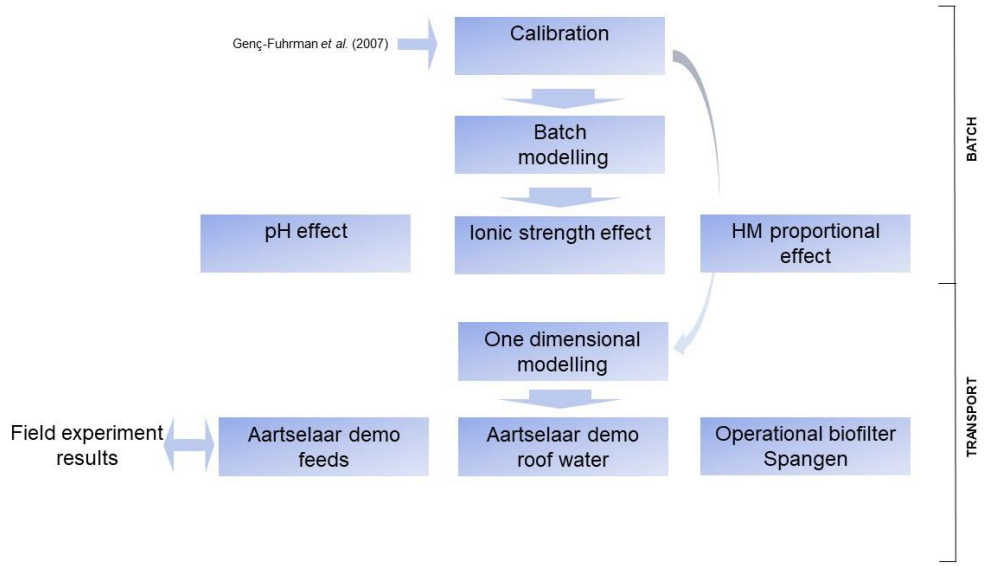

Figure 3-9 Sorption modelling approach with batch adsorption and one-dimensional simulations

3.2.2. Model calibration

Research on HM sorption by similar adsorbent material was carried out by Genç-Fuhrman *et al.* (2007) with batch adsorption tests. Regular quartz sand and IOCS were tested on 8 low to high concentration ranges of dissolved HMs. Results of Genç-Fuhrman experiments (Appendix IV) were used to calibrate the PHREEQC model on HM adsorption and used as the first basis of a representative model.

Table 3-9 shows the averaged molar ratio of HMs of the 8 solutions in the Genç-Fuhrman experiment. This averaged molar ratio was used to calibrate the model along associated data on Cd, Cu, Ni and Zn adsorption. All batch tests were recalculated to a 1 litre, so 20 g L^{-1} of sorbent media concentration (1:50 solid-to-liquid ratio). From this standard solution the concentrations were linearly expanded to model increasing concentrations in stormwater pollution. Ionic strength of 0.01 M NaCl and a buffer of 0.003 M $NaHCO_3$ were kept constant each time, pH was set to 6.5, temperature to 25 °C and a 20 g L^{-1} mass to solution ratio, according to the Genç-Fuhrman experiment. pH deviations were fixed by addition of HCl and NaOH 10 mmoles.

One-site model vs. Two-site model

SCMs can be traditionally used with weak and strong sorption sites (two-site modelling), to differentiate between low and high concentrations. On the contrary, one single type of site modelling can be applied as in Merdy *et al.* study (2009). Both adsorption methods were simulated and compared to fit the Genç-Fuhrman adsorption data for best fit.

Hydrous ferric oxide (active sites) on sorbent media

Because the Genç-Fuhrman *et al.* research (2007) did not report on the iron content of any sorbent, an iron content ratio per sorbent had to be determined first. From the results of initial leaching and product data sheet of IOCS some ranges of functional HFO content were derived and expressed in m% of iron content. Iron oxides were found in iron coated sand (AquamineralsBV, 2019) and quartz sand. It was recalculated by molar mass to an equivalent in HFO which was used in SCM. The active sites of the surface were defined by amount of sites, specific surface area and total mass of HFOs. Initially, all surface sites were in uncharged form. Conversions from HFO to Fe and vice versa were assumed with $Fe_2O_3 \cdot H_2O$ formula (89 g HFO mol^{-1} Fe). The specific surface area of amorphous HFO was assumed at 600 m^2 g^{-1}, recommended by studies of Davis and Leckie (1978). Ranges of iron content were used to determine the best settings to the Genç-Fuhrman data (Appendix IV) on a q_e-C_e plot.

Stability constant

Stability constants of surface complexation reaction in WATEQ4F database were adjusted if adsorption curves would consistently over- or underestimate. By the raise or decrease of log K coefficient for specific HMs, adsorption equilibria were shifted towards left- or right-hand side.

Table 3-9 Averaged ratio of HMs in Genç-Fuhrman (2007) research representing a typical stormwater solution.

Parameter	Unit	Genç-Fuhrman (2007) solution	
		lowest	highest
As	[µg L^{-1}]	0.22	7.26
Cd	[µg L^{-1}]	0.2	6.62
Cr	[µg L^{-1}]	0.63	20.8
Cu	[µg L^{-1}]	0.87	28.7
Ni	[µg L^{-1}]	1.1	36.3
Zn	[µg L^{-1}]	7.0	231
Na	[mmol]	13.0	13.0
Cl	[mmol]	10.0	10.0
pH	[-]	6.5	6.5
T	[°C]	25	25

3.2.3. Batch sorption modelling

Batch adsorption simulations were performed with the median values of roof water composition at the Aartselaar demo (Table 3-10). Composition was composed from the roof samples (Figure 3-4) and used make a first identification of the effects of the physical and chemical conditions.

Table 3-10 Median values of the Aartselaar roof water.

Parameter	Unit	Roof water composition Aartselaar (section 3.1.4)
As	[µg L^{-1}]	1.44
Cd	[µg L^{-1}]	0.383
Cr	[µg L^{-1}]	0.375
Cu	[µg L^{-1}]	7.25
Ni	[µg L^{-1}]	1.31
Zn	[µg L^{-1}]	58.0
Na	[mmol]	13.0
Cl	[mmol]	10.0
pH	[-]	6.5
T	[°C]	25

pH effect and ionic strength effect

To assess the performance of sorbent media under various concentrations, the adsorption capacity at equilibrium (q_e) was described by the amount of adsorbate taken up from the bulk solution by the sorbent per unit mass. This was determined at equilibrium with constant temperature and pressure:

$$q_e = \frac{adsorbed\ fraction\ [\mu g]}{adsorbent\ mass\ [g]}$$

Adsorption capacity was observed over a varying pH value from 4.0 to 12.0 on the Aartselaar water composition (Table 3-9) in a batch simulation, for both quartz sand and IOCS.
Percentage of moles adsorbed for each sorbate and the relation between pH. Also to assess the performance of pH values, the partition coefficient (K_d) for Cd, Cu, Ni and Zn were defined for both quartz sand and IOCS.

Ionic strength was simulated by changing the electrolyte, Na and Cl concentration, to 0.01M, 0.1M and 1.0M of the influent. Ionic strength effect was compared to the pH effect. Only quartz sand was simulated.

Copper and zinc ratio

The initial molar ratio of both Zn and Cu in stormwater were amplified and reduced, to analyse a variation in proportion. In section 3.1.5, Cu and Zn were determined HMs in stormwater with a wide bandwidth. Amplification factors of 0.5 and 5.0 were modelled and reviewed for both metals, while rest of the composition was kept constant. For this simulation only the effect on IOCS adsorption capacity was simulated.

Table 3-11 Settings of physical properties of sorbent media in batch model 20 g L^{-}

Batch model settings			
SURFACE #IOCS		**SURFACE #Quartz sand**	
HFO_w	9.67 *10^{-3}	HFO_w	1.00 *10^{-3}
Specific surface area	600	Specific surface area	600
Mass HFO	4.30	Mass HFO	0.45

3.2.4. Adsorption transport model

Intermezzo: introducing PHREEQC Transport

PHREEQC uses a mixing-cell approach to simulate advection. A one dimensional flow is represented by a sequence of cells. Within each cell is a volume of water and sorbent media. The solid to liquid ratio should be defined, as well as the influent composition SOLUTION 0. Water shifts from one cell to the next, mixes and aqueous and solid equilibrium are determined. By surface complexation reactions in the WATEQ4F database, equilibrium for all constituents is determined with mass and charge balances. This is repeated for each cell (Figure 3-10).

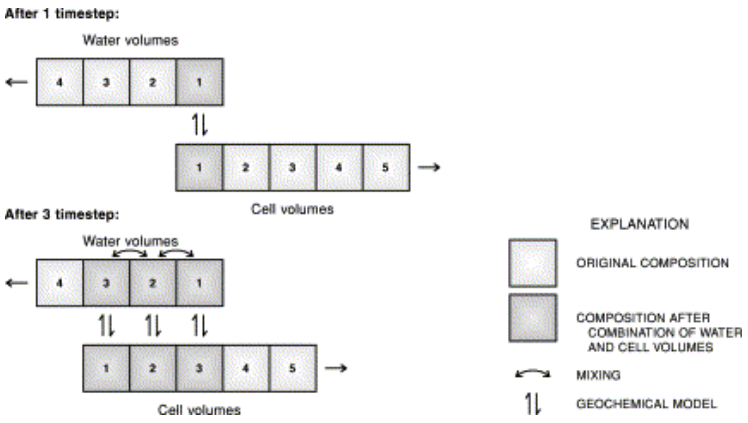

Figure 3-10 Transport and chemical processes concept for mixing cells. (Appelo and Postma, 1993)

Column settings

A one-dimensional column was simulated by 5 cells for the top 0.6 m depth, representing the filter layer of the BB. 5 cells were chosen to limit to a manageable computational capacity. Each cell represented 0.12 m depth of filter layer.
Porosity of the BB was set 0.35, so a volume of 0.65 was media. Quartz sand specific weight was 2650 g L^{-1}, resulting in 4921 g L^{-1}. This corresponded with a 1:0.2 solid-to-liquid mass ratio.
The average flow at Aartselaar was 0.5 m^3 h^{-1} m^{-2}. For simplicity of the one dimensional system this was set to 0.6 m h^{-1} linear water velocity (area of 8.4 m^2 at 30 cm filter layer). A full cycle (top to bottom) was 3600 s and 720 s per cell. Heterogeneity of the soil was not taken in account for the simulation. Dispersion was set to 0, diffusion was set to default value of 3.0 * 10^{-9} m^2 s^{-1}, flux boundary conditions (Cauchy boundary conditions) were set (Table 3-12).
1 BV was reached after 8 hours of operations.

Table 3-12 Hydraulic and physical properties of the transport model

Property	Value
Length column	0.6 m
Cells	5
Lengths	0.12 m
Porosity	0.35
Specific weight quartz sand	2.65 kg L^{-1}
Solid per liquid	4,921 g L^{-1}
Solid to liquid mass ratio	1:0.2
Dispersivities	0
Diffusion	0.3 * 10^{-9}
Shifts	4032
Time step	720
Flow direction	Forward
Boundary conditions	Flux Flux

Table 3-13 Settings of physical properties of sorbent media biofilter transport model.

Biofilter model settings			
SURFACE #IOCS		**SURFACE #Quartz sand**	
HFO_w	2.39	HFO_w	0.248
Specific surface area	600	Specific surface area	600
Mass HFO	1063	Mass HFO	110.2

Retardation and breakthrough

Aartselaar roof water composition (Table 3-10Table 3-9) was repetitively simulated as influent and transported through a one dimensional column, representing the biofilter under continuous feeding and expected influent composition.
Two columns with different media configuration were simulated, of which configuration A contained solely quartz sand and configuration B contained IOCS in the first cell and quartz sand in the remaining 4 cells (Figure 3-11). Different configuration were simulated to show the different adsorption capacities, and to show the effect of IOCS addition to the top layer at Spangen pilot and Aartselaar demo.
Cd, Cu, Ni and Zn effluent concentrations were simulated over the number of bed volumes. pH varied between 6.5 and 8.0 and fixed by HCl or NaOH. This range was similar to pH values measured at the Aartselaar demo and generated breakthrough curves.
For the same simulations, a cross section of the biofilter was created for BV values of 1,400 and 800, to show adsorption processes within the filter at start of operation and to show operational development. Dissolved Cd, Cu, Ni and Zn concentrations at equilibrium were modelled in each cell.

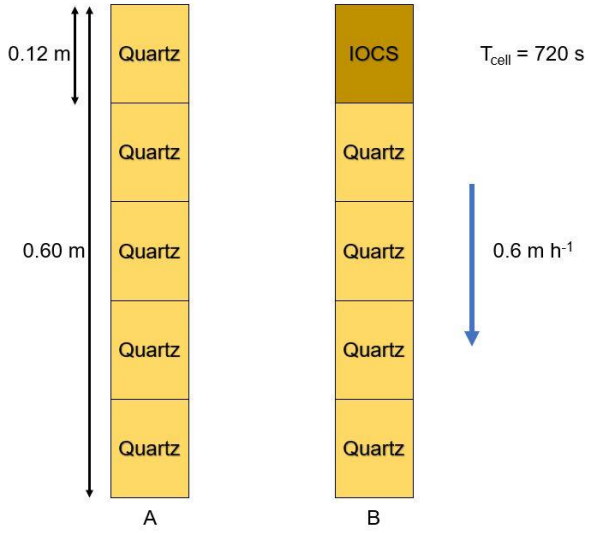

Figure 3-11 Configuration A includes only quartz sand as filter media, configuration B includes one cell with IOCS media as the top 12 cm layer.

Also, simulations with synthetic feeds were simulated with an only quartz sand filter, representing the field experiment at the Aartselaar demo. Influent compositions of feeds were based on HM compositions and operational schedule from Table 3-5 and Table 3-8 respectively. Feed A was simulated with tap water composition. pH conditions were set to 7.5, average value of all feeds. Each feed was dosed 6 BVs for low and med concentrations and 2 BV for high concentrations. After a feed, concentrations of solution in each were saved for the next feed. Rainwater, that directly falls onto the biofilter, was not included in the simulation.
Cross section concentrations of Cd, Cu, Ni and Zn in the biofilter were created at end of each cycle. Simulations cross sections were compared to the field experiment samples from the minifilter.

4. RESULTS AND DISCUSSION

4.1. FIELD EXPERIMENT RESULTS

Results of the Bluebloqs demo in Aartselaar are elaborated on pH and EC values and HM concentrations at the influent and effluent and from six depth levels in the BB. A complete list on the results is listed in the Appendix III. Not all results are discussed in this section, only what is relevant within the scope of this research. The results can be relevant for other water treatment mechanisms of the BB and of interest within the wider scope of the Bluebloqs Circular Water Systems.

4.1.1. In-situ measurements

pH

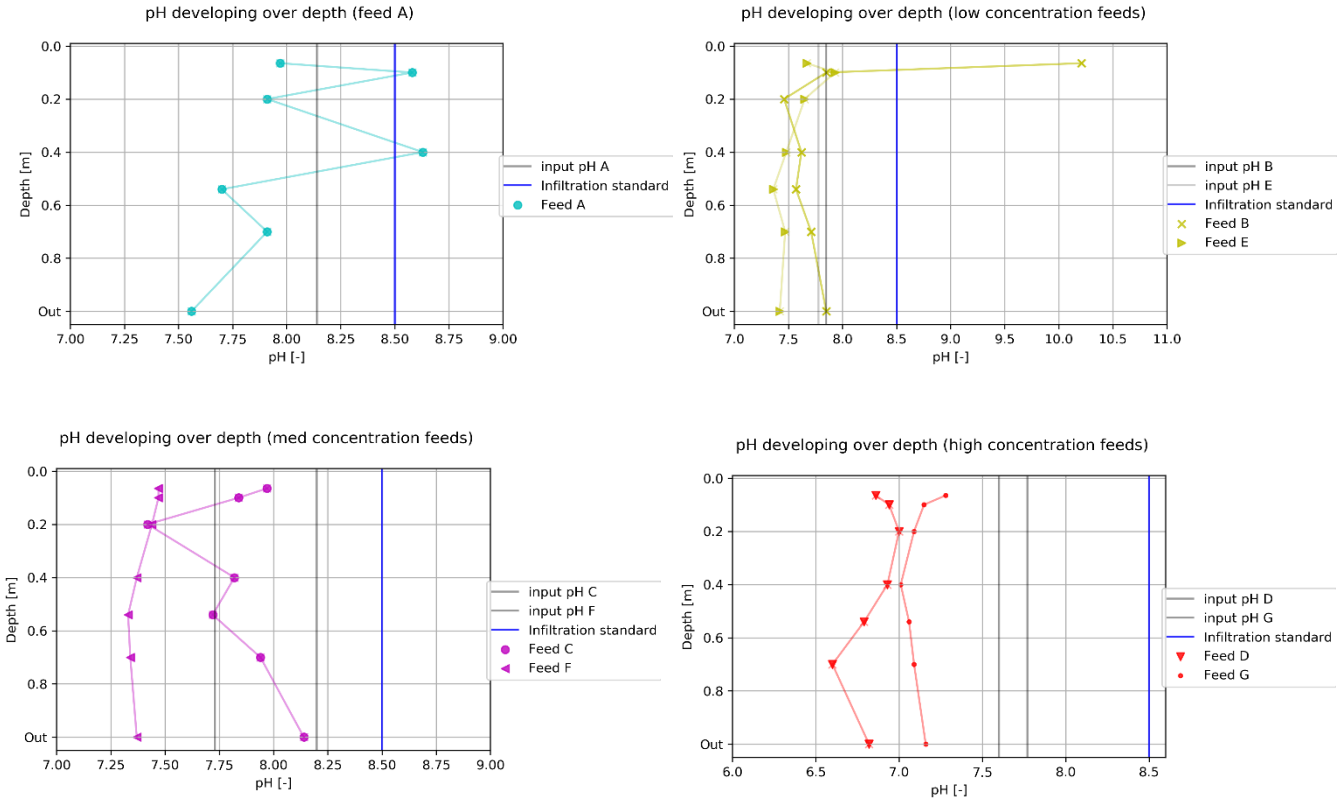

Figure 4-1 pH development over filter depth of Aartselaar demo for first cycle A (upper left), low (upper right), med (lower left) and high (lower right) pollutant dosage.

During cycle A chemical reactions of a newly installed filter increased the pH of the water samples at multiple depths, to a pH of 8. At 10 cm and 40 cm depth the pH even exceeded the infiltration limit of pH 8.5, with respectively 8.58 and 8.63. However, the median value of tap water was at pH 7.8. Explanation of this higher value remained unanswered, pH values at a later sampling period were lower.

Low dosing concentrations during cycle B and cycle E showed pH values in a range of 7.5 to 7.7, besides an ambiguous number at 5 cm during cycle B. This value was neglected. Medium concentration during cycle C and cycle F did not show clear development over depth and remained at a value 7.5 to 8.0. This was similar to the median pH value of tap water (section 3.1.4).

For the high concentration feeds with cycle D and cycle G the pH at the top layer started at 7.6 and 7.8 and decreased to a value fluctuating around 7.0 in the filter. For cycle D the deeper layer decreased to a value of 6.6. This was the lowest pH in comparison to the other cycles. Abovementioned, low pH values negatively affect the adsorption of HMs.

Overall, the pH values varied between 6.5 and 8.0 in the biofilter, which falls within the Dutch infiltration standards. Due to acidity of the soil, (quartz sand had a pH range of 5-8 as stated in section 3.1.3), the influent pH was lowered in the BB, but remained fairly constant over depth.

Electrical conductivity

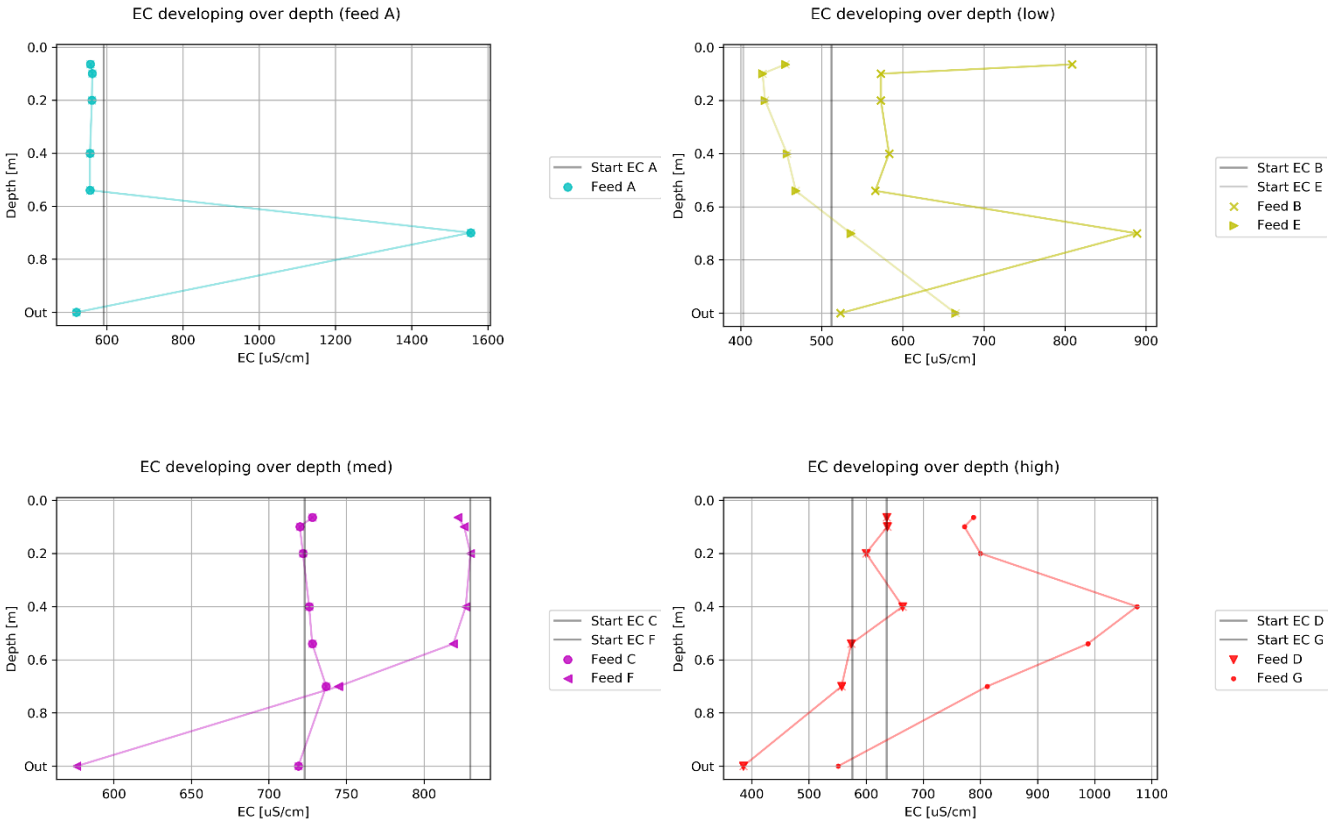

Figure 4-2 EC distribution of first cycle A (upper left), low (upper right), med (lower left) and high (lower right) concentration cycles.

EC values remained fairly constant over the first 55 cm of the BB. For measurement at 70 cm depth, EC values increased for feed A and B. Probably indirect measuring, by abstraction of water via the syringes and then placing it in cups and put the electrode to the sample, or presence of organic contaminations did not result in reliable data. Another explanation could be the effect of suction of particles stuck in the syringe or tube, during abstraction. Lowest EC values were detected during cycle E, when a low feed was dosed. However, cycle B, when also low feed was dosed, showed relatively high EC values.

EC values greatly decreased for feed A, B,D,F and G from 70 cm to the outlet. For overall treatment capacity of the BB, the transition and drainage layer cannot be excluded.

Dissolved oxygen

Dissolved oxygen was measured during cycle A and B, but delivered unusable values. By extracting water from any depth, values fluctuated up and down (from 0.7 mg L^{-1} to 8.1 mg L^{-1}) . It was recommended to log DO at fixed sampling locations.

4.1.2. Heavy metals removal efficiencies

During cycle A, a total of 10 BVs passed, no metals were synthetically added to the influent water. HM detected in the influent were collected mostly by rainwater collected of the roof. Cu, Pb, Ni and Zn showed elevated concentrations in the influent water. Comparing this to the roof water concentration of Aartselaar, Ni was relatively high. Table 4-1 shows the results of cycle A. For most of the metals, the effluent concentration was higher than the influent concentrations. This automatically resulted in negative RE values for As, Cu, Pb, Zn, Mo, Fe and Mn. For Cd, Pb and Ni the effluent concentration exceeded the infiltration standards. Elevated values were most probably related to the wash of the new material placed in the biofilter, which ended up in the effluent, seen in 3.1.2. At the moment of sampling, about 10.3 BV passed by operation of the system.

Table 4-1 Influent, effluent and removal efficiencies for Cycle A (no dose). Red values exceeded the Dutch infiltration standards.

Cycle A			
	in	out	RE [%]
Cadmium Cd (µg L^{-1})	0.05	1.06	-2190.5
Copper Cu (µg L^{-1})	9.6	13.9	-45.3
Lead Pb (µg L^{-1})	2.7	41.2	-1409.1
Nickel Ni (µg L^{-1})	89.4	53.5	40.2
Zinc Zn (µg L^{-1})	7.8	22.7	-192.0
Molybdenum Mo (µg L^{-1})	3.0	3.0	-1.3
Iron Fe (mg L^{-1})	0.05	0.10	-94.05
Manganese Mn (mg L^{-1})	0.00	0.08	-100

Specifics	
pH	7.56 – 8.58
T [°C]	22.4 – 27.7
BV	10.3

During cycle B (low) Cd, Cu, Pb were sufficiently removed by the BB, with RE's of 97.5%, 86.9%, 98.5% respectively. This was in a phase when 10 to 22 BVs passed onto the filter bed. Raised influent concentrations contributed to these high numbers. Ni was at a fairly lower RE with 69.0% with an effluent concentration of 4.6 µg L^{-1}, but still complied with the infiltration standard. Also Cu showed a relatively high effluent concentration of 5.6 µg L^{-1}. Zn was detected at 9.1 µg L^{-1}, for which the infiltration standard lies at 65 µg L^{-1} and still has some leeway. As, Fe and Mn were not synthetically dosed and showed a negative RE. A possible explanation could be leaching from fresh filter media or construction elements. All effluent concentrations complied with the Dutch infiltration standards and greatly improved compared to cycle A.

Table 4-2 Influent, effluent and removal efficiencies for Cycle B (low). No effluent values exceeded the Dutch infiltration standard.

Cycle B			
HM	in	out	RE [%]
Arsenic As (µg L^{-1})	0.9	1.1	-19.2
Cadmium Cd (µg L^{-1})	3.1	0.1	97.5
Copper Cu (µg L^{-1})	43.0	5.6	86.9
Lead Pb (µg L^{-1})	12.6	0.2	98.5
Nickel Ni (µg L^{-1})	14.9	4.6	69.0
Zinc Zn (µg L^{-1})	353	9.1	97.4
Iron Fe (mg L^{-1})	0.03	0.05	-48.6
Manganese Mn (mg L^{-1})	0.02	0.13	-546.0

Specifics	
pH	7.46 – 10.21
T [°C]	21.5 – 25.6
BV	22

During cycle C (med*)* the influent concentrations rose above the aimed for concentrations, probably due to sampling spiked water, without adequate mixing (Table 4-3). This phase was from 22 to 31 BVs. Synthetically dosed HMs had a high RE value, due to the high influent concentrations. Ni effluent concentration was still at 6.3 µg L^{-1} and the

highest of all HMs. Ni showed lowest stability constant for adsorption, compared to other HMs, which could explain a relatively higher fraction remained dissolved. Cu, Cd and Zn showed values 3.65, 0.14 and 6.02 µg L^{-1} respectively. The higher RE values compared to Ni were for the same motivation. All HMs do still comply with the infiltration standards.

Table 4-3 Influent, effluent and removal efficiencies for Cycle C (med). No effluent values exceeded the Dutch infiltration standards.

Cycle C			
	in	out	RE [%]
Arsenic As (µg L^{-1})	0.49	0.74	-50.6
Cadmium Cd (µg L^{-1})	27.0	0.14	99.5
Copper Cu (µg L^{-1})	157.1	3.65	97.7
Lead Pb (µg L^{-1})	11.42	0.09	99.2
Nickel Ni (µg L^{-1})	101.4	6.30	93.8
Zinc Zn (µg L^{-1})	2596.5	6.02	99.8
Molybdenum Mo (µg L^{-1})	3.56	3.04	14.6
Iron Fe (mg L^{-1})	0.17	0.18	-5.32
Manganese Mn (mg L^{-1})	0.00	0.02	-100

Specifics	
pH	7.42 – 8.2
T [°C]	18.1 – 20.2
BV	31.4

During cycle D (high) still all effluent values complied with the infiltration standards, although Ni was still relatively high compared to the standard (Table 4-4). This phase was from 31 to 57 BVs, there was a lot of rainfall in this period. Zn also increased a bit in the effluent compared to the two cycles prior. Influent concentrations were lower than the aimed for concentration. The pH value was relatively low for this cycle, varying between 6.6 and 7.0 over filter depth. Lower adsorption was expected and more HMs remained dissolved. However, a lower overall treatment did not stand out.

Table 4-4 Influent, effluent and removal efficiencies for Cycle D (high). No effluent values exceeded the Dutch infiltration standard.

Cycle D			
	in	out	RE [%]
Arsenic As (µg L^{-1})	0.4771	0.62	-30.0
Cadmium Cd (µg L^{-1})	6.64	0.23	96.6
Copper Cu (µg L^{-1})	66.06	2.81	95.7
Lead Pb (µg L^{-1})	52.93	0.17	99.7
Nickel Ni (µg L^{-1})	27.23	5.78	78.8
Zinc Zn (µg L^{-1})	735.1	16.52	97.8
Molybdenum Mo (µg L^{-1})	2.36	1.13	52.1
Iron Fe (mg L^{-1})	0.08	0.09	-10.94
Manganese Mn (mg L^{-1})	0.00	0.12	-4491.13

Specifics	
pH	6.6 – 7.6
T [°C]	14.0 – 17.5
BV	57.3

For Cycle E (low) the effluent value for Zn rose compared to prior cycles, while the synthetic dose was lower for this feed (Table 4-5). This was from 57 to 74 BVs. Also Ni and Cd were relatively high values in the effluent with 5.47 and 0.49 µg L^{-1} compared to earlier data. Cd even exceeded the infiltration standard. Saturation of the filter media could have an effect that more HMs remain in solution. Since pH conditions were not lower than other cycles, it was expected this caused a lower adsorption capacity of the BB.

Table 4-5 Influent, effluent and removal efficiencies for Cycle E (Low). Red values exceeded the Dutch infiltration standard.

Cycle E			
	in	out	RE [%]
Arsenic As (µg L^{-1})	0.5	0.51	-2.0
Cadmium Cd (µg L^{-1})	1.98	0.49	75.3
Copper Cu (µg L^{-1})	21.54	3.47	83.9
Lead Pb (µg L^{-1})	40.73	0.4	99.0
Nickel Ni (µg L^{-1})	9.47	5.47	42.2
Zinc Zn (µg L^{-1})	201.82	32.71	83.8
Molybdenum Mo (µg L^{-1})	2.36	2.57	-8.9
Iron Fe (mg L^{-1})	171.15	13.11	92.34
Manganese Mn (mg L^{-1})	100.51	4.59	95.43

Specifics	
pH	7.36 – 7.93
T [°C]	11.8 – 12.8
BV	74.4

For Cycle F (med*)*, 74 to 83 BVs passed, results showed the effluent concentrations of Cd and Zn exceeded the infiltration standards (Table 4-6). Again, elevated results were observed while pH conditions were not lower than prior feeds. As the highest concentrations were found during the last feed, and the conditions were not different for the other high dose feed C, it was found this was due to saturation of filter media. The Spangen pilot also showed elevated Zn values in the effluent over time. Cd was not reported as such at Spangen, but then the lower detection limit was only at 1 µg L^{-1}, so this was unclear at that location. Zn effluent concentrations showed increasing values after each cycle and for this cycle were greater than the influent concentrations.

Table 4-6 Influent, effluent and removal efficiencies for Cycle F (med). Red values exceeded the Dutch infiltration standard.

Cycle F			
	in	out	RE [%]
Arsenic As (µg L^{-1})	0.23	0.44	-91.30
Cadmium Cd (µg L^{-1})	10.57	0.49	95.36
Copper Cu (µg L^{-1})	28.81	4.25	85.25
Lead Pb (µg L^{-1})	16.07	0.24	98.51
Nickel Ni (µg L^{-1})	48.40	5.51	88.62
Zinc Zn (µg L^{-1})	13.85	88.78	-541.01
Molybdenum Mo (µg L^{-1})	3.54	2.74	22.60
Iron Fe (mg L^{-1})	0.15	0.08	45.30
Manganese Mn (mg L^{-1})	0.61	0.01	98.54

Specifics	
pH	7.33 – 7.73
T [°C]	6.3 – 9.3
BV	82.6

Cycle G (high*)* showed, just like the prior cycle, elevated Zn concentrations in the effluent, although slightly lower at 49.34 µg L^{-1} and did not exceed the infiltration standard. 82 to 94 BVs passed the BB. Cd continued to exceed the infiltration standard with 0.54 µg L^{-1} concentration. Influent concentration of Ni was extremely high and considered as an error during the analysis. pH value was between 7.0 and 7.8, not lower than earlier feeds. Higher effluent concentrations were considered by saturation of sites, which was also confirmed and elaborated by cross sectional concentrations of cycle G in 4.1.3.

Table 4-7 Influent, effluent and removal efficiencies for Cycle G (high). Red values exceeded the Dutch infiltration standard.

Cycle G			
	in	out	RE [%]
Arsenic As (µg L^{-1})	0.25	0.48	-91.6
Cadmium Cd (µg L^{-1})	3.29	0.54	83.6
Copper Cu (µg L^{-1})	33.02	3.25	90.1
Lead Pb (µg L^{-1})	56.70	0.21	99.6
Nickel Ni (µg L^{-1})	417.20	3.42	99.2
Zinc Zn (µg L^{-1})	13.93	49.34	-254.3
Molybdenum Mo (µg L^{-1})	3.37	2.29	32.1
Iron Fe (mg L^{-1})	0.19	0.01	95.4
Manganese Mn (mg L^{-1})	0.11	0.02	84.9

Specifics	
pH	7.01 – 7.77
T [°C]	6.5 – 8.1
BV	95.4

Overall, Cd was the HM hardest to comply with the infiltration standard during all the cycles and could not comply from cycle E onwards. This was after 74 BVs. Cd has a strict standard with 0.4 µg L^{-1}, so could be easily exceeded. After Ni, Cd was the HM with lowest affinity to quartz sand in the WATEQ4F database. Cu adsorption improved after the first two cycles. Cu is associated complexation formation with organic material, which could have been a higher fraction in the start-up phase. Pb seemed to be consistently removed each cycle, since Pb was associated with a relatively large particle bound fraction and filtered out, also discussed later in 4.1.4.

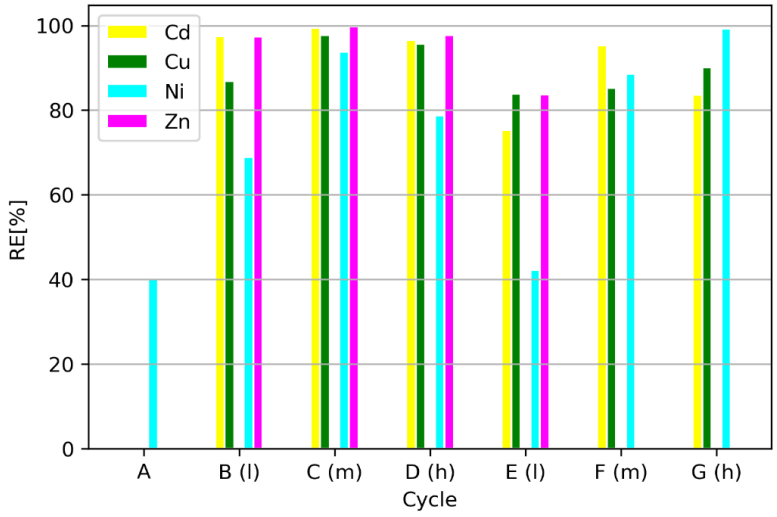

Figure 4-3 RE of Cd, Cu, Ni and Zn at Aartselaar demo, grouped for low(l), med(m) and high(h) concentrations.

Figure 4-3 shows the removal efficiencies of Cd, Cu, Ni and Zn for all cycles. Ni showed the lowest RE value for four out of six cycles with synthetic dose. Since influent values were inconsistent, it cannot be clearly stated that Ni was the HM with the lowest affinity by these results. Copper showed RE values above 80% for all cycles. Cadmium RE values were above 75%. Zinc however, showed high RE values for cycles B-D, but cycle F and G showed negative RE values, since a higher effluent concentration than the influent concentration was measured. Also reported from the Spangen demo results, elevated Zn levels ended up in the effluent water.

Figure 4-4 shows the effluent concentrations of Cd, Cu, Ni and Zn at the Aartselaar demo for all feeds. Clearly, the Cd, Cu and Ni concentrations in the first cycle were elevated, compared the cycles that followed. Cycle B-D showed sufficient removal for each HM. Higher effluent concentrations developed for cycles E-G, where Cd consistently exceeded the infiltration standard.

Since the biofilter was operated with elevated HM concentrations, a saturation of sorption sites of filter media could be an explanation for lower adsorption of Cd and Zn. The duration of this research was however too short to draw a conclusion if the trend of elevated effluent concentrations would continue or further develop to even higher effluent concentrations. Also, the influent concentrations ranged from low to high concentrations and introduce another variable.

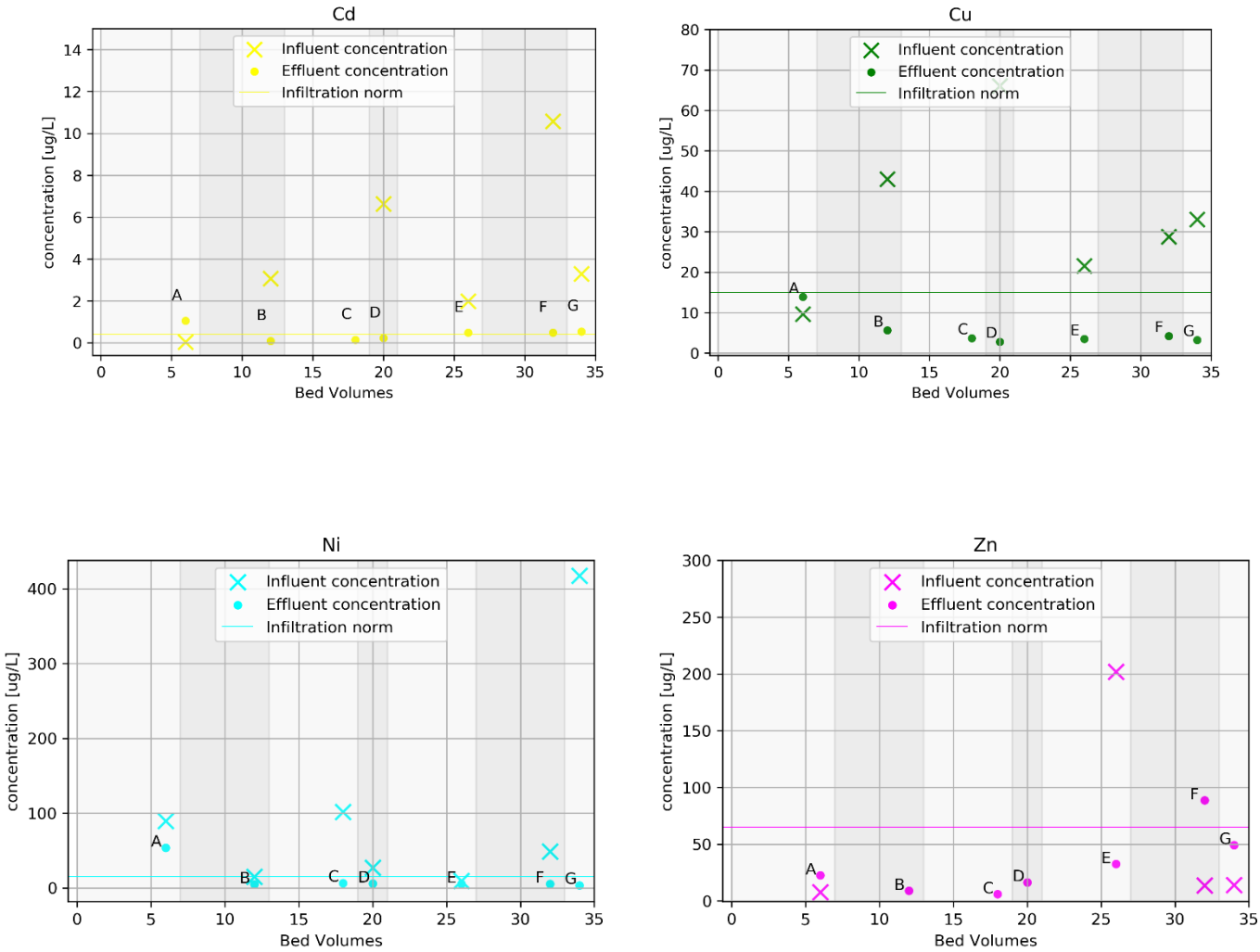

Figure 4-4 Influent and effluent concentrations of Cd, Cu, Ni and Zn for the Aartselaar Demo for each cycle. Solid lines represent HM specific infiltration standard and grey bars represent the theoretical number BVs per cycle.

4.1.3. Cross sectional heavy metal concentrations

From the overall removal of HMs, it was hard to draw conclusions on the performance of adsorption. Effluent concentrations seemed to increase in the latest measuring campaigns. Since pH values were not lower for later feeds, elevated concentrations were due to saturation of the filter media. By more HMs adsorbed, less sorption sites were available.

Cadmium

Figure 4-5 shows Cd concentrations in the biofilter for all synthetic feeds. Data showed that average concentrations of cycle B and C were below the infiltration standards. For each of the following cycles, it showed that range of concentrations increased. By more bed volumes passing the biofilter, the BB became more saturated. That also explained the higher effluent concentrations ('Out') of Cd. A clear gradual trend of concentration decrease over depth was not observed.

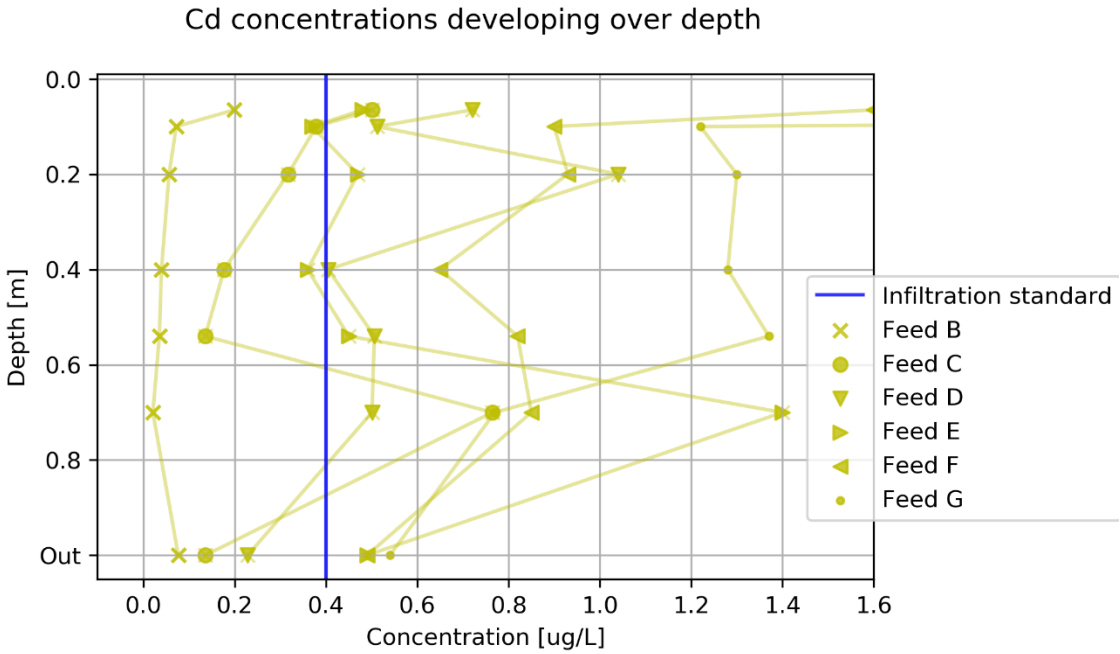

Figure 4-5 Cadmium concentrations at Aartselaar demo for various feeds over biofilter depth.

Copper

Figure 4-6 shows the Cu concentration trend over biofilter depth. It showed a clear trend, with decreasing values towards the lower depth of the BB, that shows an adsorption pattern similar to the adsorption modelling trends (later mentioned in section 0). Concentration funnelled to ranges between 3.1 and 7.4 µg L^{-1} at 70 cm depth. On average, concentrations decreased by a 0.065 µg L^{-1} cm^{-1} rate, but with a greater decrease for the first feeds. Whether high or low concentrations were dosed, seemed to have no effect on the adsorption efficiency.

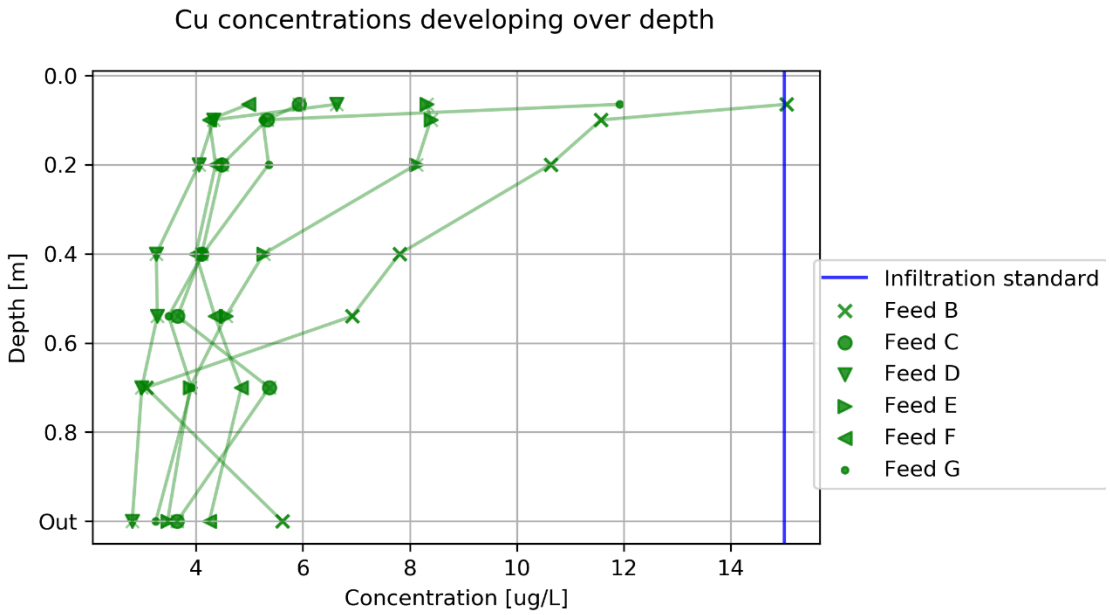

Figure 4-6 Copper concentrations at Aartselaar demo for various feeds over biofilter depth.

Nickel

Figure 4-7 shows the development of Ni in the BB. Feed A showed irregular results, with remarkably high concentrations (some are not even within the x-axis range, see Appendix III). The following cycles showed values in lower range, merely below the infiltration of 15 µg L^{-1}, so it was assumed that the first cycle enhanced a mobilization of Ni initially present on filter media. Whether low or high concentrations were dosed seemed to have no effect on the removal efficiency.

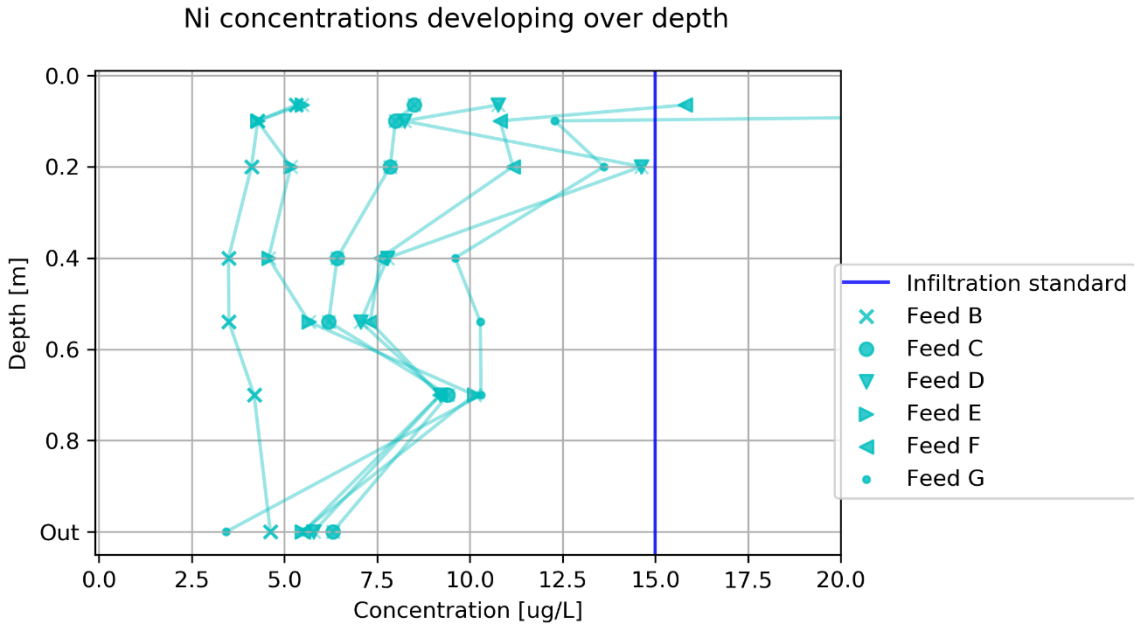

Figure 4-7 Nickel concentrations at Aartselaar demo for various feeds over biofilter depth.

Zinc

Figure 4-8 shows the Zn concentrations over depth in biofilter. The first three cycles showed low concentration in a 0-9 µg L^{-1} range. The next cycles shifted towards higher concentrations. Feed D-F showed higher concentrations at the top level of the filter layer, but decreased to values below the infiltration standard. Feed G showed that the high initial concentration was lowered over depth, but could not decrease below the infiltration standard. It showed that saturation of sorption sites could have an effect on the removal of Zn. Also, highest Zn values in the filter were detected during high synthetic feeds D and G.

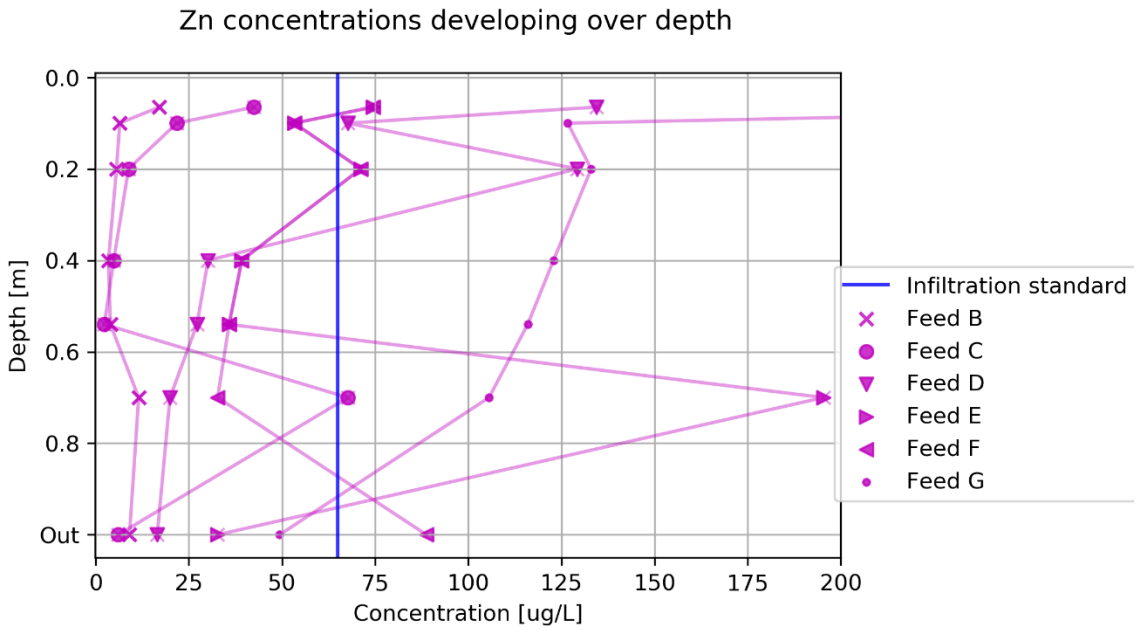

Figure 4-8 Zinc concentration at Aartselaar demo for various feeds over biofilter depth.

Overall, the highest removal was often in the top 5 cm of the filter bed for all HMs. This could be by adsorption, but it was also believed to be removed by precipitation and mechanical filtration. HM fractions can be particle bound and filtered out. It was hard to distinguish what fraction was removed by adsorption, or by other treatment processes.

Since there was a newly build system, the BB did not develop to steady state conditions during the field experiment. The demo was built in summer and research was conducted from summer to winter. Growth of roots by vegetation, die-off of vegetation, settlement of filter media were all processes during the research, introducing unknown conditions. Also, growth of active microbiology could range from several weeks to several months, depending on conditions. Since temperature decreased, it could be likely that no mature biology and there was no ‘bio’ in biofilter.

Since the biofilter was only 4m^3, it was subject to short-circuiting flow along the edges, with a sloped base. For smaller systems, short-circuiting resulted in different contact time, allowing for water passing along the edges. Also, influence of drainage pipes, overflow pipes, the minifilter and foundation elements could introduce short-circuiting flow in sand filters.

4.1.4. Particle bound fractions of heavy metals

Both filtered and unfiltered samples were collected from cycle E. Unfiltered samples showed a clearly elevated concentration of iron and lead compared to 0.45 µm filtered samples. For influent water, 67% of lead fraction was dissolved and 68% for iron. This indicated that a significant part of Fe was attached to particles, as beforementioned. For the effluent the fraction decreased to 33% and 19% respectively, while the absolute concentrations decreased. Manganese dissolved fraction decreased from 100% in influent to 22% in effluent.

Table 4-8 Filtered and unfiltered sampling results of Cycle E on influent and effluent concentrations of HMs and iron and manganese

Cycle E	Influent			Effluent		
	filtered	unfiltered	fraction dissolved	filtered	unfiltered	fraction dissolved
Arsenic As (µg L^{-1})	0.5	0.64	78%	0.51	0.62	82%
Cadmium Cd (µg L^{-1})	1.98	2.02	98%	0.49	0.52	94%
Copper Cu (µg L^{-1})	21.54	23.84	90%	3.47	3.88	89%
Lead Pb (µg L^{-1})	40.73	60.54	67%	0.4	1.23	33%
Nickel Ni (µg L^{-1})	9.47	9.4	100%	5.47	5.64	97%
Zinc Zn (µg L^{-1})	201.82	207.3	97%	32.71	37.92	86%
Iron Fe (µg L^{-1})	171.15	253.1	68%	13.11	67.37	19%
Manganese Mn (µg L^{-1})	100.51	100.08	100%	4.59	20.59	22%

Also Pb showed a 33% of the influent was particle bound, and 22% of As. Compared to Boogaard *et al.* (2005), Figure 2-3, more HMs from Aartselaar roof water were dissolved fraction, but also showed for Pb and Fe higher fraction particle bound than other HMs. Presence of sediments was expected to be lower for roof water than street runoff, resulting in a higher dissolved fraction for this research.

4.1.5. Initial leaching of metals from filter media

Since Cycle A showed ambiguous high concentrations in the effluent water, various fresh and used filter media were tested on initially present components. Fresh sands, IOCS and used sands from the operation Spangen biofilter were evaluated. Concentrations of metals from each washed sorbent are depicted in Table 4-9. With 50 mL eluent, the total leached mass HM per mass sorbent was determined.

Table 4-9 HM eluent concentrations from 5 types of filter media.

	Mn	Ni	Zn	Pb	Cu	Cd	As	Fe		
	µg L^{-1}	µg L^{-1}	µg L^{-1}	µg L^{-1}	µg L^{-1}	µg L^{-1}	µg L^{-1}	µg L^{-1}	µg g^{-1}	m%
Fresh filter sand FFS	15.6	3.32	9.67	13.8	3.48	0.00	1.26	7810	78.1	0.008
Used filter sand UFS	39.6	2.37	28.7	14.0	5.02	0.00	5.02	14800	148	0.015
Fresh coarser sand FCS	6.85	1.12	17.9	5.56	2.60	0.00	0.60	3980	39.8	0.004
Used coarser sand UCS	2380.0	1.76	65.8	38.78	2.45	0.02	1.26	24200	242	0.024
IOCS	n.d.	14.4	23.3	36.5	1.25	0.63	16.1	375000	3750	0.375

Results showed that used quartz sands leach metals, as well as the fresh sands, which must have been present initially in its composition. Concentration of Mn, Zn, Pb, Cu, As and Fe were higher in eluents of UFS than FFS. The higher concentrations of used sand was related to the adsorption of HM pollutants during the six months of operation. The higher Ni concentrations in FFS compared to UFS remained unclear. Concentration of Mn, Ni, Zn, Pb, As, Cd and Fe were also higher in eluents of UCS. Cu showed the opposite effect.

Noteworthy were the relatively high concentrations of Fe, Mn, Pb and Zn in the UCS. It was expected that higher Zn concentrations would be detected in UFS, due to higher specific surface area than coarse particles, however

opposite occurred. Also, elevated Zn effluent concentrations were observed for the Spangen pilot. A possible explanation could be that Zn acid leached from the filter layer to mobilized to the transition layer of the BB.

Fe of the coated sand was above detection limit of the ICP-MS and was extrapolated from calibration curve, which made the value less accurate. According to the data sheet of Fe-coated sand (Aquaminerals) 13-14 m% Fe was defined. However, only 0.375 m% Fe leached in the leaching test.

Only 0.375 m% of iron of the IOCS was determined and fairly low compared to the material data sheet, which stated a 13.5 m% of iron. This major difference in iron content showed that the initial leaching test results were not reliable to use. However, it indicated that from fresh filter sand and fresh coarse sand HMs were initially present.

The high concentration in the effluent during Cycle A could be related to the initial presence of HMs on fresh filter media.

4.2. SORPTION MODEL RESULTS

Each of the simulation used the “Fix_H+” in an EQUILIBRIUM_PHASES data block to adjust the pH. NaOH or HCl (depends on pH) was added or removed for each solution equilibrium.

4.2.1. Heavy metal speciation

Of four main HMs of interest pH-distributions are presented in Figure 4-9 for a Aartselaar roof water (Table 3-9). All HMs were mainly present in cationic species. The most important species for Cd were Cd^{2+} and $CdCl^{+}$ for lower pH values and complicated arrangement for pH values > 9.0, where anionic $Cd(CO_3)_2^{2-}$ dominated. $CuHCO^{+}$ was mainly present for pH < 6.5 and for pH > 8 $Cu(OH)_2$ was dominant. Cationic Ni^{2+} and $NiHCO_3^{+}$ were the most important species for pH < 6.0 and $Ni(CO_3)_2^{2-}$ was for pH > 9.0. Zn^{2+} and $ZnHCO_3^{+}$ dominated for pH < 7.0, while non-charged $ZnCO_3$ in the pH-range 7.0-9.5 was dominant and above pH 9.5 $Zn(OH_2)_2$ was mainly present.

Speciation of all HMs showed that at lower pH values mostly free cations and positively charged complexes, while for higher pH-values rather the non-charged and anionic aqueous complexes were formed.

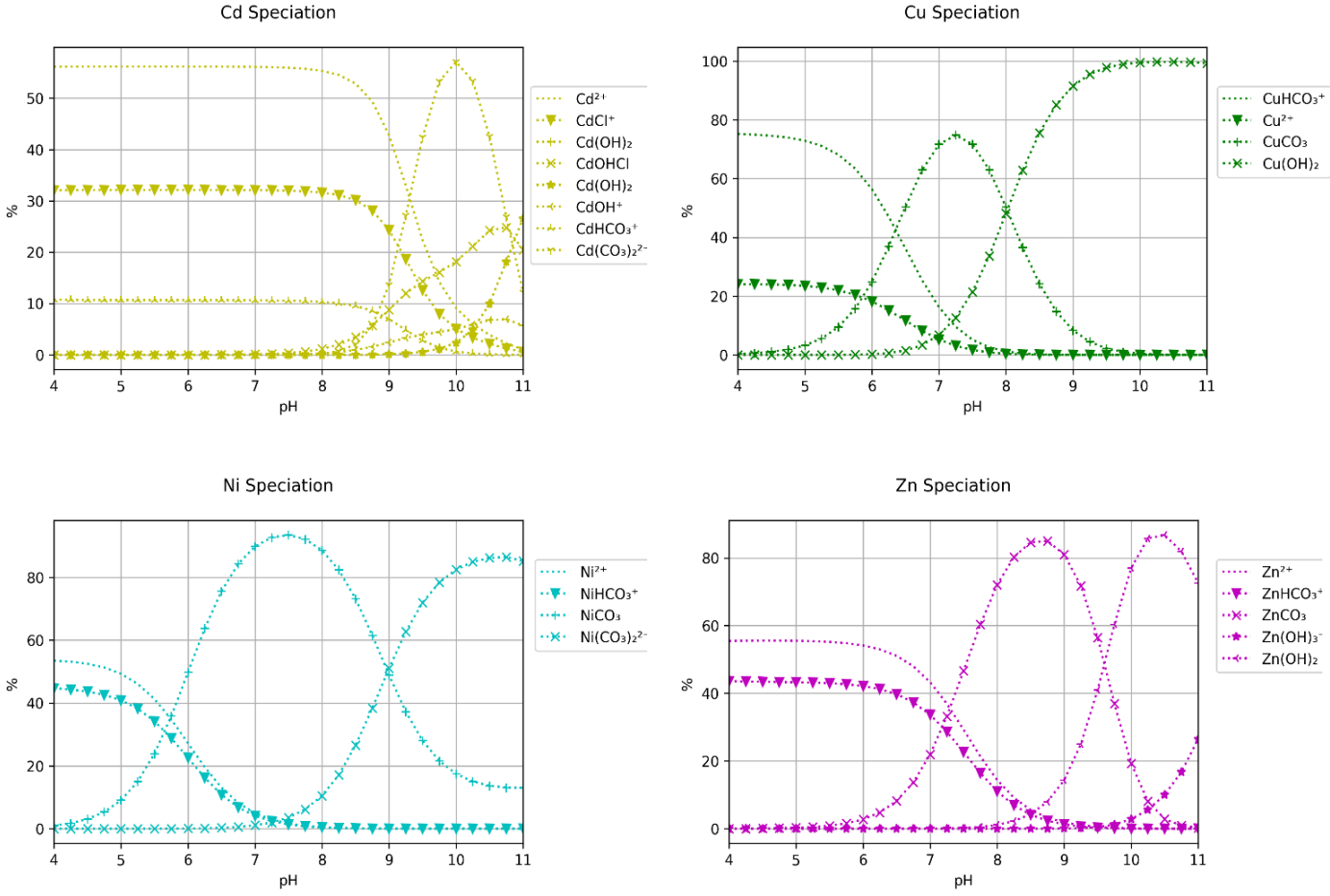

Figure 4-9 - Speciation of Cd, Cu, Ni and Zn in typical stormwater with 0.01M NaCl ionic strength and 0.003 M $NaHCO_3$

4.2.2. Sorption model calibration

One binding site model vs. two binding sites model

Figure 4-10 shows the comparison between a one type of site two sites model of four main HMs, compared to the Genç-Fuhrman data. Two type of sites (weak or strong) (dashed line) showed an overestimation for low concentrations relative to the experiment data. At higher concentrations most of the HMs adsorbed to weak binding sites. A typical S-curve established when weak sites started to predominate the strong sites in the system. This also caused preferential adsorption of Cu over other HMs. This is elaborated in Figure 4-11.

By using only weak sites (solid line, Figure 4-10) the adsorption lines showed better results, especially for the lower concentrations. The number of weak site moles remained the same, the number of strong site moles was set to zero. The S-curve in the q_e-C_e plot was not present in the one type of site model and showed a line resembling linear adsorption for low concentrations. For higher initial/equilibrium concentrations, the difference between the two models was negligible.

HM concentration were often found in low concentration range of 0-10 µg L^{-1} (Figure 3-4 and Table 3-4), with the exception of zinc, but this was also not above 1 mg L^{-1}. Since the one site model showed the best results for the lowest concentration, this was used for the following simulations.

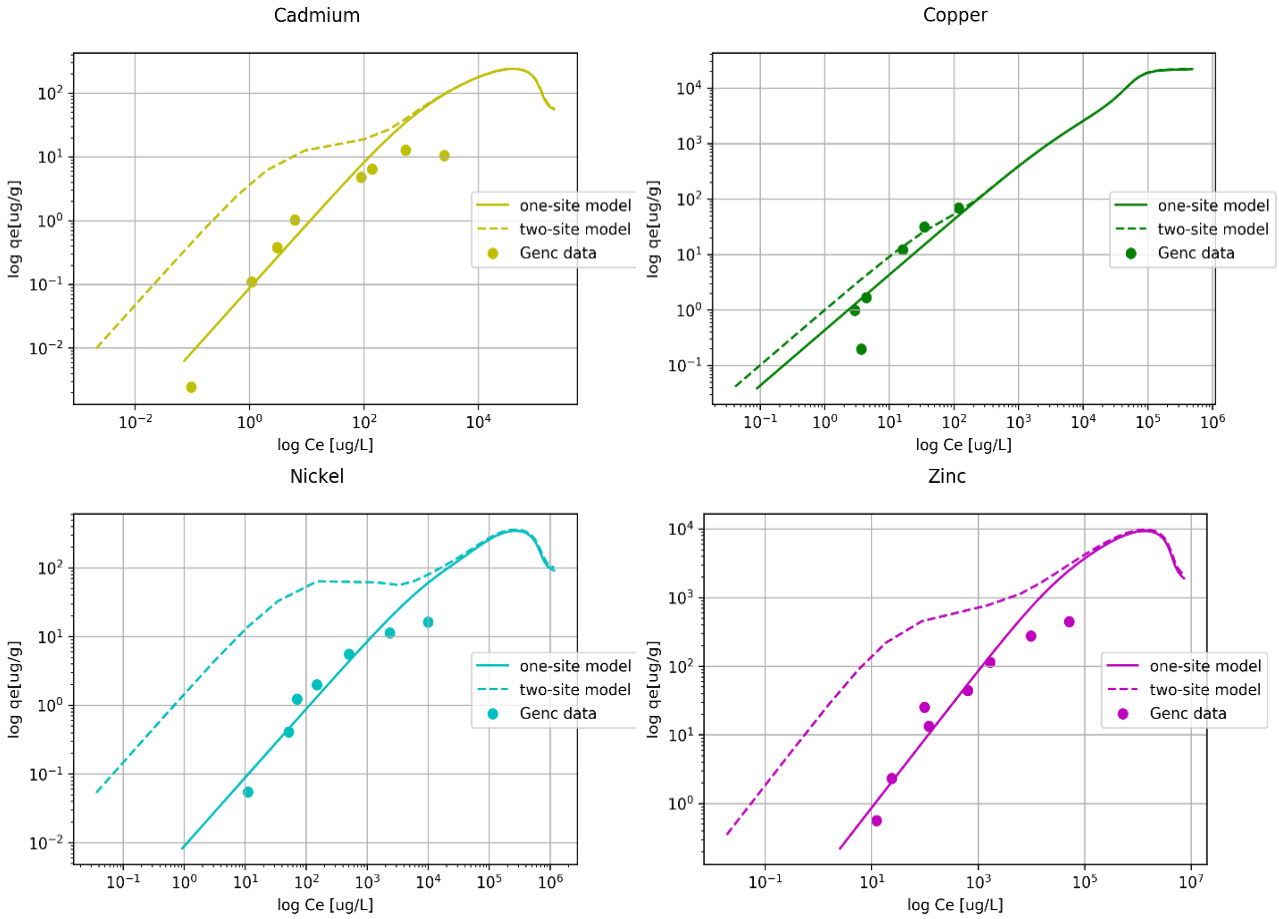

Figure 4-10 Comparison of one-site model and two binding site model to the Genç-Fuhrman (2007) data for adsorption on IOCS.

Strong sorption site saturation

By increasing the initial concentrations of the solutions, a saturation of the strong binding sites occurred. This explained the observed S-curve in the two binding site model.
At low initial concentrations each HM in solution was adsorbed to a strong binding site. For these conditions, strong

site adsorption was dominant over weak binding site adsorption. However, when initial concentrations of HM increased, saturation of strong binding sites occurred. Figure 4-11 shows the effect of saturation of strong binding sites. Competition for adsorption binding sites occurred in higher concentration, when the number of HM moles exceeded the number of moles of strong binding sites. This competition for strong binding sites resulted in a preferred adsorption and had the effect that HMs with lowest affinity remained as solutes. This preferred adsorption occurred in Cu>Zn>Cd=Ni order, since the figure showed that Cu adsorbed increased at high concentrations, while Zn, Cd and Ni decreased.
The adsorption model showed this for the two binding site model, when strong sites were merely covered by Cu ions and relatively more Ni, Cd and Zn species remained in solution, which created the abovementioned S-curve. Notice that the same occurred for even higher concentrations towards weak binding site saturation and the total adsorption of Ni, Cd and Zn even decreased.

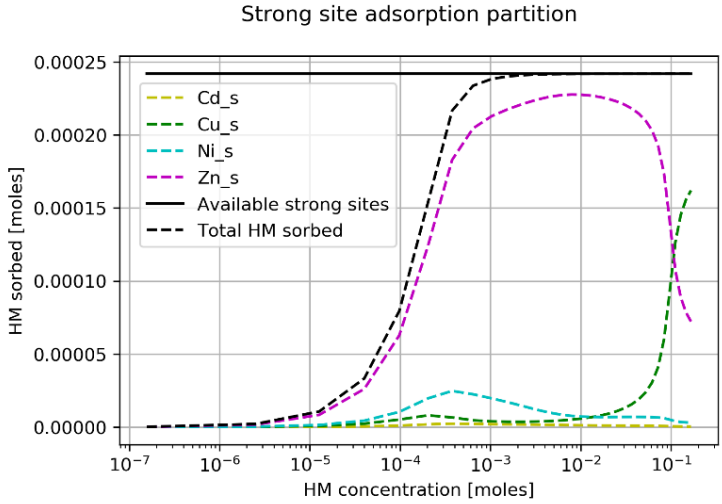

Figure 4-11 Adsorption on the strong sites of the filter media with initial HM ratios as in Genç-Fuhrman typical stormwater with a mixture of HMs. It depicts the preferred adsorption for Cu when increasing HM concentrations and saturation of the sites occurs.

Iron content (active sites) effect on adsorption

The 13.5 m% iron content of IOCS showed the best fit for Cu, Ni and Zn, depicted in Figure 4-12. 13.5 m% was the iron content reported in the product data sheet. The q_e-C_e curves fitted the Genç-Fuhrman data for Cu, Ni and Zn. A 20 m% iron content overestimated the adsorption of Ni and Zn, while for Cu it showed a reasonable fit. The latter showed no significant difference with 13.5 m% iron content. Also 0.375 m% was simulated, to show the results of the initial leaching test (section 4.1.5), which was clearly an underestimation for IOCS adsorption capacity for all four HMs.

Cd sorption was underestimated by all three iron contents, even for higher assumed iron content of 20 m%. Since 13.5m% showed to have an appropriate fit for all the other three HMs, this was chosen as appropriate. The log K value for Cd (weak) site adsorption was set from -2.91 to -2.0 to also fit 13.5 m% iron content with the Genç-Fuhrman IOCS sorption data. This adjustment rose the adsorption curve vertically upwards.

Table 4-10 Surface complexation parameters applied for model calibration to Genç-Fuhrman et al., (2007) in a 20 g L^{-1} batch simulation

Figure	Model	Media	m%	Strong sites [mol]	Weak sites [mol]	Specific surface area [m2 g^{-1}]	Mass [g]
Figure 4-10	One site model	IOCS	13.5	0	$9.67 * 10^{-3}$	600	4.30
	Two sites model			$2.42 * 10^{-4}$			
Figure 4-12	One site model	IOCS	0.375	0	$1.00 * 10^{-3}$	600	0.12
			13.5		$9.67 * 10^{-3}$		4.30
			20.0		$1.79 * 10^{-3}$		6.37
Figure 4-13	One site model	Quartz sand	0.33 (Fe_2O_3)	0	$1.65 * 10^{-4}$	600	0.07
			1.4		$1.00 * 10^{-3}$		0.45
			2.5		$1.79 * 10^{-3}$		0.80

Ratio
20 g L^{-1}

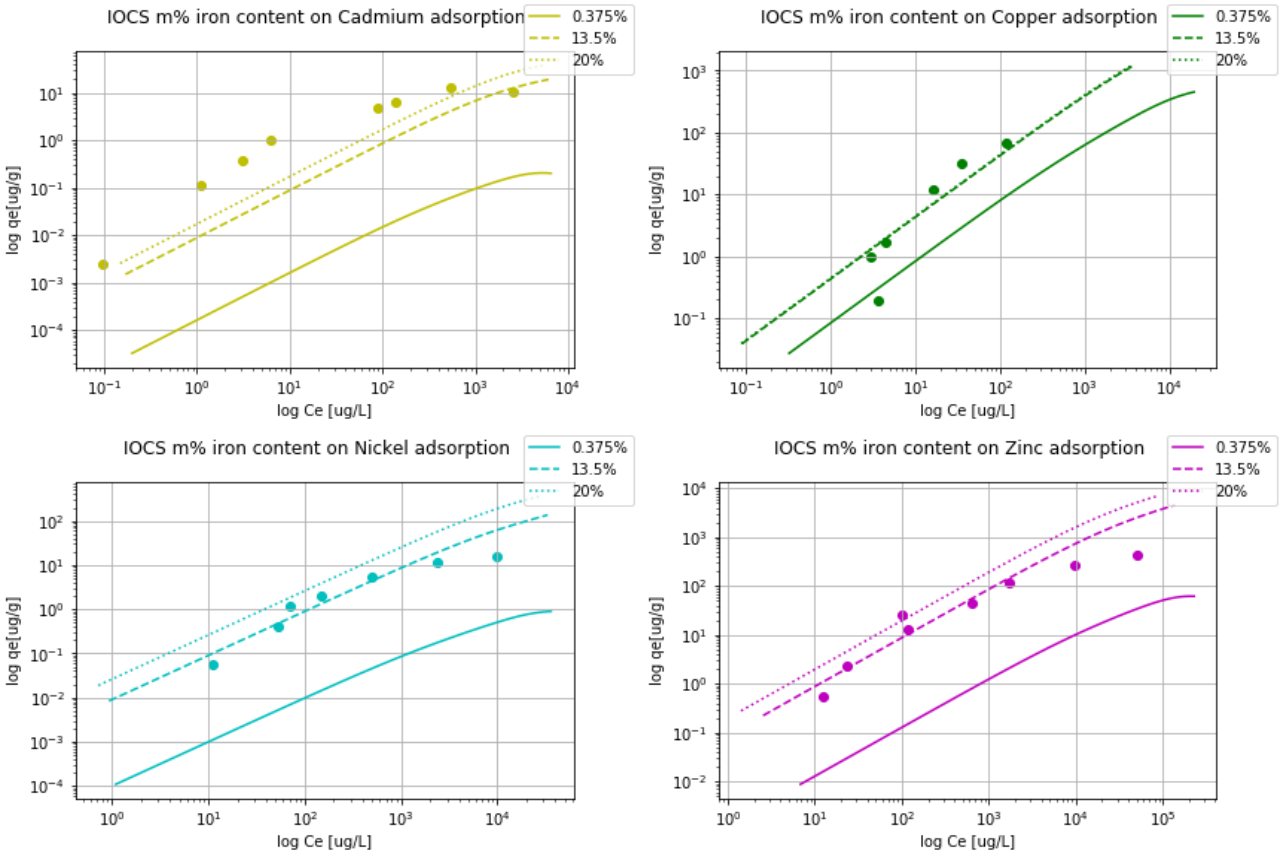

Figure 4-12 Adsorption on IOCS by tweaking the iron content to fit the Genç-Fuhrman (2007) data on batch adsorption for Cd, Cu, Ni and Zn.

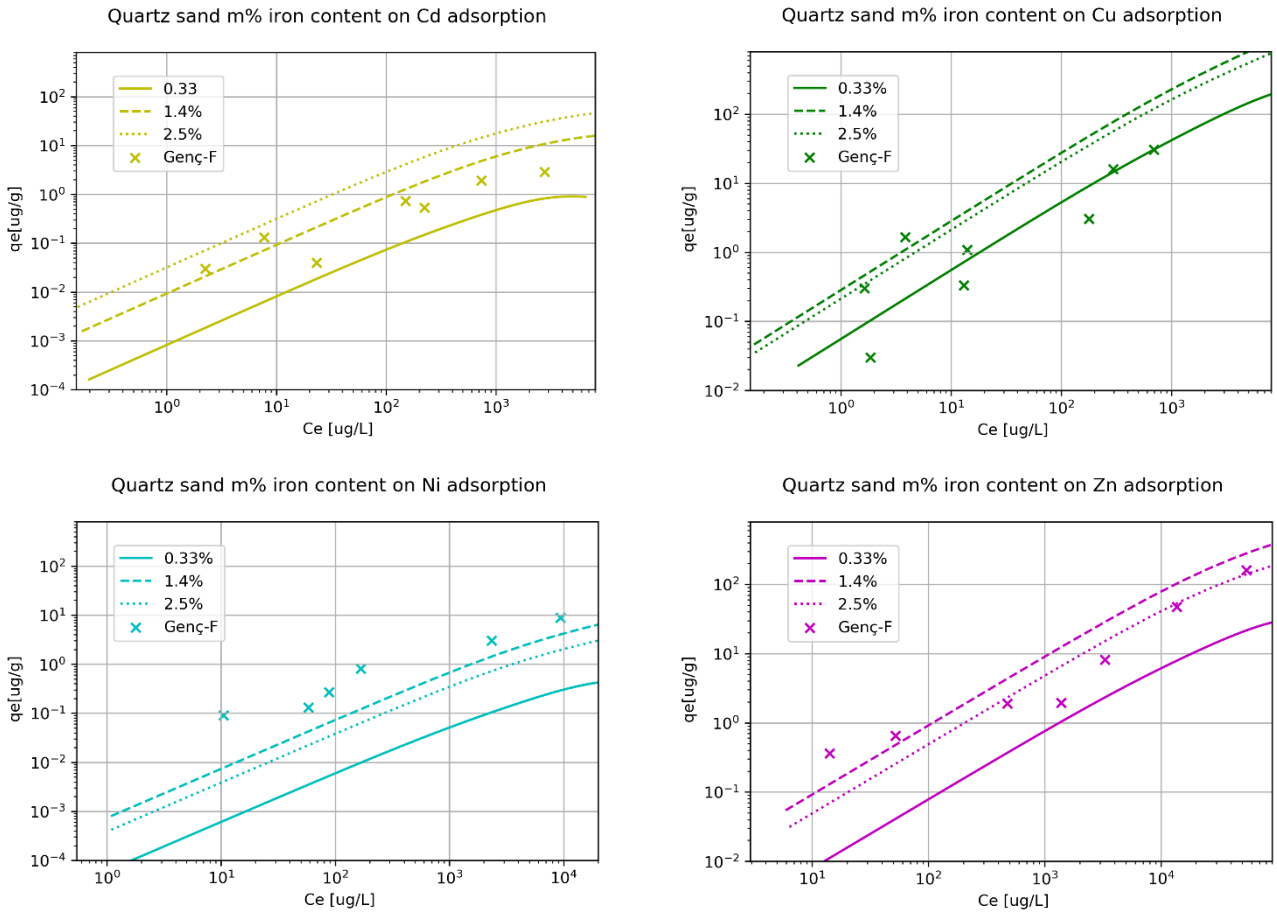

Figure 4-13 Adsorption on quartz sand by tweaking the iron content to fit the Genç-Fuhrman (2007) data on batch adsorption for Cd, Cu, Ni and Zn.

To fit the quartz sand iron content, iron contents of 0.33 m%, 1.4 m% and 2.5 m% were simulated. Product data sheet of quartz sand reported an iron content of 0.33 m% in Fe_2O_3 (Certicon, 2018). Figure 4-13 shows that quartz sand adsorption capacity was underestimated for Ni, Zn and Cd, thus contained more sorption sites. The 2.5 m% overestimated the Cd and Zn adsorption. Best fit was for quartz sand when 1.4 m% of iron content was simulated, but overall quartz sand resulted in a less good fit than IOCS

For 1 g of solid, quartz sand has 5.0 * 10^{-5} mol sorption sites, 600 m^2 g^{-1} surface area and 0.0225 g HFO. For 1g IOCS, this is 4.835 * 10^{-4} mol sorption sites, 600 m^2 g^{-1} surface area and 0.215 g HFO.

Surface complexation model vs. Freundlich isotherm

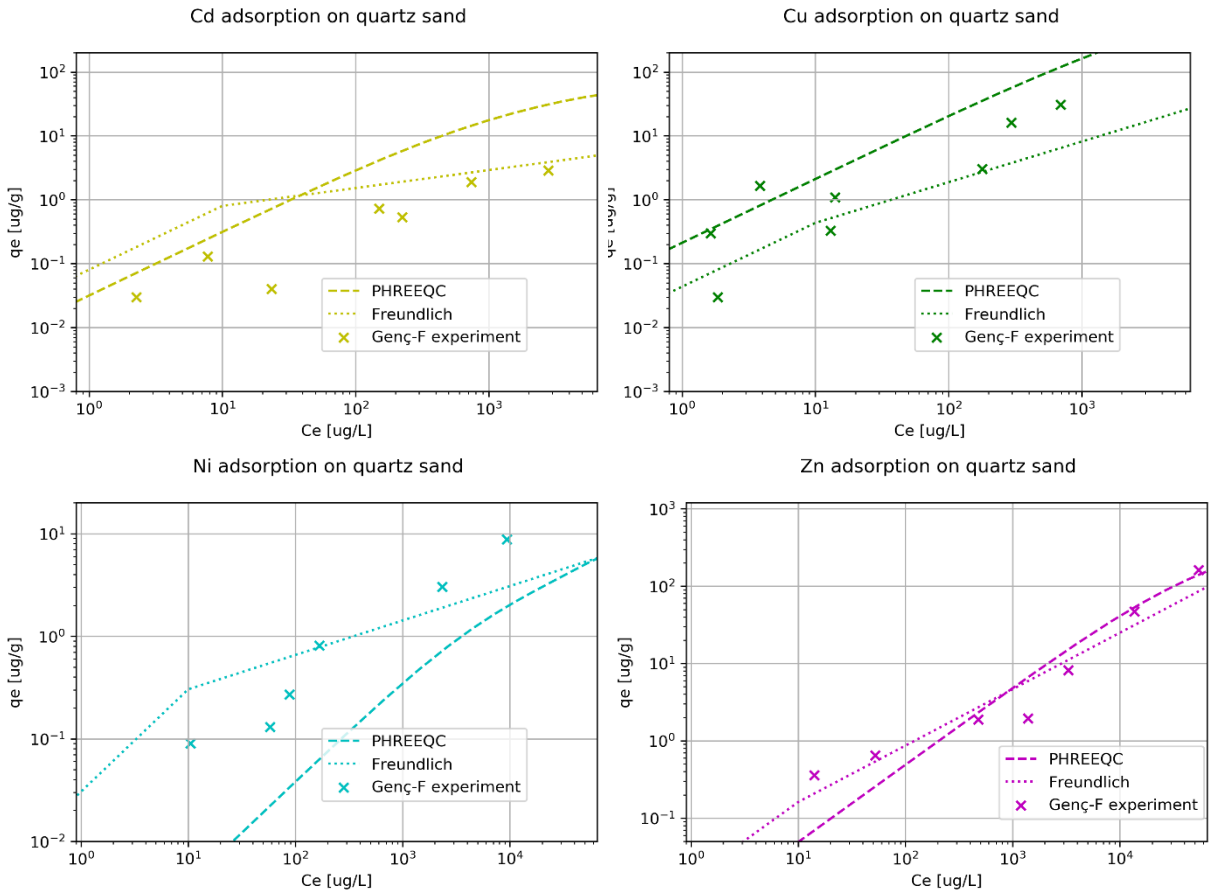

Figure 4-14 Comparison of PHREEQC surface complexation modelling and Freundlich isotherm to fit data of Genç-Fuhrman (2007) batch quartz sand adsorption experiment.

Figure 4-14 shows the comparison of the *Freundlich* isotherm, derived from the best fit on Genç-Fuhrman sorption data, and the surface complexation modeling for quartz sand. The Freundlich isotherm formed a typical straight line along the log-scale axes, but the SCM curved for the higher concentrations. The SCM overestimated the adsorption of Cd, while the *Freundlich* isotherm slightly overestimated lower concentrations. For Ni adsorption, the SCM underestimated lower concentrations and *Freundlich* isotherm showed a better fit. However, for both Cu and Zn adsorption SCM showed a proper fit.
Figure 4-15 shows adsorption of Cd, Cu, Ni and Zn on IOCS for *Freundlich* isotherm and PHREEQC SCM. SCM ill fitted the adsorption of Cd, Ni and Zn, where Cu adsorption was a better fit. The complexity of fitting SCM to data lies in overestimation adsorption for one HM and underestimate for other HMs.

Table 4-11 Freundlich isotherm constants for Genç-Fuhrman sorption data.

	Quartz sand		**IOCS**	
	K_f	n	K_f	n
Cd	0.42	0.28	0.07	0.80
Cu	0.10	0.64	0.41	0.78
Ni	0.14	0.34	0.17	0.47
Zn	0.03	0.73	0.24	0.75

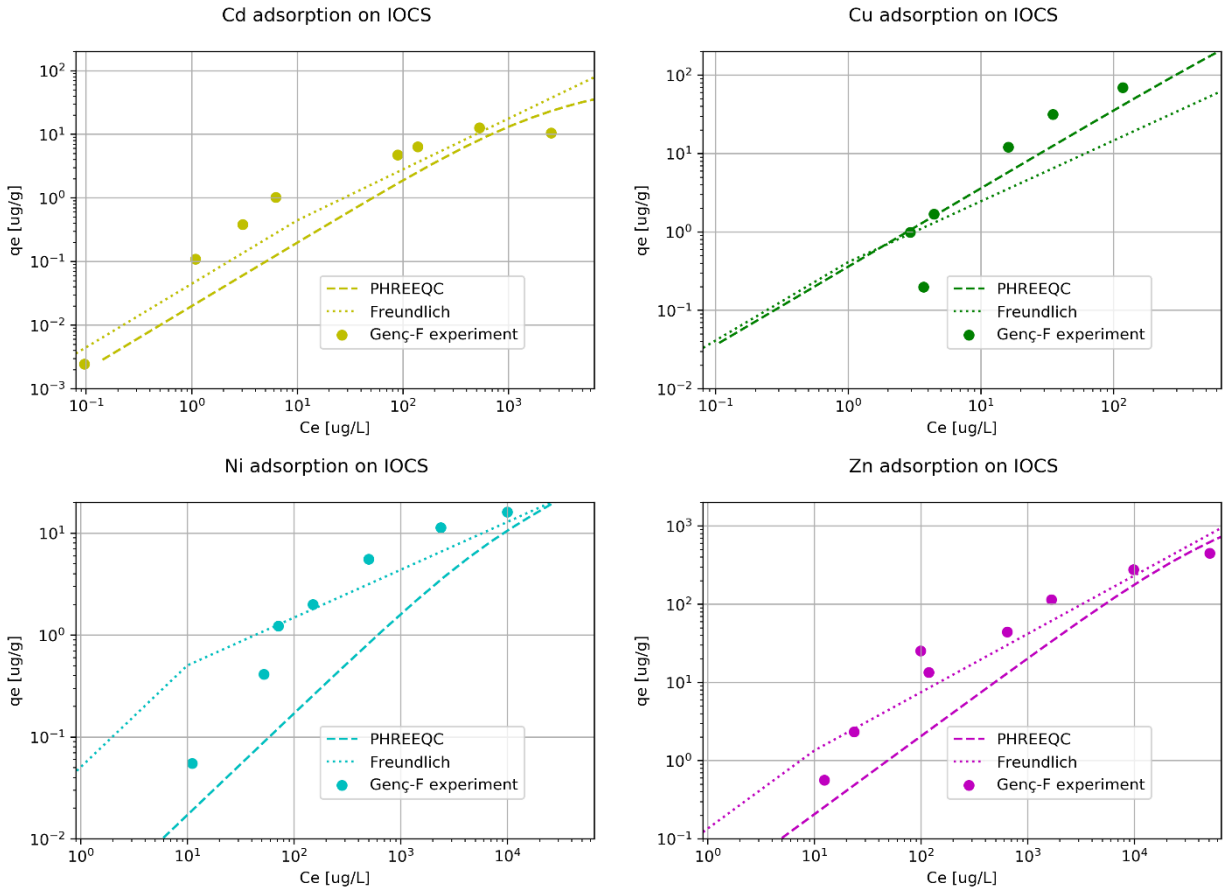

Figure 4-15 Comparison of PHREEQC surface complexation modelling and Freundlich isotherm to fit data of Genç-Fuhrman (2007) batch IOCS adsorption experiment.

4.2.3. pH-effect on adsorption

Batch experiment adsorption

Figure 4-16 shows the effect on adsorption for various pH values on Cd, Cu, Ni and Zn adsorption. Median values of the Aartselaar roof water concentrations were simulated as initial solution. At pH of 6.5 conditions, 80%, 10%, 10% and 1% was adsorbed on quartz sand for Cu, Cd, Zn and Ni respectively. At pH 8.0, 100% of Cd and Cu was sorbed, 97 % of Zn and 40% of Ni. For IOCS, pH 6.5 resulted in 90%, 60%, 50% and 15% adsorption of Cu, Zn, Cd and Ni. At pH 8.0 all Cu, Zn and Cd was adsorbed and 90% of Ni.

Copper showed relatively the best adsorption of each of the simulated HMs, especially in lower pH conditions. Higher pH values showed better adsorption for all HMs for both IOCS and quartz sand. Furthermore, IOCS showed a better adsorption capacity than quartz sand, due to the higher surface area and more sorption sites as a result of a higher iron content. Ni was the most obstinate sorptive and showed only full adsorption from a pH of 10 or higher for IOCS. For quartz sand this was even higher at pH value of 10.5.

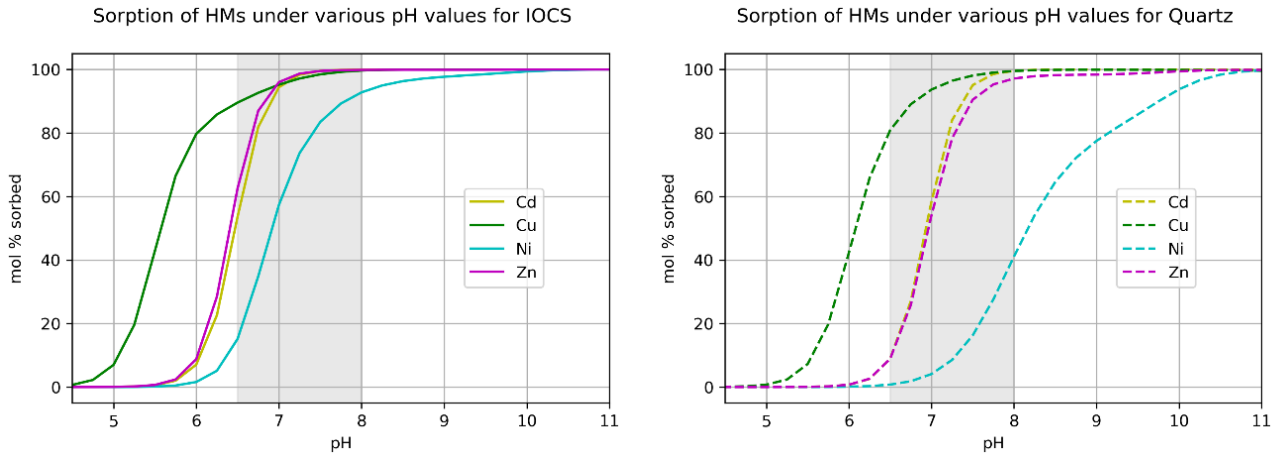

Figure 4-16 Simulated pH effect on the adsorption equilibrium by IOCS (left) and quartz sand (right) of Cd, Cu, Ni and Zn for Aartselaar roof water compositions (solid-to-liquid 1:50) with 0.01M NaCl ionic strength and 0.003 M $NaHCO_3$. Grey area is the pH range of water at the Aartselaar demo.

The range of pH from insignificant to nearly complete adsorption was very narrow for Cu, Zn and Cd. It reflects the protonation of the sorbent surface. A lower pH affected the state of the sorbent to higher positively charged surface, whereas a higher pH set the surface charge to a more negative charge and attracted the cations. An increase on O^- groups on the surface of the sorbent material caused an increased attraction of the HM ions. This affected the attraction of the positively charged HMs in solution.

K_d values for batch experiment settings

Figure 4-17 shows the partition coefficient K_d for a 1:50 solid-to-liquid ratio for both IOCS and quartz sand. K_d values of quartz sand at pH of 6.5 were 4.24 , 9.81 $*10^{-2}$, 9.77 $*10^{-2}$ and 7.71 $*10^{-3}$ for Cu, Cd, Zn and Ni respectively. The order of values resembled the earlier mentioned adsorption percentages order. At pH 8.0 the order changed to K_d values of 228, 201, 34.0 and 0.697 for Cd, Cu Zn and Ni respectively. IOCS showed higher K_d values for similar conditions. At pH 6.5 K_d values of 8.58, 1.67, 1.16 and 0.178 for Cu, Zn, Cd and Ni respectively were established. At pH 8.0 K_d values rose to 2.15 * 10^3, 6.98, 282 and 12.9 for Cd, Zn, Cu and Ni. Table 4-12 and Table 4-13 show more partition coefficients for other pH values.

Cu adsorption showed a typical development, where the IOCS K_d-value approached similar values of quartz sand between pH values of 6.5 to 8.0. Apparently, the number of sorption sites less affected the Cu adsorption than while pH conditions had a significant effect. Whereas for the other HMs IOCS greatly increased the K_d values and resulted in a greater retardation. Cd adsorption to quartz sand showed to have the highest gradient by changing the pH conditions, at least in the range of 6.5 to 8.0.

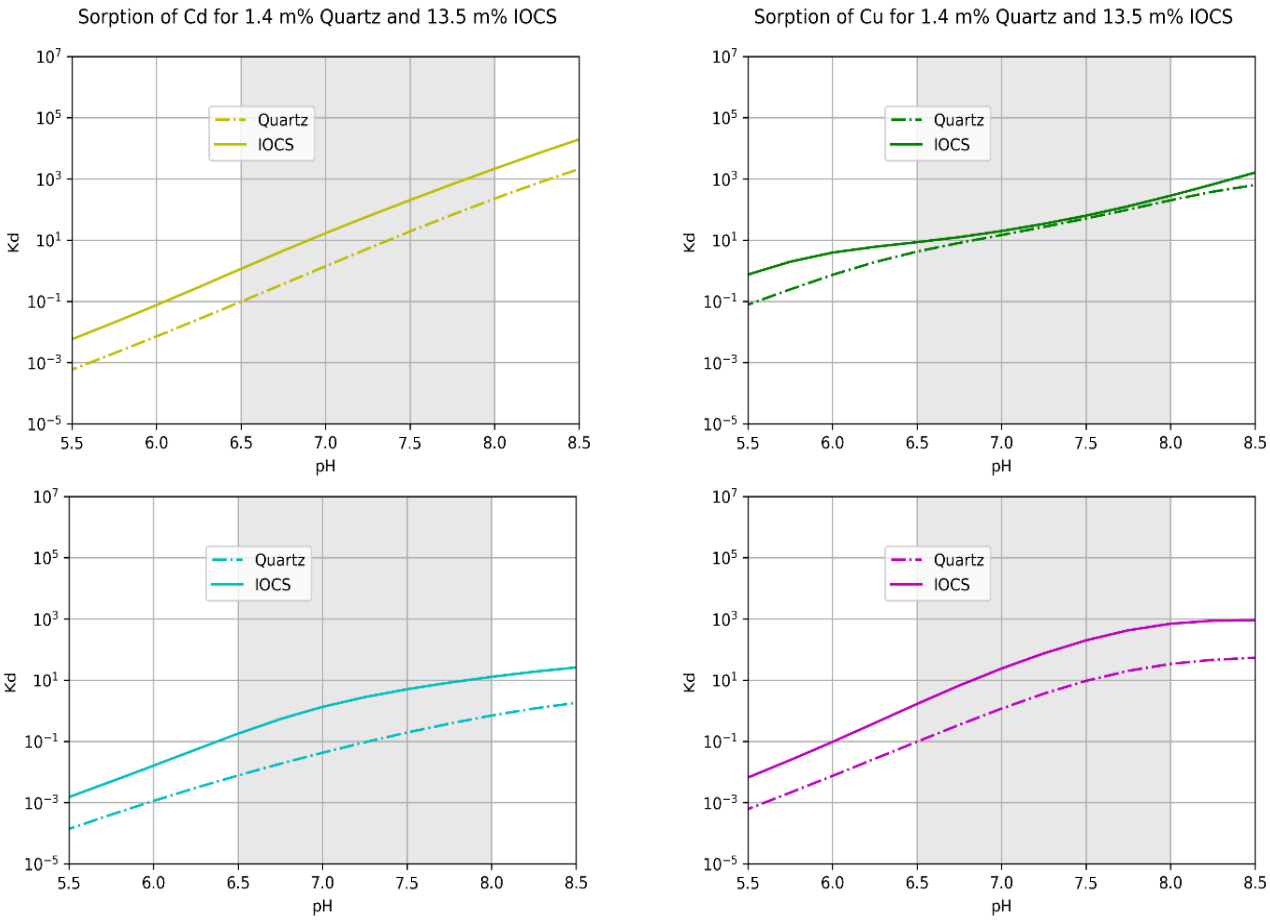

Figure 4-17 Partition coefficient K_d as a function of pH for adsorption of Cd (upper left), Cu (upper right), Ni (lower left) and Zn (lower right) on IOCS and quartz sand, modelled for Aartselaar roof water with 0.01M NaCl ionic strength and 0.003 M $NaHCO_3$ in a 1:50 solid-to-liquid ratio. Grey area is the pH range at the Aartselaar demo.

Table 4-12 K_d values for IOCS in a 1:50 and 1:0.2 solid-to-liquid ratio on Cd, Cu, Ni and Zn adsorption for Aartselaar roof water concentrations.

K_d IOCS	**1:50 (batch)**				**1:0.2 (biofilter)**			
HM	Cd	Cu	Ni	Zn	Cd	Cu	Ni	Zn
pH 6.5	1.16	8.58	0.178	1.67	20.1	$1.58 * 10^4$	178	566
pH 7.0	16.8	19.9	1.34	23.9	339	$4.91 * 10^4$	$1.71 * 10^3$	$5.88 * 10^3$
pH 7.5	203	63.4	5.05	199	$7.63 * 10^3$	$2.50 * 10^5$	$1.83 * 10^4$	$6.12 * 10^4$
pH 8.0	$2.15 * 10^3$	282	12.9	698	$2.72 * 10^5$	$1.87 * 10^6$	$1.95 * 10^5$	$6.87 * 10^5$

K_d value for biofilter settings

Figure 4-18 shows the development of the partition coefficient for biofilter settings (1:0.2 ratio solid-to-liquid ratio).. Again, highest K_d values were reached at highest pH values in case of all four HMs. At pH 6.5 the K_d values for quartz sand were 33.9, 38.5, 130 and $3.82 * 10^4$ for Cd, Ni, Zn and Cu respectively. For IOCS, this was 20.1, 178, 566 and $1.58 * 10^4$ for Cd, Ni, Zn and Cu respectively. At pH 8.0, K_d values rose to $1.95 * 10^5$, $2.72 * 10^5$, $6.87 * 10^5$ and $1.95 * 10^5$ for Ni, Cd, Zn and Cu respectively

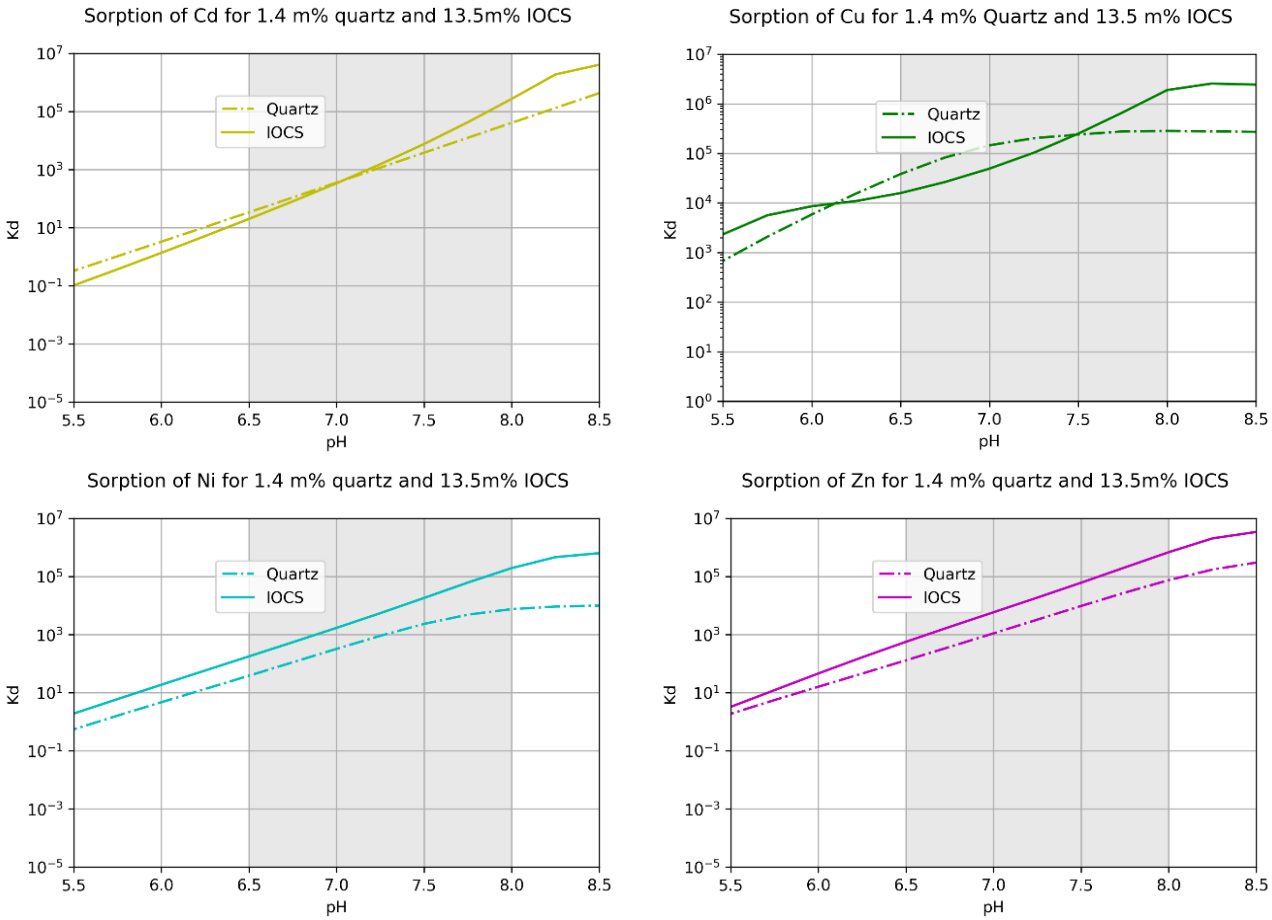

Figure 4-18 Partition coefficient K_d as a function of pH for adsorption of Cd (upper left), Cu (upper right), Ni (lower left) and Zn (lower right) on IOCS and quartz sand, modelled for Aartselaar roof water with 0.01M NaCl ionic strength and 0.003 M $NaHCO_3$ in a 1:0.2 solid-to-liquid ratio. Grey area is the pH range of water at the Aartselaar demo.

For IOCS, more sorption sites were available relative to water volume, so one would expect higher K_d values. This was clearly seen for Ni and Zn adsorption. However, Cd and Cu showed lower K_d values in acidic conditions (pH < 7.0). The pH was fixed by addition of HCl (by the FIX_PH iterative command). A significant HCl was dosed to satisfy the fixed pH conditions, and as a result additional Cl^- formed complexes with the HMs. This was clearly seen by the K_d development for Cd and Cu adsorption, where adsorption by quartz sand was higher than IOCS. For quartz sand, 4.145 * 10^{-2} moles of HCl was added to fix pH 6.5, but IOCS this was even 0.7532 moles HCl.

Table 4-13 K_d values for quartz sand in a 1:50 and 1:0.2 solid-to-liquid ratio on Cd, Cu, Ni and Zn adsorption for Aartselaar roof water concentrations

K_d quartz sand	**1:50 (batch)**				**1:0.2 (biofilter)**			
HM	Cd	Cu	Ni	Zn	Cd	Cu	Ni	Zn
pH 6.5	9.81 *10^{-2}	4.24	7.71 *10^{-3}	9.77 *10^{-2}	33.9	3.82 *10^{4}	38.5	130
pH 7.0	1.41	14.8	4.27 *10^{-2}	1.18	358	1.45 * 10^{5}	323	1.11 *10^{3}
pH 7.5	19.3	50.9	0.195	9.52	3.83 *10^{3}	2.40 * 10^{5}	2.34 *10^{3}	9.66 *10^{3}
pH 8.0	228	201	0.700	34.0	4.08 *10^{4}	2.83 * 10^{5}	7.55 *10^{3}	7.50 *10^{4}

4.2.4. Ionic strength effect on adsorption

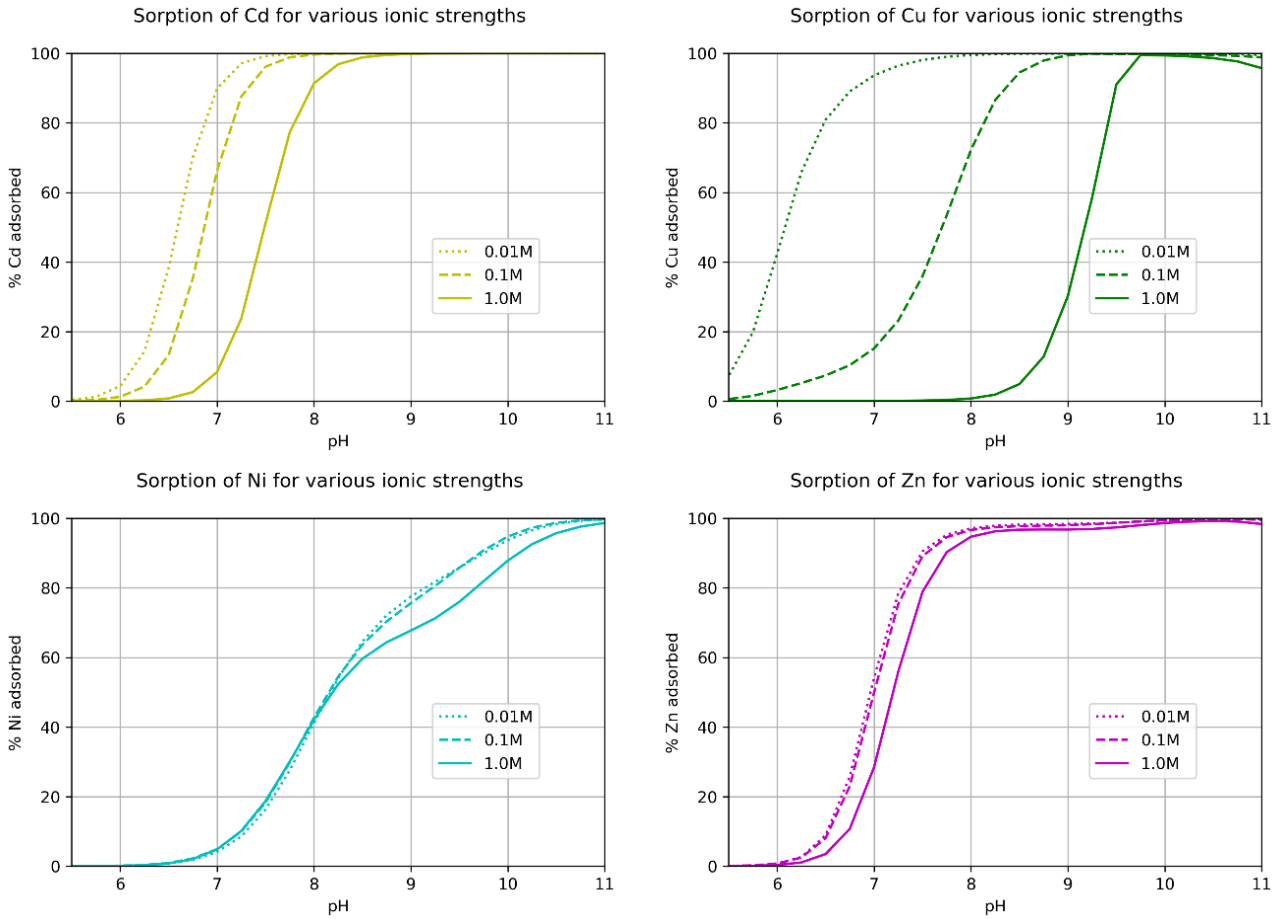

Figure 4-19 Simulated pH effect on the adsorption for quartz sand of Cd, Cu, Ni and Zn for Aartselaar roof water compositions (solid-to-liquid 1:50) with 0.01M, 0.1 and 1.0 NaCl ionic strength and 0.003 M $NaHCO_3$.

Figure 4-19 shows the effect of increasing ionic strengths in the stormwater compositions. An increase of the ionic strength resulted for each HM in lower adsorption. This resembled the classical ionic strength effect. The greatest effect was for Cu adsorption, with a shift of full adsorption from pH 8.0 to pH 10.0 for I=0.01M and I=1.0M respectively. Ni adsorption was less affected and mostly above the pH 8.0, where higher ionic strength decreased the adsorption.
HMs formed aqueous complexes with Cl^- and less was adsorbed to the surface. This was most specifically the case for Cu-Cl complexes and Cd-Cl complexes. Also, ionic strength affects the Debye length and suppresses the diffuse layer. Table 4-14 shows that the surface potential and Debye length decrease by increasing ionic strength.

Table 4-14 Charge, surface potential and Debye length development by variation of the ionic strength

	Charge density [C m^{-2}]			**Surface Potential ψ_0 [V]**			**Debye length κ^{-1} [m]**
	pH = 7.0	pH = 8.0	pH = 9.0	pH = 7.0	pH = 8.0	pH = 9.0	pH = 7-9
I = 0.01	$3.066 * 10^{-6}$	$-2.048 * 10^{-5}$	$-5.703 * 10^{-5}$	$3.821 * 10^{-3}$	$-2.444 * 10^{-2}$	$-5.667 * 10^{-2}$	$3.066 * 10^{-9}$
I = 0.1	$9.712 * 10^{-6}$	$-2.048 * 10^{-5}$	$-1.186e * 10^{-4}$	$4.659 * 10^{-3}$	$-2.060 * 10^{-2}$	$-4.899 * 10^{-2}$	$9.694 * 10^{-10}$
I = 1.0	$3.317 * 10^{-5}$	$-8.691 * 10^{-5}$	$-2.344 * 10^{-4}$	$5.018 * 10^{-3}$	$-1.303 * 10^{-2}$	$-3.317 * 10^{-2}$	$3.066 * 10^{-10}$

An ionic strength of 1.0M is unlikely to occur for stormwater under regular conditions, but Na and Cl concentrations can increase 1 or 2 order of magnitude as a result of road salting (Brown *et al.*, 1997). The simulations show that a salt shock pulse has a significant effect on adsorption for all metals. A range of ionic strength of 0.01 to 0.1M is more likely and this still has a significant effect on Cu and Cd adsorption.

4.2.5. Zinc ratio effect in stormwater runoff

Figure 4-20 shows the effect of the increase and decrease of Zn concentrations in typical stormwater. By changing the molar ratio of Zn in the influent stormwater, the adsorption of Ni and Cd was affected only for very high concentrations. By increasing the Zn concentration by a factor f_n = 5.0, the Cd and Ni adsorption was affected negatively at higher equilibrium concentrations. Greatest drop of q_e was 1.32 *10^2 and 2.24 *10^2 , for Cd and Ni respectively in these conditions. By half of the Zn concentration f_n = 0.5, the adsorption of the same HMs was increased and had a positive effect. Cd adsorption increased with a q_e rise of maximally 1.1 *10^2 and Ni adsorption increased with q_e rise of 1.98 *10^2.

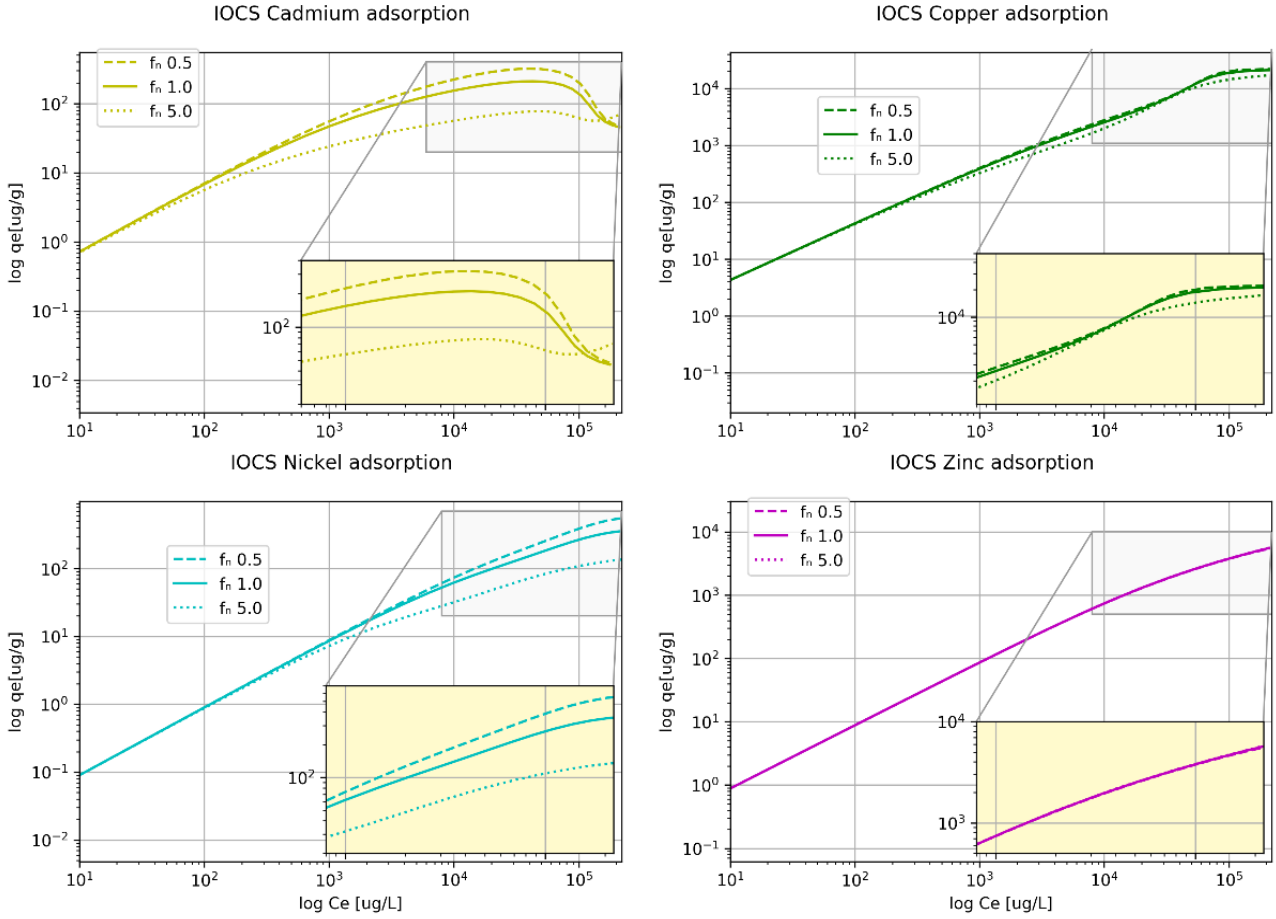

Figure 4-20 Cd, Cu, Ni and Zn sorption effects on IOCS by an Zn ratio increase or decrease for Aartselaar roof water at pH 6.5 with 0.01M NaCl ionic strength and 0.003 M $NaHCO_3$. A higher concentration of Zn in stormwater results in a negative effect of the adsorption of Cd and Ni and reduced effect on Cu for elevated equilibrium concentrations. A lower Zn concentration has the opposite effect.

4.2.6. Copper ratio effect in stormwater runoff

Figure 4-21 shows the influence of copper concentration on the adsorption of other HMs by IOCS. By increasing the Cu ratio with a factor 5.0, the Zn adsorption was negatively affected and resulted in lower adsorbed concentration. An increased Cu concentration resulted in a lower adsorption of Cd and Ni. Cu ions were competitive on the sorption sites of the IOCS. Also Zn adsorption was highly affected by the change of Cu concentrations. By adsorption of Cu, the potential to adsorb other HMs from the solution decreased.

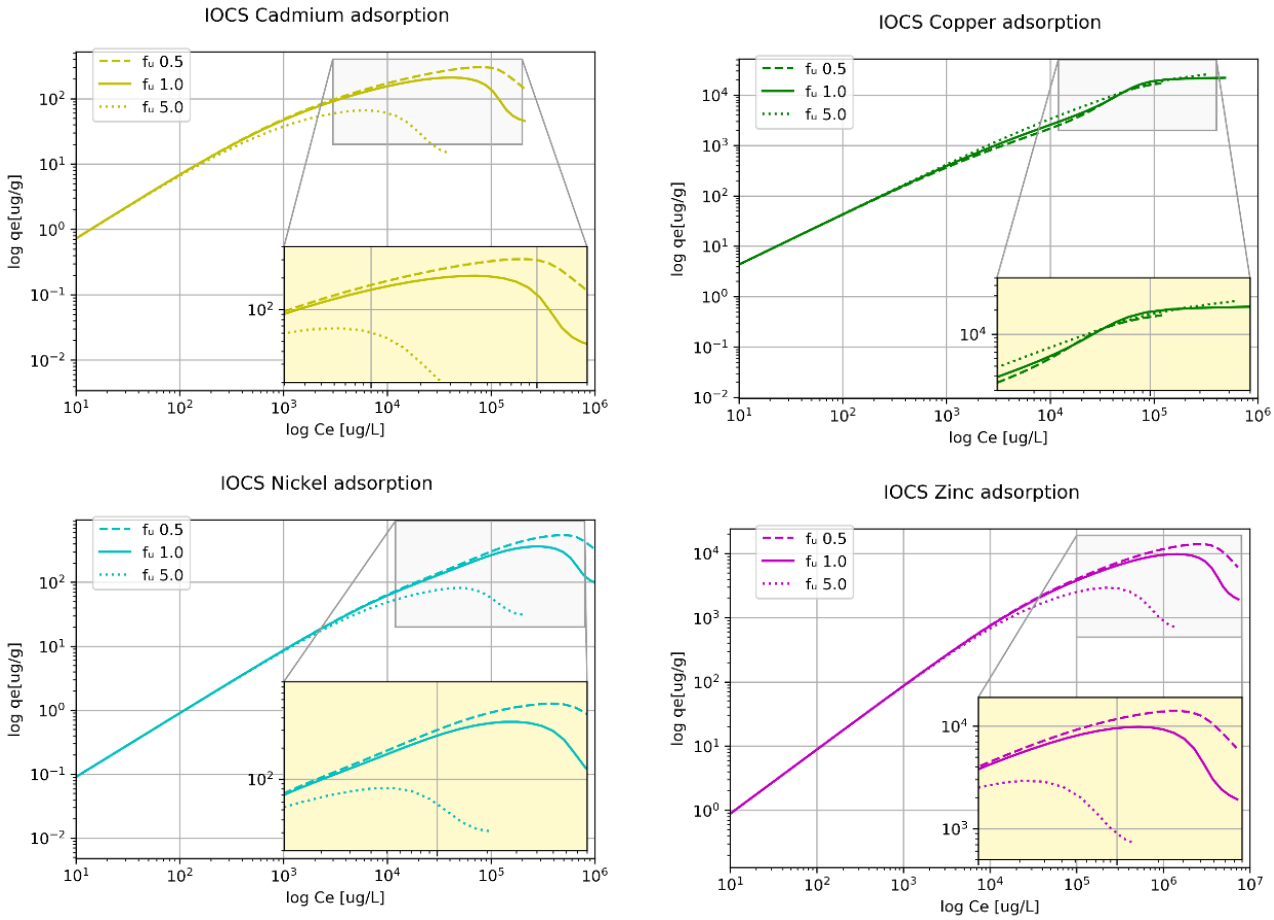

Figure 4-21 Cd, Cu, Ni and Zn sorption effects on IOCS by an Cu ratio increase or decrease for Aartselaar roof water at pH 6.5 with 0.01M NaCl ionic strength and 0.003 M $NaHCO_3$. A higher concentration of Cu in stormwater results in a negative effect of the adsorption of Cd, Ni and Zn for elevated equilibrium concentrations. A lower Cu concentration has the opposite effect.

4.2.7. Breakthrough curves Aartselaar demo roof water

To represent the flow of stormwater passing biofilter, a one dimensional column consisting of 5 cells was simulated. When average influent concentrations, chemical and physical conditions and solid-to liquid ratio are known, the model can predict the effluent concentration development over water volumes passed and development of the concentrations within the biofilter. For the Aartselaar demo, this was a 1:0.2 solid-to-liquid ratio (see section 3.2.4).

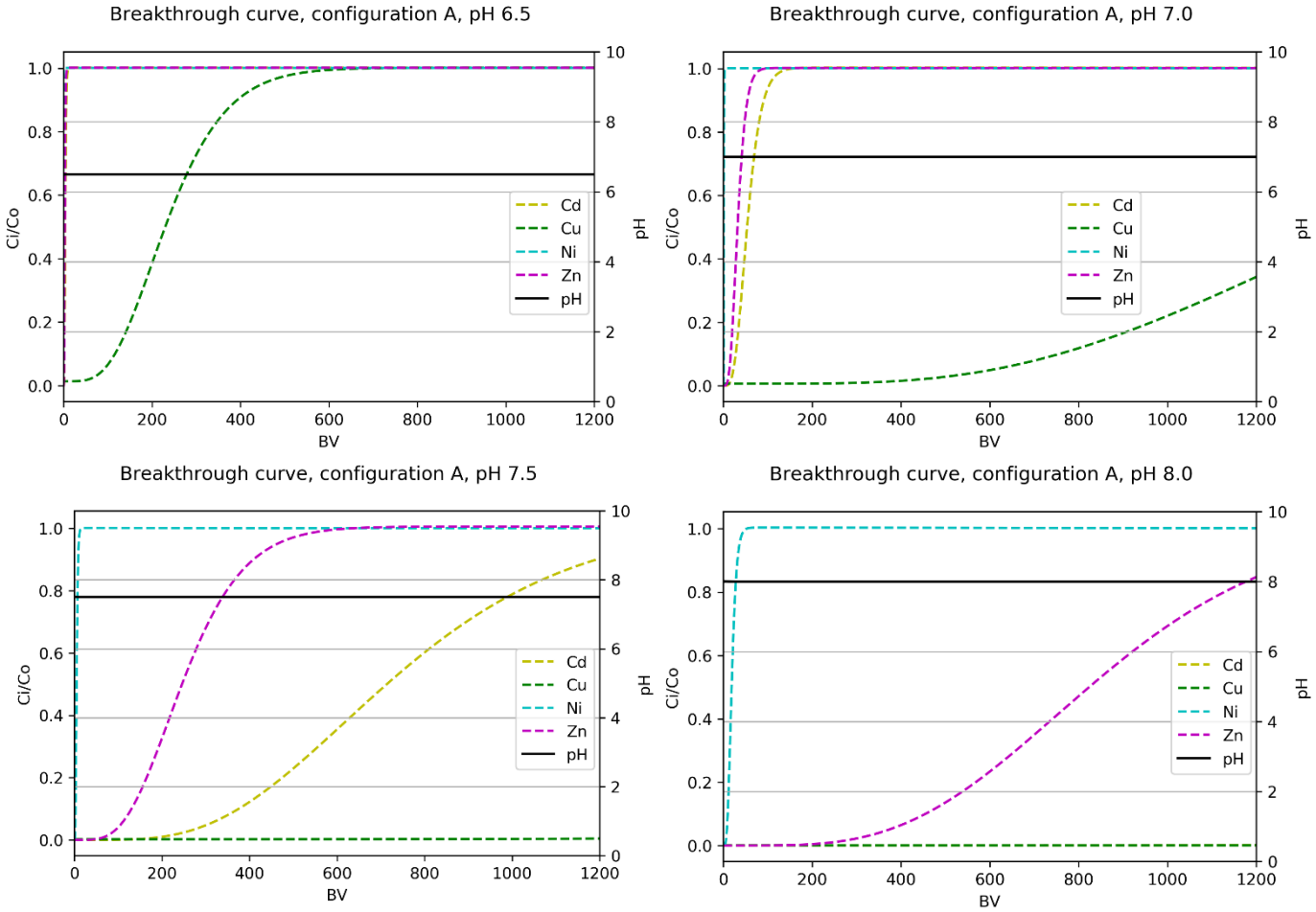

Figure 4-22 Breakthrough curves configuration A for pH 6.5 (upper left), pH 7.0 (upper right), pH 7.5 (lower left) and pH 8.0 (lower right). Aartselaar roof water composition is simulated with 0.01M NaCl ionic strength and 0.003 M $NaHCO_3$.

Figure 4-22 shows the pH effect on HM adsorption for configuration A. Clearly, it showed that a higher pH value has a positive effect on the adsorption for all HMs and delayed the breakthrough. Cu showed that it was best adsorbed of the simulated HMs, which was already seen in the batch simulations with preferred adsorption. Full breakthrough (C_i/C_0 = 1.0) for Cu occurred only after 560 BVs for pH 6.5 conditions.
Ni breakthrough curves showed that Ni was most obstinate to adsorb and remove from the stormwater. Even higher pH values showed fast breakthrough in comparison to other HMs, although it improved in comparison to a lower pH. Zn adsorption showed how susceptible it was for pH values. At pH 6.5, all Zn passed the quartz sand configuration, whereas at pH 8.0 a C_i/C_o = 0.8 was reached at approximately 1200 BV. Zn in effluent water can thus be efficiently decreased by increasing the pH in the system. Cd showed also the relevance of the system pH on its adsorption. At pH 8.0, all Cd was still removed from the stormwater in the 1200 BV simulated. Cu sorption was best for each simulation and showed full breakthrough at 600 BV at pH 6.5, some breakthrough started 300 BV at pH 7.0 and full adsorption occurred at pH 7.5 and 8.0 up to 1200 BV.

Table 4-15 50% breakthrough for simulation A and B for Aartselaar roof water under various pH conditions.

	Configuration A				Configuration B			
50% Breakthrough [BV]	Cd	Cu	Ni	Zn	Cd	Cu	Ni	Zn
pH 6.5	3.88	230	0.5	2.9	8.75	533.5	0.625	6.35
pH 7.0	54.3	1445	1.25	32	125	3380	2.625	74.6
pH 7.5	714	5755	5.13	246	1666	13.6 *10^3	11.9	577
pH 8.0	7280	13.1 * 10^3	18.9	825	17008	31.3 * 10^3	43.9	1948

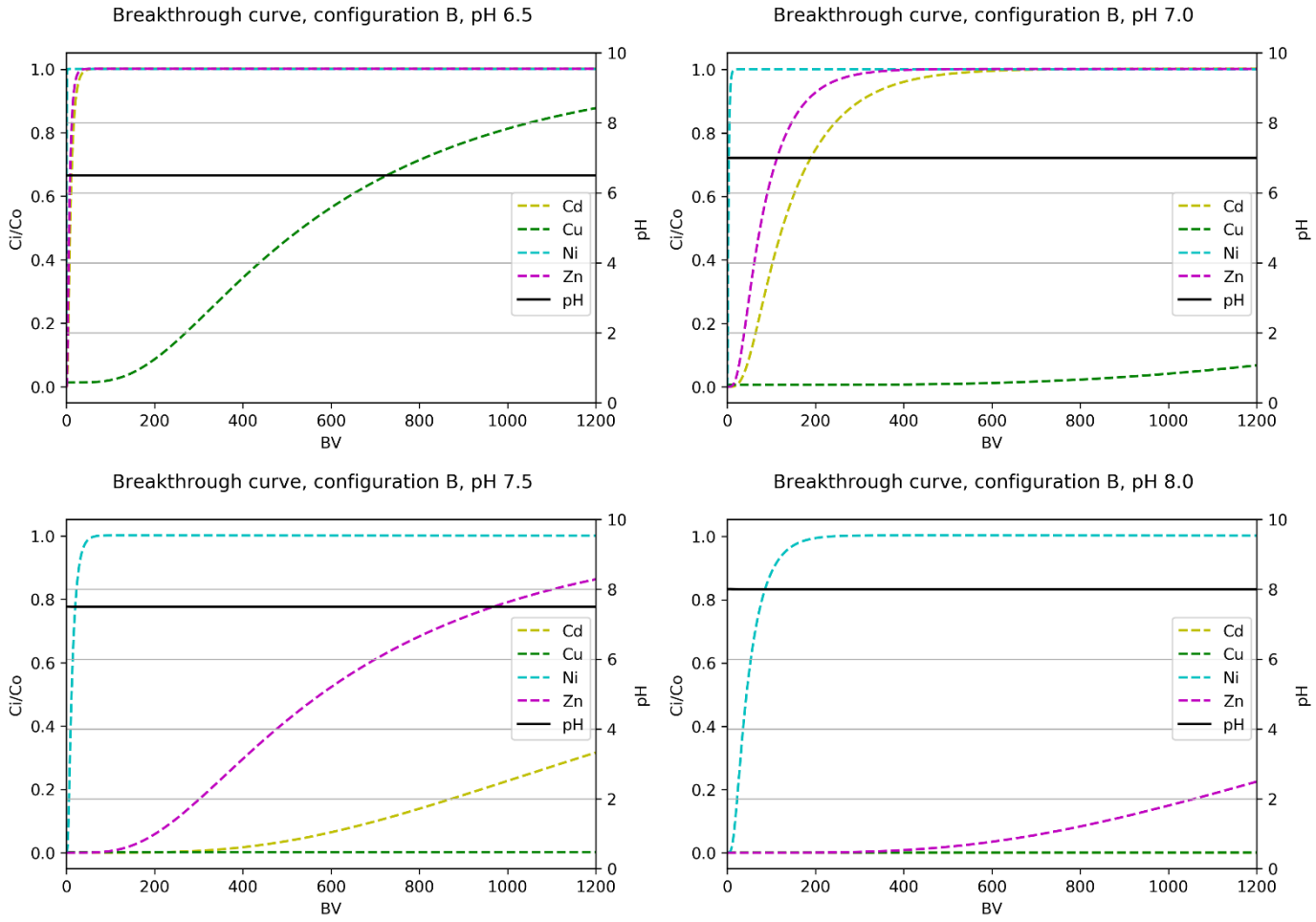

Figure 4-23 Breakthrough curves configuration B for pH 6.5 (upper left), pH 7.0 (upper right), pH 7.5 (lower left) and pH 8.0 (lower right). Aartselaar roof water composition is simulated with 0.01M NaCl ionic strength and 0.003 M $NaHCO_3$.

Figure 4-23 shows that configuration B, with upper cell IOCS instead of quartz sand, has an improved adsorption capacity in comparison to configuration A. IOCS significantly delays the breakthrough for each HM. Table 4-15 shows when 50% breakthrough occurred for both configuration under various pH conditions. Configuration B showed a delayed breakthrough for all HMs, since IOCS has more available sorption sites. For pH 7.0, 7.5 and 8.0, the simulation of one cell of IOCS delayed the breakthrough by a factor ±2.36 for all HMs.

For both configuration A and B, increasing pH value from 7.0 to 8.0 had a similar delayed breakthrough factor for HM specifically. Breakthrough was delayed with a factor 9.2, 15.8, 25.9, and 135.1 for Cu, Ni, Zn and Cd respectively. This was also confirmed by batch simulations, when the Cd K_d partition coefficient showed to greatest increase by increasing pH (section 4.2.3).

Ni showed to be the hardest metal to remove by adsorption. When the initial concentrations of Ni in the influent stormwater are too high, this can cause trouble for effluent water quality standards. Comparing this to the results of the field experiment, it was seen that overall RE of nickel was lowest of all HMs. However, Ni effluent concentrations were not similar to influent concentrations, which the sorption model however predicted. In contrast, Zn did end up in the effluent water, which could have been by a saturation effect, but more research can confirm this.

4.2.8. Cross section development Aartselaar demo roof water

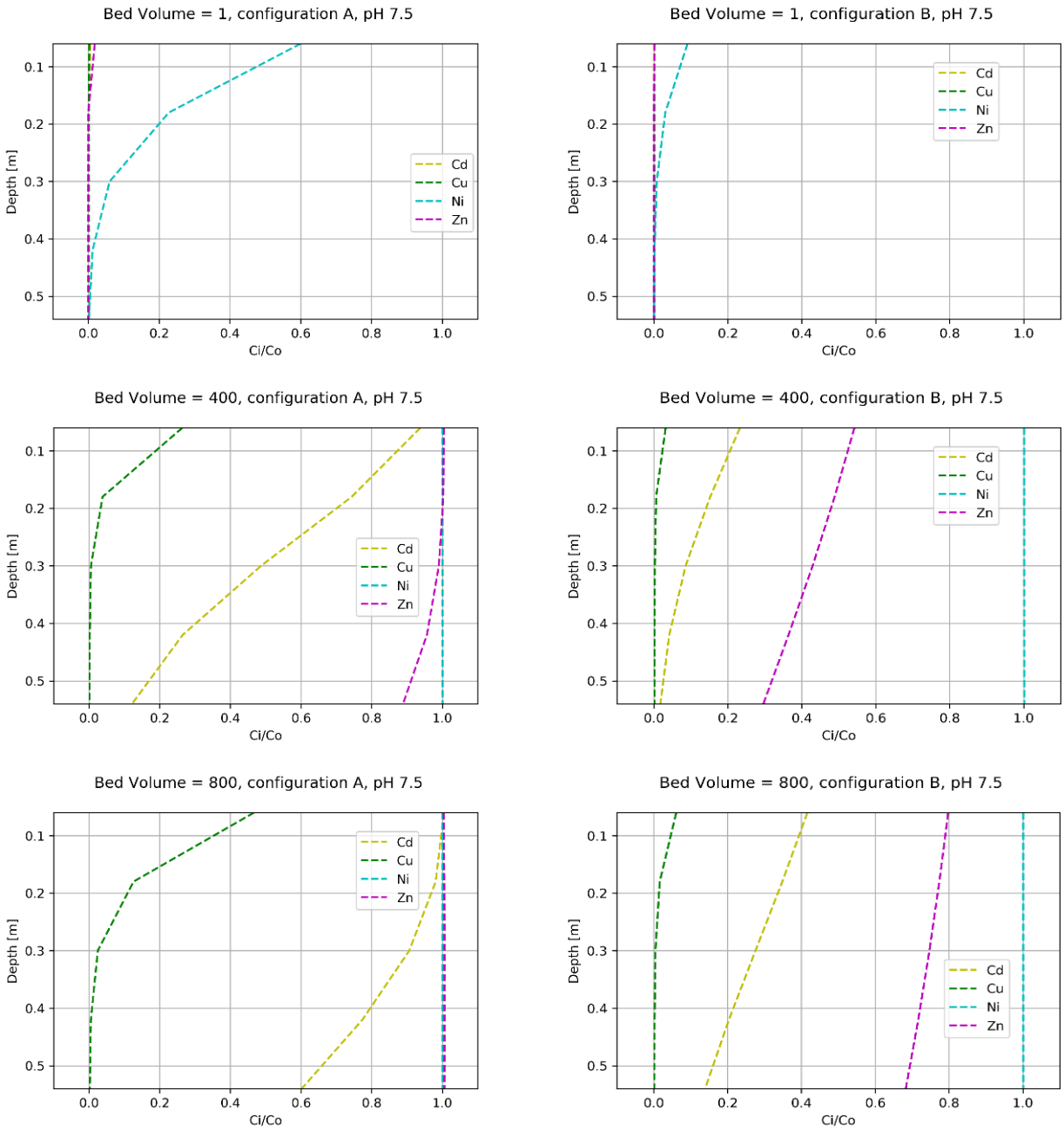

Figure 4-24 Aartselaar roof water HM adsorption, depicting the concentrations in the biofilter for pH 7.5 conditions at various moments of operation. Left: configuration A (only quartz sand) Right: configuration B (one cell IOCS, four cells quartz sand).

Figure 4-24 shows the HM concentration in the water relative to the influent concentration for configuration A, at three moments during the life cycle. After 1 BV, Ni showed its low affinity to adsorb to quartz sand. In the top layer (0.06m depth), only 40% of the Ni was sorbed to the media. 400 BV showed a $C_i/C_o = 1.0$ for Ni, which resulted to no adsorption at any location in the biofilter. Only a small part of the Zn was adsorbed, only active in the bottom layer of the filter. Notice that 0.54 m depth in Figure 4-24 and Figure 4-22 are interrelated.

Figure 4-24 also shows configuration B, for similar cross sections at the same time of operation. The effect of adding IOCS showed lower concentration of HM throughout the biofilter. Despite the high adsorption capacity of IOCS, Ni remained the obstinate HM to remove.

Cross sectional concentrations of HMs in the water showed a gradually decreasing trend towards the biofilter bottom. From the field experiments, this was only a result for Cu concentrations over depth for all cycles.

4.2.9. Aartselaar demo synthetic feeds

To compare the sorption model to a field experiment, feeds were simulated and cross sections were established, plotted against field data. Appendix VV shows simulations without field data. Transport flow was modelled with average constant conditions, only the influent compositions was changed. It was expected to have different outcomes as temperature and pH conditions changed and rainwater directly falling onto the biofilter was not included. Furthermore, cross sectional data was discussed to be biased by lack of steady state and short-circuiting (see section 4.1.3). Comparing both methods validated outcomes and emerged different settings, that allowed for discussion.

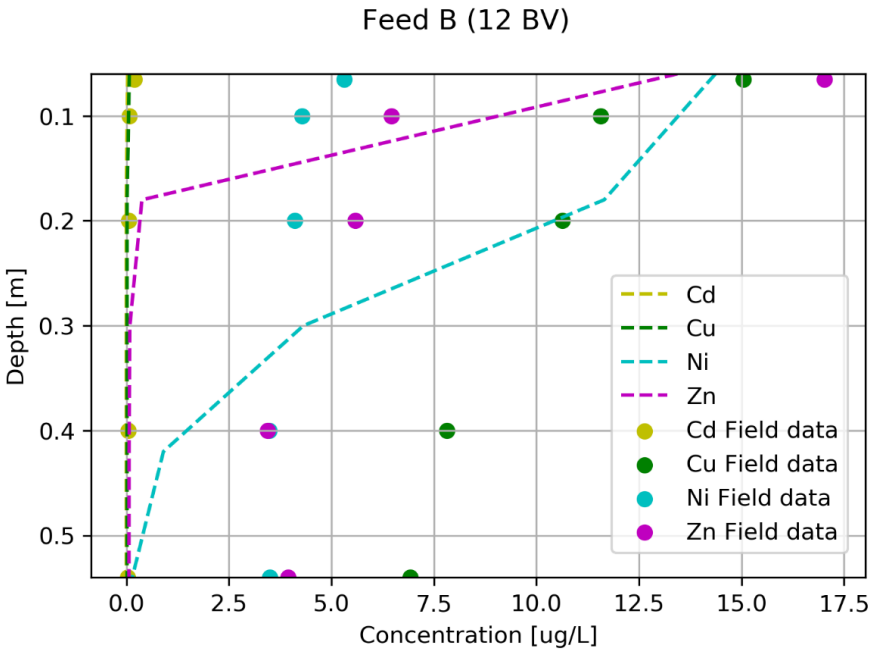

Figure 4-25 Synthetic feed B comparison sorption model and field data

From batch experiments, the relatively high affinity of Cu and Cd adsorption on quartz sand. Feed simulations confirmed this, as for each feed the Cu and Cd concentrations were 0 along filter depth. Zn and Ni showed a relatively lower adsorption affinity, and were gradually removed over depth .

For feed B with synthetic HMs dosed (low). Sorption model showed full adsorption of Cu and Cd at the top of the filter. Zn was showed full adsorption, but only over 30 cm depth, and full adsorption of Ni was established over 0.54 m. Field data did not correspond with model predictions, especially Cu adsorption was overestimated by the model. Higher solubility of Cu than expected could also be due to presence of organic ligands in the system forming aqueous complexes .

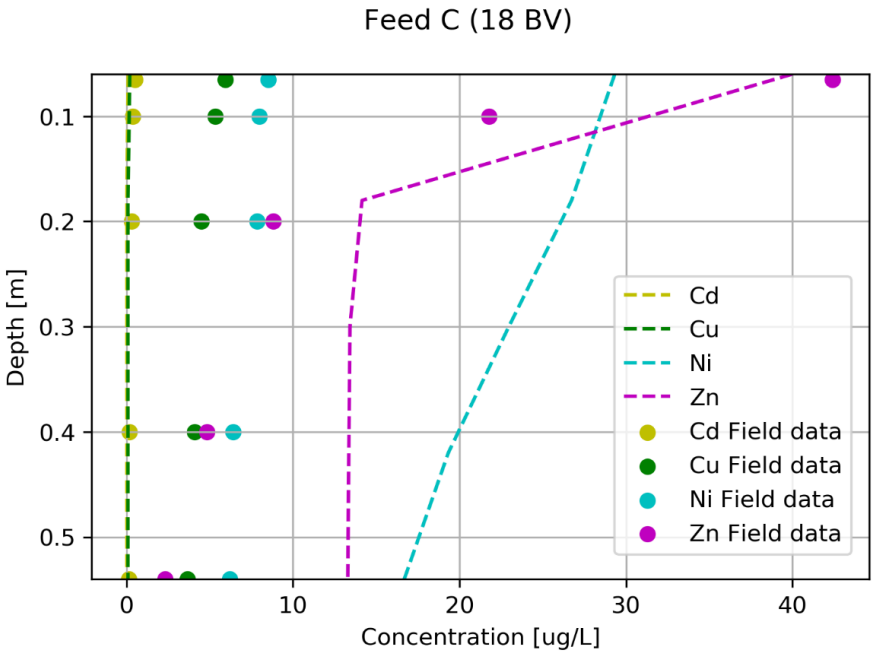

Figure 4-26 Synthetic feed C comparison sorption model and field data

Feed C, depicted in Figure 4-26, showed for both field data and model highest decrease of Zn in the BB top 20 cm. Zn sorption simulation showed best fit along data. Ni adsorption in the model was underestimated compared to the field data. Since Zn was determined with a higher affinity for HFO binding sites, it was better adsorbed than Ni, despite the higher concentration. Cd and Zn affinities are nearly the same, but the lower initial Cd concentration lead to full adsorption. Cu adsorption was higher for the sorption model than observed in the field experiment. It was seen in 4.2.2 that Cu adsorption was slightly overestimated for low concentrations, but field experiment concentrations showed partitioning and slight decrease over depth.

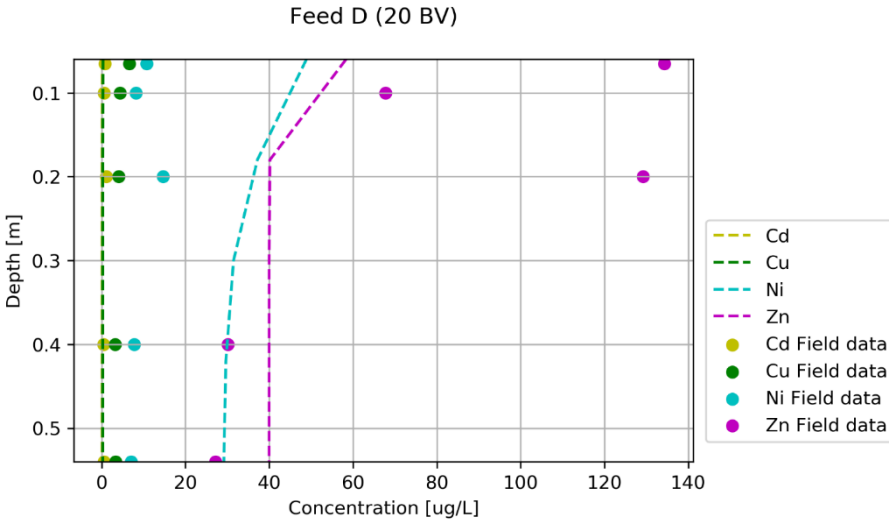

Figure 4-27 Synthetic feed D comparison sorption model and field data

Figure 4-27 shows results of feed D. The high Zn concentration at 0.2 m depth was not following the trend and could be by short-circuiting along vegetation roots. If that value was neglected, the model showed a reasonable fit along the Zn concentrations. pH value during this sampling round was around 7.0, which was 0.5 log units lower than simulated. Therefore, adsorption by the model could be overestimating the sorption of HMs.

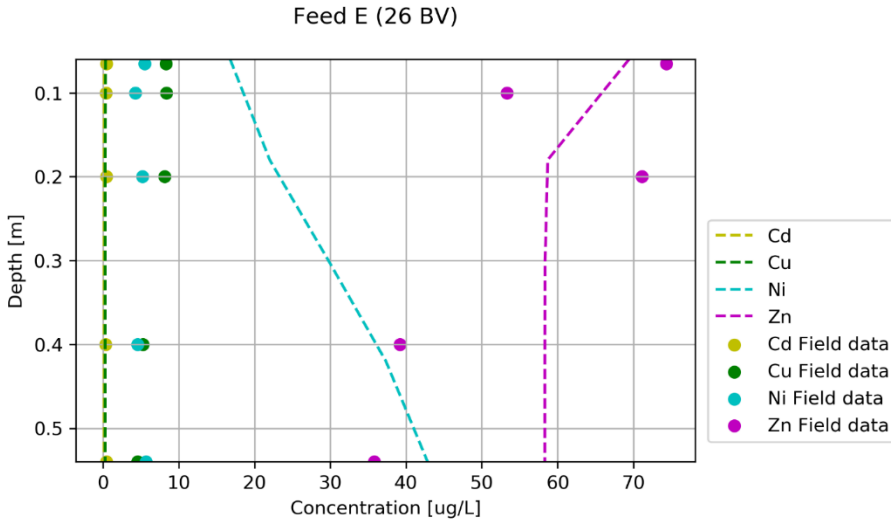

Figure 4-28 Synthetic feed E comparison sorption model and field data

Figure 4-28 shows results of feed E. For this low concentration feed, the sorption model showed high Ni concentrations for deeper layers. This effect was caused by the high concentration of the prior feed. By the lower affinity of Ni to quartz sand, more remained in solution during the prior feed. This was not observed for field data, since the effect of rainwater falling directly on the BB in between sampling periods was not taken in account for the model. Zn field data showed a reasonable fit with the sorption model, with highest sorption in the top 20 cm. Compared to the prior feed D, higher Zn concentrations were found due to saturation of sorption sites of the media.

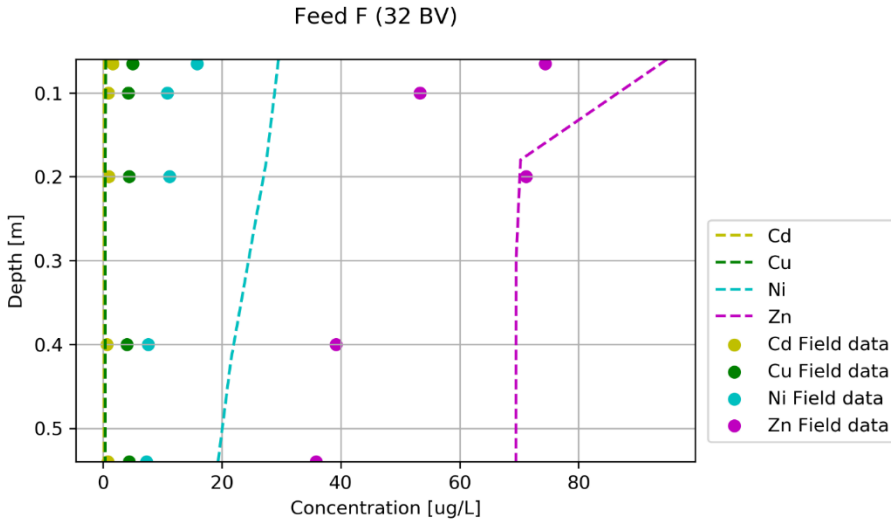

Figure 4-29 Synthetic feed F comparison sorption model and field data

Figure 4-29 shows results of feed F. Field data showed higher concentrations of Ni, compared to prior feeds, also by saturation of filter media. However, the model still underestimated the Ni removal. Zn adsorption in both sorption model and field experiment deteriorated compared to the prior feed, as an effect of media saturation. Modelling underestimated sorption of Ni and Zn.

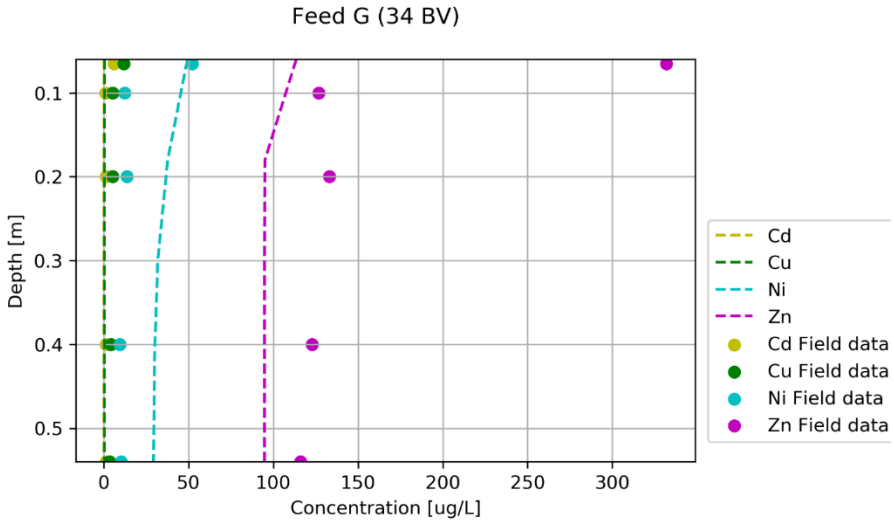

Figure 4-30 Synthetic feed G comparison sorption model and field data

Figure 4-30 shows feed G when high concentrations were modelled and dosed. For high concentrations, modelling of Zn adsorption overestimated, but a reasonable fit. Similar to high Zn concentrations in batch adsorption (section 4.2.2), the model showed overestimation compared to Genç-Fuhrman data.

Comparing the model to field data, it resulted in a good prediction to compare HMs to each other. Both field experiment results and sorption model showed the effect of saturation of sorption sites, resulting in increased dissolved concentrations of Ni and Zn over time. Overall, Ni adsorption was consistently underestimated in the model compared to the field data. This could be due to the relatively poor fit in the batch calibration or other treatment processes not taken in account. On the contrary, Cd and Cu were overestimated by the sorption model, possibly for the contrary reason. However, Zn concentration showed the best fit of all HMs, which was also observed in model calibration.

The sorption model confirmed the saturation of sorption sites of filter media, as seen in field experiment results in section 4.1.3. However, for the field experiment this was only observed for increasing effluent concentrations of Cd and Zn when more BVs passed. Since Ni had a lower affinity for quartz sand than other HMs, also the saturation effect was clearly observed in cross sectional data. Cu was best adsorbed in both the sorption model and confirmed by the field data, due to the high affinity for quartz sand and also noticed in the Genç-Fuhrman *et al.* (2007) experiment.

4.2.10. Practical application of sorption model to the Spangen biofiltration system

Practical application and implementation of sorption model for stormwater biofilters

The sorption model shows how the adsorption varies for various influent compositions and environmental conditions. In urban context all of these factors can be very location specific and differ for each site. Also specific scenarios that suddenly change the conditions (road salt during freezing, acid rain) can be studied.

It can also quantify the efficiency of the filter media (configuration) on the removal of HMs. The combination of sorbent media can be simulated to remove most effectively a proportion of HMs in the influent.

Utilisation of this sorption model can be used for the design guidelines of a biofilter and predict the lifespan of a biofilter. When proportions of influent water and the location-specific circumstances of the system are known, the model can predict the adsorption and removal of contaminants. Subsequently, the life duration and status of the biofilter can be determined and when and which maintenance measure has to be taken.

It should be taken in account that this sorption model is under development and it demands more validation towards an improved output.

When the sorption model is applied to the existing Spangen pilot, the condition of the biofilter can estimated. Table 4-16 shows the input parameters for the initial water. Since the pilot was in operation since September 2018, approximately 310 BV passed the biofilter up to the moment of this writing (February 2020). Backflushes and rainwater directly on the biofilter are not taken in account for this calculation.

Table 4-16 Averaged values of the influent water at Spangen. The actual numbers of As, Cd, Pb and Ni are lower as the lower detection limit was noted in the reference. Design and statistics of the Spangen pilot.

Spangen average influent water composition	
T [°C]	16.6
pH [-]	7.2
Heavy Metals	
As µg L-1]	4.00
Cd µg L-1]	1.00
Cu µg L-1]	5.00
Pb µg L-1]	5.00
Ni µg L-1]	5.00
Zn µg L-1]	155.14

Properties of Spangen pilot	
Volume Spangen [m3]	81
Surface area [m2]	90
Filter layer [m]	0.6
Porosity	0.35
Linear water velocity [m h-1]	0.33
Total volume passed 20 Oct 2018 - 19 Jan 2020 [m3]	25709
Bed Volumes	310
Volume Spangen [m3]	81

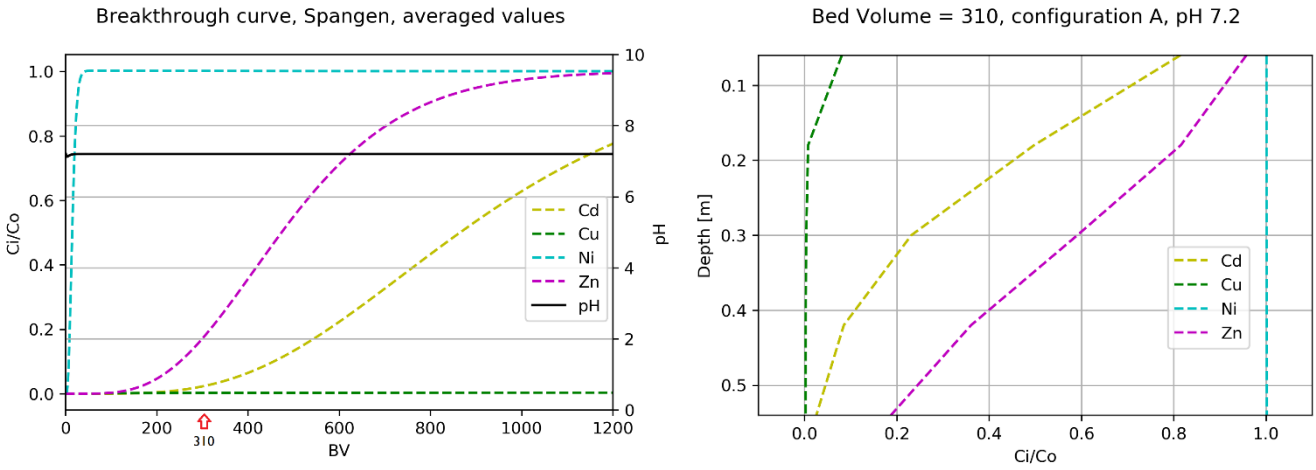

Figure 4-31 Simulation of average influent water on a 0.6 m quartz sand filter bed. On the left the breakthrough curves for Cd, Cu, Ni and Zn.

In January 2020, the number of BV was approximately 310 since start of operation. Figure 4-31 shows the development of breakthrough and the cross section development of the HM concentrations at 310 BV. Ni showed breakthrough in an early stage, full breakthrough occurred at 20 BV. Cu showed full adsorption up to 1200 BV and Cd was just at the start of its breakthrough. Zn showed that a 0.2 fraction of the influent water concentration ended up in the effluent. This was about 31 µg L^{-1}. By further operation, the Zn effluent concentration will increase. At a C_i/C_o of 0.42, this is at 410 BV, the Zn concentration in the effluent will be above the infiltration limit.

Comparing this to the data from Spangen, there are similar observations (Figure 4-32). At the start of the operation, no alarming Zn effluent concentration were noticed. However, 26th of February 2019 (±81 BV), 76 Zn µg L^{-1} was detected. 3 of the last 5 sampling rounds showed an Zn level above the infiltration standards. The KWR report stated that water in the filter bed was not refreshed and became anoxic and lead to mobilization of Zn (Zuurbier and van Dooren, 2019). Additionally, the adsorption model showed the relevance of saturation of the filter bed, the competition of other metals and pH effects, that decreased the adsorption of Zn.

Also Ni and As were reported to the have higher effluent than influent concentrations at Spangen. The minimum detection limit of Ni was at 5.0 µg L^{-1} and therefore no clear observation was to be made, although the low influent concentrations made less of concern for this system. The simulation showed that no Ni was sorbed by the bed at 310 BV, so if a sudden increase of Ni in the influent would appear, the adsorption model showed that the biofilter will not adsorb the Ni and can be found in the effluent.

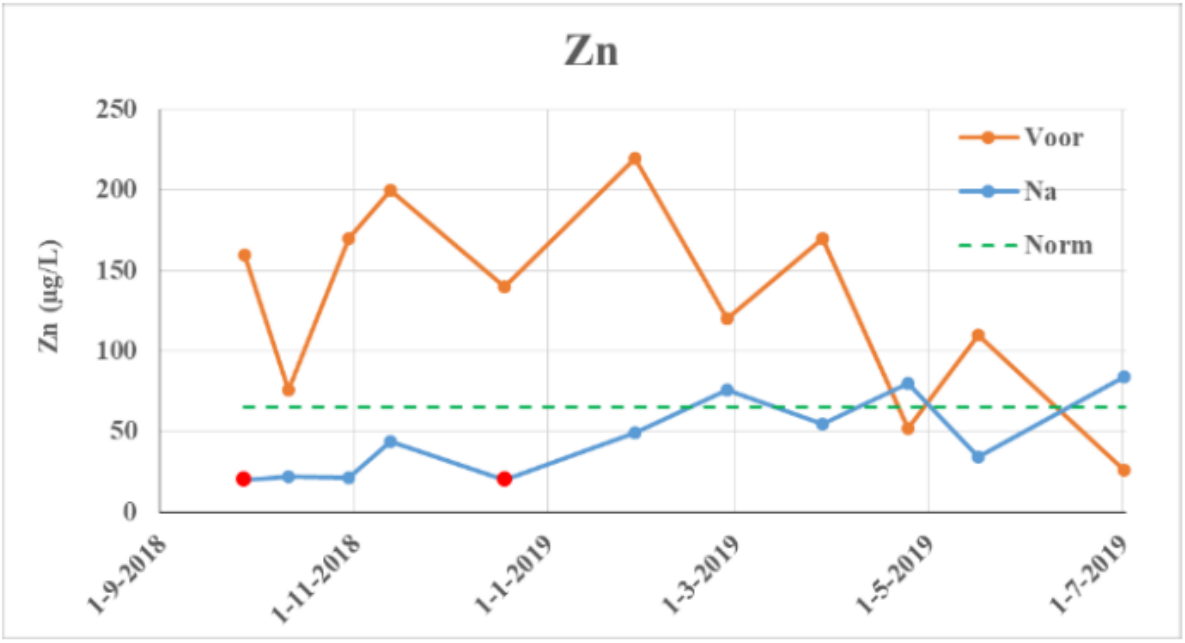

Figure 4-32 Concentration of zinc in stormwater at Spangen before biofiltration ("Voor"), after biofiltration ("Na") and the Dutch infiltration standard for zinc ("Norm"). Red dots is under detection limit (Zuurbier and van Dooren, 2019).

5. CONCLUSIONS

5.1. MODELLING THE ADSORPTION OF HEAVY METAL POLLUTANTS

The PHREEQC surface complexation model showed that the program is able to predict and analyse the adsorption mechanisms of HMs on filter media. Using a relatively simple approach, it holds promise that extrapolated adsorption behaviour of HMs can be predicted reasonably well for batch simulations, as well as one dimensional transport simulations. Furthermore, the surface complexation sorption model can be applied to assess the quantitative effect of various environmental conditions on retardation and breakthrough in the BB, and similar biofiltration systems.

The sorption model uses surface complexation reactions from the WATEQ4F database, composed of reactions between solid surface and aqueous solutes, which are specified by stability constants. Hereby, surface complexation modelling enabled extrapolation for different physical and chemical conditions, such as higher or lower pH values, while it takes into account the effect on surface charge for the complexation reactions.

The most important parameters that can be adjusted in the model are: influent composition, pH values and, of lesser importance, ionic strength. The filter media characteristics can be described by the number of HFO active sorption sites on the media, specific surface area and mass of HFO. The affinity of the surface and the solutes can be described by the complexation reactions and the associated stability constant.

In this study, the model was calibrated to Genç-Fuhrman *et al.* (2007) batch experiment data for adsorption of Cd, Cu, Ni and Zn on quartz sand and IOCS. It showed the best fit for adsorption with low HM concentrations in stormwater, with one type of binding site. Quartz sand was best represented with 0.0225 g HFO g^{-1} and 5.0 * 10^{-5} mol g^{-1} sorption sites, IOCS with 0.215 g HFO g^{-1} and 4.835 * 10^{-4} mol g^{-1} sorption sites. Stability constant for Cd adsorption was set to log k = -2.0, other sorption reactions were kept similar to the database. For higher concentrations (mg L^{-1} range), the model deviated from the experimental data and was less accurate.

A comparison of the established sorption model with data from the field experiment showed averaged results, but a good prediction to compare HMs to each other. Ni adsorption was underestimated by the model, while Zn, Cd and Cu were overestimated. Overall, the most similarity in between model results and field data was shown for Zn adsorption. Highest adsorption was observed at the top of the filter media. From the cross sectional data from the field experiment, only Cu showed a gradually decreasing trend of concentration at each cycle. It was not distinguished what fraction was removed by adsorption, or by precipitation-filtration processes.

The application of the sorption model on the Spangen biofilter showed the ability to characterise the current state of the BB after one year of operation, and to predict that after 410 BV the biofilter might not deliver a treatment capacity to guarantee the infiltration standards. With average concentrations and a constant pH of 7.2, the biofilter was simulated to have a 1.0, 0.2, 0.03 and 0 C_i/C_o rate in the effluent for Ni, Zn, Cd and Cu respectively.

5.2. EFFECT OF VARIATION IN CHEMICAL AND PHYSICAL CONDITIONS IN STORMWATER ON THE REMOVAL EFFICIENCY OF HEAVY METALS

Variations in low, med or high concentrations in the synthetic feed in the field experiment showed no clear difference from one another on the removal efficiency. For all feeds, a high RE value was established for all dosed HMs. After the sorption model simulated after a high concentration feed D, elevated Ni concentrations were found in the next feed E in at 54 cm depth. Such an effect was not observed with field data.

Adsorption of HMs showed to be highly influenced by pH conditions in the stormwater. For the field experiment, pH range was measured 6.5 to 8.0, defining a key condition in adsorption. In a 1:50 solid-to-liquid batch simulation, when pH values were increased from 6.5 to 8.0, K_d values of quartz rose from 9.81 *10^{-2}, 4.24, 7.71*10^{-3} and 9.77 *10^{-2} to 228, 201, 0.7 and 34.0 for Cd, Cu, Ni and Zn respectively. The same simulation for IOCS resulted in an increase from 1.16, 8.58, 0.178 and 1.67 to 2.15 *10^3, 282, 12.9 and 698 for Cd, Cu, Ni and Zn respectively. Also, for one dimensional transport the breakthrough of each HM was delayed by increasing the pH. For the media with only quartz configuration simulation at pH 6.5, 50% breakthrough occurred at 0.5, 2.875, 3.875 and 230 BV for Ni, Zn, Cd and Cu adsorption respectively. By increasing the pH with one log unit to pH 7.5, 50% breakthrough was retarded to 5.125, 246, 714 and 5755 BV for Ni, Zn, Cd and Cu, respectively.

The effect of ionic strength of the solution affected the total adsorption of HMs, but to a lesser extent than pH conditions. HMs formed more aqueous complexes with Cl^- by a higher ionic strength, therefore less was adsorbed to the surface, lowering the solutes charge and remained in solution. For Cd adsorption, with an ionic strength of 0.01M full adsorption was at pH 7.5 and with an ionic strength of 1.0M full adsorption increased to a pH value of 9.0. The greatest effect was for Cu adsorption, for a solution with I of 0.01M, full adsorption occurred at pH of 8.0. For Ni adsorption, a significant effect of elevated ionic strength only occurred at higher pH values (> 8.0).

An increased initial proportion of Cu in the influent water, caused preferred adsorption of Cu over Zn, Ni and Cd, especially for higher initial concentrations, as seen in section 4.2.6. An increased initial concentration of Zn showed lesser adsorption of Ni and Cd, however Cu adsorption was influenced to a lower extent. This was caused by the high affinity of Cu to the filter media and to a lower extent for Zn. Cu and Zn concentrations can increase when building materials composed of these metals are present in the stormwater catchment area.

5.3. INFLUENCING THE ADSORPTION PROCESSES FOR EFFICIENT REMOVAL OF HEAVY METALS IN THE BLUEBLOQS BIOFILTER

Adsorption capacity of IOCS was found to be merely higher than the adsorption capacity of quartz sand. In a 20 g L^{-1} batch adsorption simulation with a composition based on Aartselaar roof water, full adsorption of Cd, Cu and Zn occurred at a pH of 7.5 on IOCS. For quartz sand this only happened at a pH of 8.0 and 9.0 for Cd and Zn respectively. Also for one dimensional transport simulations IOCS showed a higher adsorption capacity. In a 5 cell transport simulation with Aartselaar roof water, when one quartz sand cell was replaced by IOCS, 50% breakthrough was delayed from 246 to 577 BVs for Zn, from 714 to 1666 BVs for Cd, from 5.125 to 11.875 BVs for Ni and from 5755 to 50 * 10^3 BVs for Cu. Breakthrough was hereby extended by a factor ±2.36 for all mentioned HMs.

Increasing the pH of the water solution improved adsorption of all HMs. By increasing the pH from 7.0 to 8.0 in a one dimensional transport simulation, breakthrough of Cu was delayed with a factor 9.2, Ni by 15.8, Zn by 25.9, 135.1. This was for a simulation with only quartz sand as well as for a simulation with one cell replaced by IOCS. Increase of pH showed to be most effective to improve BB treatment on HM removal.

For the first feed in the field experiment, effluent HM concentrations were higher than influent concentrations, while no synthetic HMs were dosed. Influent water was water from the roof augmented with tap water, with negligible HM concentrations This indicates that during the start-up phase, wash-off from fresh quartz sand and IOCS can occur, which leads to negative RE values. Consequently, this leads to exceedance of the Dutch infiltration standards.

In general, the field experiment showed a high RE for low, med and high HM concentrations, without clear difference between these feeds. However, results showed that Cd and Zn were less efficiently removed when more BVs passed the biofilter. For the last three cycles, Cd concentrations in the effluent rose to 0.49, 0.49 and 0.54 µg L^{-1}, exceeding the Dutch infiltration standards. For Zn, the last two cycles showed 88.78 and 49.34 µg L^{-1}, of which the first concentration exceeds the Dutch infiltration standard. The sorption model showed that after a longer period of operation, a breakthrough can occur and concentrations in the effluent might rise. In order to derive a better conclusion whether saturation was indeed causing elevated effluent concentrations, more cycles are required to be analysed.

6. RECOMMENDATIONS

The results of this study show that more research is needed to be able to derive more clear conclusions. Following recommendations aim to help improve the performance of the Bluebloqs biofiltration system for the removal of HMs, and for further improvement of the reliability of the sorption model. Also, practical recommendations are addressed, to improve and maintain good condition of the BB during operation. For remaining unanswered questions or when parameters were assumed, further research is recommended.

6.1. DESIGN GUIDELINES

Application of limestone buffers is often mentioned in literature as an easy addition to biofilters, as it neutralizes protons and increases soil pH. In other research, it was also added to effectively remove phosphorus species from stormwater (Hossain, Chang and Wanielista, 2009). Limestone can thus increase overall adsorption capacity of the BB, as this research showed the effect of pH increase. Carbonates from limestone can however inhibit the transfer of HMs to the roots of the plants, mentioned in section 2.4 (Wang *et al.*, 2015) (Bolan *et al.* 2003). Further research should be conducted to determine the use of limestone in the filter media and the subsequent effects on HM and nutrient removal.

When high Ni concentrations are detected in influent water, different media in the BB might be considered. Natural zeolite was reported to remove 90% of Ni in a 10g to 100 ml solution batch experiment (Reddy, Xie and Dastgheibi, 2014). Additionally, Mitani *et al.*(1995) found an increase in the removal efficiency when ionic strength was increased while swollen chitosan beads were used as filter media.

From the positive results on the high adsorption capacity of IOCS, one could consider to readily apply the IOCS in all layers. However, the physical properties cause a low hydraulic conductivity by precipitate formation (Benjamin *et al.*, 1996). In this research, IOCS and quartz sand are separately simulated, but reasonably a mix of IOCS and quartz sand throughout the filter layer is a considerable design option, to create an increased adsorption capacity over the depth of the filter bed.

During the Quick Scan of a design, a classification of pollution in catchment area can help to identify the limitations of a BB implementation. For example, by identifying the pollutants per object and the volume of this object in the catchment area, an estimation of the influent composition of HMs can be determined. An appropriate BB design can be established and tested by applying the sorption model.

6.2. SORPTION MODEL

More detailed information of the total Fe fraction on each material and an improved definition of the active sites on sorbent media would benefit the PHREEQC model calibration, and the followed design guidelines and design parameters. The forms of iron coating on the filter media also influence the adsorption capacity of the media, affecting chemical and physical conditions as the specific surface area. Calibration of the sorption model was based on Genç-Fuhrman and colleagues' data, in which limited characteristics of the sorbent media were reported. Brunauer-Emmett-Teller (BET) analysis or scanning electron microscope (SEM) techniques are frequently used to characterise metal adsorption sites and could determine the number of sorption sites of filter media (Lai, Lo and Chiang, 2000).

Additional batch adsorption experiments should be incorporated to improve the calibration of the sorption model. It is recommended to incorporate various pH values, specifically for low HM concentrations. Additionally, column experiments can eb conducted to validate transport simulations. By means of this, it is expected that results from the sorption model will further improve.

Redox potential and oxidation state were not addressed within this research, but do have an effect on adsorption and mobilization of HM species (Bradl, 2004). This was also suspected from the remobilization of Zn at the Spangen pilot, which resulted in elevated concentrations to the effluent (Zuurbier and van Dooren, 2019).

The sorption model only incorporates adsorption, other processes were out of scope within this research. Biological and physical processes can affect the adsorption and overall treatment efficiency of the biofilter, as mentioned in section 2.4, therefore one could consider to incorporate and combine these processes in a treatment model.

6.3. OPERATION & MONITORING

Model results showed the importance of the pH value in the system. Lower pH values could however occur by all sorts of events, like waste spills and acid rain events, having a significant effect on the performance of the biofilter. Continuous monitoring data in field experiments can provide more insights into the effect of drops and spikes of pH values. Also, the point of data collection did not show the presence of peak influent and effluent data (which could have been the case in this research). Interactive control actions, i.e. closing off the intake of water, can respond to anomalies and prevent negative effects, also commonly used in water distribution systems (Kara *et al.*, 2016). Also, the sorption model could be applied to show the effect of pH drops and if acid leaching occurs of adsorbed HMs. This is also a known phenomenon for soil contamination research (Fonseca *et al.*, 2011).

The contact time of the contaminated water with the sorbent media should be investigated to see the effect on the performance of the biofilter. By controlling the flow to the biofilter and the emptying rate in the drainage tank, the residence time in the biofilter can be changed. The SURFACE command in PHREEQC is not time dependent, so a kinetic adsorption function (KINETICS) can show the effects of residence time.

Unfortunately, the results from the Aartselaar demo were hard to interpret since the influent composition showed great variety. The mix of roof water augmented with tap water and a synthetic stormwater solution did not allow for creating real conditions set-up. An increase of the catchment area to compensate the lack of sufficient stormwater volume, appropriate to the size of the biofilter, can help improve the set-up of the field experiment.

The Aartselaar demo showed inconsistent results. With the fluctuation of multiple parameters, the results on HM adsorption were hard to conclude. The ratio of tap water and stormwater varied throughout the feeding of the system, which may have had a significant impact on the performance of the system due to different initial concentrations. Also, the measured influent concentrations did not seem to match the dosed synthetic concentrations. A water tank stirring system can help improve mixing of synthetic pollutants and the bulk water.

At Aartselaar, effluent samples were collected from the drainage standing pipe, being this the first accessible point to collect water after water passes the biofilter. However, removal processes that occurred in the bottom drainage layer of the BB and within the drainage pipe were not taken into account. Water sample collection directly after passing the biofilter, for example by a tapping point, will better represent BB processes and the comparison of field measurement with the sorption model and theory.

Pb and Fe concentrations have shown an immediate drop in the top layer of the filter bed, according to Aartselaar field measurements. It is assumed that Pb precipitated onto particles and was removed by filtration. Likewise, the sorption model shows the highest removal in the top layer by adsorption since the start of the simulation. An analysis on the quantity of metal accumulation onto sorbents over the period of usage of the BB is highly recommended. Accumulation in the top layer can cause clogging, which is known as the main drawback of biofiltration systems.

6.4. MAINTENANCE & RISKS

The sorption model shows that after certain time of operation and number of BVs, adsorption in the bed deteriorates when less sorption sites are available and (too) high effluent concentrations remain in the effluent water. To prevent the risk of aquifer contamination and maintain a functional filter bed, filter media should be replaced or regenerated in time.

A risk assessment on potential effects of HMs to ecosystems or exposure to humans is recommended. Accumulation of HMs (as seen for Pb and Fe at Aartselaar) in the top layers can represent a potential health risk, as the BB is usually located in public space areas.

A. CONTACT INFORMATION

Author

Name: Pim Versteeg

E-mail: pim@fieldfactors.com

Student Number: 4194438

Graduation committee

1st supervisor: B.M. van Breukelen

Organisation: TU Delft

Faculty: Civil Engineering & Geosciences

Section: Sanitary Engineering

E-mail: B.M.vanBreukelen@tudelft.nl

2nd supervisor: L.C. Rietveld

Organisation: TU Delft

Faculty: Civil Engineering & Geosciences

Section: Sanitary Engineering

E-mail: L.C.Rietveld@tudelft.nl

External supervisor: P.J. Stuijfzand

Organisation: TU Delft - KWR

Faculty: Civil Engineering & Geosciences

Section: Geo-Engineering

E-mail: P.J.Stuyfzand@tudelft.nl

Supervision Field Factors

Company supervisor: K. Peña

Organisation: Field Factors

E-mail: kp@fieldfactors.com

B. REFERENCES

Abbar, B. *et al.* (2017) 'Experimental investigation on removal of heavy metals (Cu2+, Pb2+, and Zn2+) from aqueous solution by flax fibres', *Process Safety and Environmental Protection*. Institution of Chemical Engineers, 109(November 2019), pp. 639–647. doi: 10.1016/j.psep.2017.05.012.

Abdel-Shafy, H. I. and Mansour, M. S. M. (2016) 'A review on polycyclic aromatic hydrocarbons: Source, environmental impact, effect on human health and remediation', *Egyptian Journal of Petroleum*. Egyptian Petroleum Research Institute, 25(1), pp. 107–123. doi: 10.1016/j.ejpe.2015.03.011.

Al-Anbar, M. A. (2011) 'Thermodynamics Approach in the Adsorption of Heavy Metals', *Thermodynamics - Interaction Studies - Solids, Liquids and Gases*, (November 2011). doi: 10.5772/21326.

Ali, I. and Gupta, V. K. (2007) 'Advances in water treatment by adsorption technology', *Nature Protocols*, 1(6), pp. 2661–2667. doi: 10.1038/nprot.2006.370.

Appelo (2017) *PHREEQC version 3 downloads*. Available at: https://www.hydrochemistry.eu/ph3/index.html (Accessed: 8 October 2019).

Appelo, C. A. J. and Postma, D. (1993) *Geochemistry, Groundwater and Pollution*, *Vadose Zone Journal*. doi: 10.2136/vzj2005.1110br.

AquamineralsBV (2019) *Iron pellets and granulate*, *https://aquaminerals.com/iron-pellets/*.

ATSDR (2004) *Toxic profile copper*. Available at: https://www.atsdr.cdc.gov/ToxProfiles/tp132-c1-b.pdf.

Badawy, N. A. and Alkhalik, E. A. (2009) 'Effect of ionic strength on the adsorption of copper and chromium ions by vermiculite pure clay mineral', 170(3), pp. 1204–1209. doi: 10.1016/j.jhazmat.2009.05.100.

Ball and Nordstrom (1991) 'WATEQ4F'.

BC Ground Water Association (2007) 'Iron & Manganese in Groundwater', *The British Columbia Ground Water Association*.

Benjamin, M. M. *et al.* (1996) 'Sorption and filtration of metals using iron-oxide-coated sand', *Water Research*, 30(11), pp. 2609–2620. doi: 10.1016/S0043-1354(96)00161-3.

Bhargava, S. (2013) 'Ecological consequences of The Acid rain', *IOSR Journal of Applied Chemistry*, 5(4), pp. 19–24. doi: 10.9790/5736-0541924.

Blecken, G. T. *et al.* (2009a) 'Impact of a submerged zone and a carbon source on heavy metal removal in stormwater biofilters', *Ecological Engineering*, 35(5), pp. 769–778. doi: 10.1016/j.ecoleng.2008.12.009.

Blecken, G. T. *et al.* (2009b) 'Influence of intermittent wetting and drying conditions on heavy metal removal by stormwater biofilters', *Water Research*. Elsevier Ltd, 43(18), pp. 4590–4598. doi: 10.1016/j.watres.2009.07.008.

Bolan, N. S., Adriano, D. C. and Curtin, D. (2003) 'Soil acidification and liming interactions with nutrientand heavy metal transformationand bioavailability', *Advances in Agronomy*, 78, pp. 215–272. doi: 10.1016/S0065-2113(02)78006-1.

Boogaard, F. *et al.* (2014) 'Stormwater Quality Characteristics in (Dutch) Urban Areas and Performance of Settlement Basins', *Challenges*, 5(1), pp. 112–122. doi: 10.3390/challe5010112.

Boogaard, F. C., van Mossevelde, T. and Schipper, P. N. M. (2005) *Kwaliteitsaspecten infiltreren stedelijk water beter bekeken, Stowa Rapport 2005-23*, *STOWA*. Utrecht.

Borkovec, M. and Westall, J. (1983) 'Solution of the Poisson-Boltzmann equation for surface excesses of ions in the diffuse layer at the oxide-electrolyte interface', *Journal of Electroanalytical Chemistry*, 150(1–2), pp. 325–337. doi: 10.1016/S0022-0728(83)80214-9.

Bradl, H. B. (2004) 'Adsorption of heavy metal ions on soils and soils constituents', *Journal of Colloid and Interface Science*, 277(1), pp. 1–18. doi: 10.1016/j.jcis.2004.04.005.

van Breukelen, B. M. and Griffioen, J. (2004) 'Biogeochemical processes at the fringe of a landfill leachate pollution plume: potential for dissolved organic carbon, Fe(II), Mn(II), NH4, and CH4 oxidation.', *Journal of contaminant hydrology*, 73(1–4), pp. 181–205. doi: 10.1016/j.jconhyd.2004.01.001.

Van Breukelen, B. (2017) *CIE4495-13 Fundamentals of Water Treatment Module 4 Sorption Processes*.

Brezonik, P. L. and Stadelmann, T. H. (2002) 'Analysis and predictive models of stormwater runoff volumes, loads,

and pollutant concentrations from watersheds in the Twin Cities metropolitan area, Minnesota, USA', *Water Research*, 36(7), pp. 1743–1757. doi: 10.1016/S0043-1354(01)00375-X.

Brolsma, R. and Molenaar, R. (2015) *Application of Urban Water Balance Model for Utrecht Station Area Why a simple urban water balance model*.

Brown, C. J. *et al.* (1997) 'Water Quality in the Headwater Area', in *Urbanization and Recharge in the Vicinity of East Meadow Brook*. Part 4. New York.

Brown, R. R., Keath, N. and Wong, T. H. F. (2009) 'Urban water management in cities: historical, current and future regimes', *Water Science and Technology*, 59(5), pp. 847–855. doi: 10.2166/wst.2009.029.

Burkhardt, M. *et al.* (2011) 'Leaching of additives from construction materials to urban storm water runoff', *Water Science and Technology*, 63(9), pp. 1974–1982. doi: 10.2166/wst.2011.128.

Cao, H., Tsai, F. T.-C. and Rusch, K. A. (2010) 'Salinity and Soluble Organic Matter on Virus Sorption in Sand and Soil Columns', *Ground Water*. John Wiley & Sons, Ltd, 48(1), pp. 42–52. doi: 10.1111/j.1745-6584.2009.00645.x.

Cederkvist, K. *et al.* (2013) 'Behaviour of chromium(VI) in stormwater soil infiltration systems', *Applied Geochemistry*. doi: 10.1016/j.apgeochem.2013.05.011.

Certicon (2018) *Partijkeuring ijzerzand - Batch 12112018*.

Chandra Mouli, P., Venkata Mohan, S. and Reddy, S. J. (2005) 'Rainwater chemistry at a regional representative urban site: Influence of terrestrial sources on ionic composition', *Atmospheric Environment*, 39(6), pp. 999–1008. doi: 10.1016/j.atmosenv.2004.10.036.

Chesterfield (2019) *Stormwater Utility | Chesterfield County, VA*. Available at: https://www.chesterfield.gov/300/Stormwater-Utility?PREVIEW=YES (Accessed: 3 October 2019).

ClimateData (2019) *Klimaat Antwerpen: Klimatogram, Temperatuur grafiek en Klimaat tabel voor Antwerpen*. Available at: https://nl.climate-data.org/europa/belgie/vlaanderen/antwerpen-714869/ (Accessed: 2 October 2019).

CNT (2014) *The Prevalence and Cost of Urban Flooding*.

Contin, M. *et al.* (2007) 'Enhanced soil toxic metal fixation in iron (hydr)oxides by redox cycles', *Geoderma*, 140(1–2), pp. 164–175. doi: 10.1016/j.geoderma.2007.03.017.

Davis, A. P., Shokouhian, M. and Ni, S. (2001) 'Loading estimates of lead, copper, cadmium, and zinc in urban runoff from specific sources', *Chemosphere*, 44(5), pp. 997–1009. doi: 10.1016/S0045-6535(00)00561-0.

Davis, J. A. and Leckie, J. O. (1978) 'Surface ionization and complexation at the oxide/water interface', *Journal of Colloid and Interface Science*, 67(1).

Deletic, A. (1998) 'The first flush load of urban surface runoff', *Water Research*, 32(8), pp. 2462–2470. doi: 10.1016/S0043-1354(97)00470-3.

Deltares (2018) *Droogte in Nederland: uitdaging voor het waterbeheer*. Available at: https://www.deltares.nl/nl/blog/droogte-nederland-uitdaging-voor-het-waterbeheer/ (Accessed: 21 October 2019).

Derouane, E. G. and Chang, C. D. (2000) 'Confinement effects in the adsorption of simple bases by zeolites', *Microporous and Mesoporous Materials*. Elsevier Sci B.V., 35–36, pp. 425–433. doi: 10.1016/S1387-1811(99)00239-5.

Devi, R. R. *et al.* (2014) 'Removal of iron and arsenic (III) from drinking water using iron oxide-coated sand and limestone', *Applied Water Science*, 4(2), pp. 175–182. doi: 10.1007/s13201-013-0139-5.

Duncan, H. P. (1999) *Urban Stormwater Quality: A Statistical Overview*. Available at: https://ewater.org.au/archive/crcch/archive/pubs/pdfs/technical199903.pdf.

Dzombak, D. A. and Morel, F. M. M. (1990) 'Surface Complexation Modeling: Hydrous Ferric Oxide', in *Surface Complexation Modeling*. doi: 10.1002/9780470642665.

Eckelberry, R. (2016) *The Water Revolution Moving To A Decentralized System*, *Water Online*. Available at: https://www.wateronline.com/doc/the-water-revolution-moving-to-a-decentralized-system-0001 (Accessed: 8 January 2020).

ECORYS (2019) 'Economische schade door droogte in 2018'.

Eriksson, E. *et al.* (2007) 'Selected stormwater priority pollutants - a European perspective', *Science of the Total Environment*, 383(1–3), pp. 41–51. doi: 10.1016/j.scitotenv.2007.05.028.

Fernández-Remolar, D. C. (2014) 'Encyclopedia of Astrobiology', *Encyclopedia of Astrobiology*, pp. 1–4. doi: 10.1007/978-3-642-27833-4.

FieldFactors (2019) *Urban Waterbuffer Spangen | Field Factors*. Available at:

https://fieldfactors.com/en/projects/urban-waterbuffer-spangen (Accessed: 24 February 2020).

Fonseca, B. *et al.* (2011) 'Mobility of Cr, Pb, Cd, Cu and Zn in a loamy sand soil: A comparative study', *Geoderma*. Elsevier B.V., 164(3–4), pp. 232–237. doi: 10.1016/j.geoderma.2011.06.016.

Fränkische Rohrwerke (2016a) *Rigofill*.

Fränkische Rohrwerke (2016b) *Sedipoint*.

Gall, J. E., Boyd, R. S. and Rajakaruna, N. (2015) 'Transfer of heavy metals through terrestrial food webs: a review', *Environmental Monitoring and Assessment*, 187(4). doi: 10.1007/s10661-015-4436-3.

Geiger, F. *et al.* (2010) 'Persistent negative effects of pesticides on biodiversity and biological control potential on European farmland', *Basic and Applied Ecology*, 11(2), pp. 97–105. doi: 10.1016/j.baae.2009.12.001.

Genç-Fuhrman, H., Mikkelsen, P. S. and Ledin, A. (2007) 'Simultaneous removal of As, Cd, Cr, Cu, Ni and Zn from stormwater: Experimental comparison of 11 different sorbents', *Water Research*, 41(3), pp. 591–602. doi: 10.1016/j.watres.2006.10.024.

Glibert, P. M. *et al.* (2005) 'The Role of Eutrophication in the Global Proliferation of Harmful Algal Blooms: New Perpectives and New Approaches', *Oceanography*, 18(2), pp. 198–209.

Göbel, P., Dierkes, C. and Coldewey, W. G. (2007) 'Storm water runoff concentration matrix for urban areas', *Journal of Contaminant Hydrology*, 91(1–2), pp. 26–42. doi: 10.1016/j.jconhyd.2006.08.008.

Graham, N. J. D. and Collins, M. R. (2014) 'Slow Sand Filtration', in *Progress in Slow Sand Filtration and Alternative Biofiltration Processes*. London, UK: IWA, pp. 3–16.

Haque, M. M., Rahman, A. and Samali, B. (2016) 'Evaluation of climate change impacts on rainwater harvesting', *Journal of Cleaner Production*. Elsevier Ltd, 137, pp. 60–69. doi: 10.1016/j.jclepro.2016.07.038.

Hatt, B. *et al.* (2009) 'Adoption guidelines for stormwater biofiltration systems'.

Hatt, B. E., Deletic, A. and Fletcher, T. D. (2007) 'Stormwater reuse: Designing biofiltration systems for reliable treatment', *Water Science and Technology*, 55(4), pp. 201–209. doi: 10.2166/wst.2007.110.

Hatt, B. E., Fletcher, T. D. and Deletic, A. (2009) 'Hydrologic and pollutant removal performance of stormwater biofiltration systems at the field scale', *Journal of Hydrology*, 365(3–4), pp. 310–321. doi: 10.1016/j.jhydrol.2008.12.001.

van Hattum, T. *et al.* (2016) 'Towards water smart cities: climate adaptation is a huge opportunity to improve the quality of life in cities.', *Alterra-rapport - Wageningen University and Research Centre*, p. 60 pp.

Hayes, K. F. and Leckie, J. O. (1987) 'Modeling ionic strength effects on cation adsorption at hydrous oxide/solution interfaces', *Journal of Colloid And Interface Science*, 115(2), pp. 564–572. doi: 10.1016/0021-9797(87)90078-6.

Hejazi, M. I. *et al.* (2014) 'Integrated assessment of global water scarcity over the 21st century under multiple climate change mitigation policies', *Hydrology and Earth System Sciences*, 18(8), pp. 2859–2883. doi: 10.5194/hess-18-2859-2014.

Hendricks, D. W. (2006) *Water Treatment Unit Processes: Physical and Chemical*. CRC Press.

Hoegh-Guldberg, O. *et al.* (2015) *Impacts of 1.5°C of Global Warming on Natural and Human Systems*, *Global Warming of 1.5 ºC. An IPCC SPecial Report on the impacts of global warming of 1.5 ºC above pre-industrial levels and related global greenhouse gas emission pathways, in the context of strengthening the global response to the threat of climate chang*.

Hossain, F., Chang, N.-B. and Wanielista, M. (2009) 'Modeling Kinetics and Isotherms of Functionalized Filter Media for Nutrient Removal from Stormwater Dry Ponds', *Environmental Progress & Sustainable Energy*, 29(3), pp. 319–333.

HowStuffWorks (2019) *Why Is Salt Used to Melt Ice on the Roads in Winter? | HowStuffWorks*. Available at: https://science.howstuffworks.com/nature/climate-weather/atmospheric/road-salt.htm (Accessed: 2 October 2019).

Istanbulluoglu, E. (2018) *Sewer Overflows [Powerpoint slides]*.

Jenssen, P. and Pandey, M. (2012) *Centralised and Decentralised Systems for Water and Sanitation*. Available at: https://sswm.info/sswm-university-course/module-2-centralised-and-decentralised-systems-water-and-sanitation (Accessed: 9 December 2019).

Jeppu, G. P. and Clement, T. P. (2012) 'A modified Langmuir-Freundlich isotherm model for simulating pH-dependent adsorption effects', *Journal of Contaminant Hydrology*. Elsevier B.V., 129–130(December 2017), pp. 46–53. doi: 10.1016/j.jconhyd.2011.12.001.

Jonkman, S. N. *et al.* (2004) 'Cost benefit analysis of flood damage mitigation in the Netherlands', *HERON*, 49(1).

Kara, S. *et al.* (2016) 'Real time monitoring and control in water distribution systems for improving operational efficiency', *Desalination and Water Treatment*, 57(25), pp. 11506–11519. doi: 10.1080/19443994.2015.1069224.

Karge, H. G. and Weitkamp, J. (2008) *Fundamentals of Adsorption Equilibrium and Kinetics in Microporous Solids*. Springer. doi: 10.1007/978-3-540-73966-1.

Khaodhiar, S. *et al.* (2000) 'Copper, chromium, and arsenic adsorption and equilibrium modeling in an iron-oxide-coated sand, background electrolyte system', *Water, Air, and Soil Pollution*, 119(1–4), pp. 105–120. doi: 10.1023/A:1005109325539.

KMI (2019) 'Klimaatstatistieken van de Belgische gemeenten Antwerpen', pp. 1–6. Available at: https://www.meteo.be/resources/climatology/climateCity/pdf/climate_INS11002_nl.pdf.

KNMI (2011) *De Bosatlas van het Klimaat 1981-2010*. Noordhoff, Groningen.

KNMI (2018) *De droogte van 2018: Een analyse op basis van het potentiële neerslagtekort*.

Kremer (2014) *Veiligheidsinformatieblad: Kwarts*.

Kremer (2015) 'Prestatieverklaring kwartszand'.

Kulshrestha, U. *et al.* (1999) 'Measurements of acid rain over Indian Ocean and surface measurements of atmospheric aerosols at New Delhi during INDOEX pre-campaigns', *JSTOR*, 76(7), pp. 968–972. Available at: https://www.jstor.org/stable/24101374 (Accessed: 3 March 2020).

Kumar, U. (2011) 'Thermodynamics of the Adsorption of Cd(II) from Aqueous Solution on NCRH Cylinder', *International Journal of Environmental Science and Development*, 2(5), pp. 334–336. doi: 10.7763/ijesd.2011.v2.147.

Kummu, M. *et al.* (2016) 'The world's road to water scarcity: Shortage and stress in the 20th century and pathways towards sustainability', *Scientific Reports*. Nature Publishing Group, 6(May), pp. 1–16. doi: 10.1038/srep38495.

Lai, C. H., Lo, S. L. and Chiang, H. L. (2000) 'Adsorption/desorption properties of copper ions on the surface of iron-coated sand using BET and EDAX analyses', *Chemosphere*. doi: 10.1016/S0045-6535(99)00534-2.

Landsberg, H. E. (1981) *The Urban Climate*. 28th edn. Academic Press.

Langergraber, G. (2005) 'The role of plant uptake on the removal of organic matter and nutrients in subsurface flow constructed wetlands: A simulation study', *Water Science and Technology*, 51(9), pp. 213–223.

Leigh, N. G. and Lee, H. (2019) 'Sustainable and resilient urban water systems: The role of decentralization and planning', *Sustainability (Switzerland)*, 11(3). doi: 10.3390/su11030918.

Lemmen, G. and Boogaard, F. (2007) *STOWA Database Regenwaterkwaliteit*.

Lennard-Jones, J. E. (2014) 'Adsorption and Mineral Surface Reactions - Slides - Lecture 24'. Ithaca, New York: Cornell University, pp. 1–14.

Li, M. *et al.* (2016) 'Phosphate adsorption on metal oxides and metal hydroxides: A comparative review', *Environmental Reviews*, 24(3), pp. 319–332. doi: 10.1139/er-2015-0080.

Liu, Q. *et al.* (2019) 'Aluminum-impregnated biochar for adsorption of arsenic(V) in urban stormwater runoff', *Journal of Environmental Engineering (United States)*, 145(4), pp. 1–10. doi: 10.1061/(ASCE)EE.1943-7870.0001503.

Lo, S.-L., Jeng, H.-T. and Lai, C.-S. (1997) 'Characteristics and Adsorption Properties of Iron-Coated Sand', *Water Science and Technology*, 35(7), pp. 63–70. doi: 10.1192/bjp.111.479.1009-a.

Lützenkirchen, J. (1997) 'Ionic strength effects on cation sorption to oxides: Macroscopic observations and their significance in microscopic interpretation', *Journal of Colloid and Interface Science*, 195(1), pp. 149–155. doi: 10.1006/jcis.1997.5160.

Macnamara, J. and Derry, C. (2017) 'Pollution removal performance of laboratory simulations of Sydney's Street stormwater biofilters', *Water (Switzerland)*, 9(11). doi: 10.3390/w9110907.

McGrane, S. J. (2016) 'Impacts of urbanisation on hydrological and water quality dynamics, and urban water management: a review', *Hydrological Sciences Journal*. Taylor & Francis, 61(13), pp. 2295–2311. doi: 10.1080/02626667.2015.1128084.

Merdy, P., Gharbi, L. T. and Lucas, Y. (2009) 'Pb, Cu and Cr interactions with soil: Sorption experiments and modelling', *Colloids and Surfaces A: Physicochemical and Engineering Aspects*, 347(1–3), pp. 192–199. doi: 10.1016/j.colsurfa.2009.04.004.

Metcalf, L. and Eddy, H. P. (2003) *Wastewater Engineering*.

Mitani, T. *et al.* (1995) 'Effects of ionic strength on the adsorption of heavy metals by swollen chitosan beads', *Journal of Environmental Science and Health*, 30(3), pp. 669–674. doi: 10.1080/10934529509376224.

Muhammad, N. *et al.* (1997) 'Removal of heavy metals by slow sand filtration', in *23rd WEDC Conference*. Durban, South Africa, pp. 167–170.

Nair, S., Karimzadeh, L. and Merkel, B. J. (2014) 'Surface complexation modeling of Uranium(VI) sorption on quartz in the presence and absence of alkaline earth metals', *Environmental Earth Sciences*, 71(4), pp. 1737–1745. doi: 10.1007/s12665-013-2579-5.

NASA (2011) *Glossary*. Available at: https://earthobservatory.nasa.gov/glossary (Accessed: 18 March 2020).

Nicolopoulou-Stamati, P. *et al.* (2016) 'Chemical Pesticides and Human Health: The Urgent Need for a New Concept in Agriculture.', *Frontiers in public health*, 4(July), p. 148. doi: 10.3389/fpubh.2016.00148.

Oki, T. (2006) 'Global Hydrological Cycles and World Water', *Science*, (August), pp. 1068–1073. Available at: http://research.bpcrc.osu.edu/hydro/publications/OkiKanae_GlobalHydro_Science.pdf.

Page, D. *et al.* (2010) 'Characterising aquifer treatment for pathogens in managed aquifer recharge', *Water Science and Technology*, 62(9), pp. 2009–2015. doi: 10.2166/wst.2010.539.

Parkhurst, B. D. L. and Appelo, C. A. J. (1999) 'User ' S Guide To Phreeqc (Version 2)— a Computer Program for Speciation , and Inverse Geochemical Calculations', *Exchange Organizational Behavior Teaching Journal*, (Version 2).

Patel, H. (2019) 'Fixed - bed column adsorption study : a comprehensive review', *Applied Water Science*. Springer International Publishing, 9(3), pp. 1–17. doi: 10.1007/s13201-019-0927-7.

Payne, E. *et al.* (2015) *Adoption Guidelines for Stormwater Biofiltration Systems Cities as Water Supply Catchments*.

Payne, T. E. *et al.* (2013) 'Environmental Modelling & Software Guidelines for thermodynamic sorption modelling in the context of radioactive waste disposal', *Environmental Modelling and Software*. Elsevier Ltd, 42, pp. 143–156. doi: 10.1016/j.envsoft.2013.01.002.

Peralta-Videa, J. R. *et al.* (2009) 'The biochemistry of environmental heavy metal uptake by plants: Implications for the food chain', *International Journal of Biochemistry and Cell Biology*, 41(8–9), pp. 1665–1677. doi: 10.1016/j.biocel.2009.03.005.

Pimentel, D. (1995) 'Amounts of pesticides reaching target pests: Environmental impacts and ethics', *Journal of Agricultural and Environmental Ethics*, 8(1), pp. 17–29. doi: 10.1007/BF02286399.

Ranjan, P. and Prem, M. (2018) 'Schmutzdecke- A Filtration Layer of Slow Sand Filter', *International Journal of Current Microbiology and Applied Sciences*, 7(07), pp. 637–645. doi: 10.20546/ijcmas.2018.707.077.

Reddy, K. R., Xie, T. and Dastgheibi, S. (2014) 'Removal of heavy metals from urban stormwater runoff using different filter materials', *Journal of Environmental Chemical Engineering*. Elsevier Ltd, 2(1), pp. 282–292. doi: 10.1016/j.jece.2013.12.020.

Rijsberman, F. R. (2006) 'Water scarcity: Fact or fiction?', *Agricultural Water Management*, 80(1-3 SPEC. ISS.), pp. 5–22. doi: 10.1016/j.agwat.2005.07.001.

Sahmoune, M. N. (2019) 'Evaluation of thermodynamic parameters for adsorption of heavy metals by green adsorbents', *Environmental Chemistry Letters*. Springer International Publishing, 17(2), pp. 697–704. doi: 10.1007/s10311-018-00819-z.

Saladrich Català, C. (2019) *ANALYSIS OF BLUEBLOQS BIOFILTER BB1.0*, *Field Factors*.

Schijven, J. F. and de Roda Husman, A. M. (2005) *Effect of climate changes on waterborne disease in The Netherlands*, *Water Science and Technology*.

Sidhu, J. P. S. *et al.* (2012) 'Prevalence of human pathogens and indicators in stormwater runoff in Brisbane, Australia', *Water Research*. Elsevier Ltd, 46(20), pp. 6652–6660. doi: 10.1016/j.watres.2012.03.012.

Søberg, L. C., Viklander, M. and Blecken, G. T. (2014) 'The influence of temperature and salt on metal and sediment removal in stormwater biofilters', *Water Science and Technology*, 69(11), pp. 2295–2304. doi: 10.2166/wst.2014.161.

Speed, D. E. (2016) *Environmental aspects of planarization processes*, *Advances in Chemical Mechanical Planarization (CMP)*. Elsevier Ltd. doi: 10.1016/B978-0-08-100165-3.00010-3.

Spekreijse, P. (2019) 'Urban Water Buffer Rotterdam Sorption of Heavy Metals', (June).

Stietiya, M. H. (2010) 'Sorption mechanisms of zinc in different clay minerals and soil systems as influenced by various natural ligands', (May), p. 214.

STOWA (2007) 'Database Regenwater'.

Streat, M., Hellgardt, K. and Newton, N. L. R. (2008) 'Hydrous ferric oxide as an adsorbent in water treatment. Part 1. Preparation and physical characterization', *Process Safety and Environmental Protection*, 86(1 B), pp. 1–9. doi: 10.1016/j.psep.2007.10.007.

Tekerlekopoulou, A. G., Pavlou, S. and Vayenas, D. V. (2013) 'Removal of ammonium, iron and manganese from potable water in biofiltration units: A review', *Journal of Chemical Technology and Biotechnology*, 88(5), pp. 751–773. doi: 10.1002/jctb.4031.

Tilley, E. *et al.* (2014) *Compendium of Sanitation Systems and Technologies*. 2nd edn. Duebendorf, Switzerland.

Tschapek, M. and Wasowski, C. (1986) 'The wall effect of potential for determining the iep of quartz sand', *Electrochimica Acta*. Pergamon, 31(6), pp. 691–693. doi: 10.1016/0013-4686(86)87036-0.

US Environmental Protection Agency (2013) 'Extra_Polycyclic Aromatic Hydrocarbons (PAHs) Fact Sheet', *Environmental Health*, pp. 1–2. doi: 10.1016/j.egypro.2014.03.002.

USEPA (2000) *Technical Fact Sheet: Proposed Rule for Arsenic in Drinking Water and Clarification to Compliance and New Source Contaminants Monitoring*, *EPA*.

USGS (2014) *Common pollutants of concern and sources in stormwater runoff - Minnesota Stormwater Manual*. Available at: https://stormwater.pca.state.mn.us/index.php/Common_pollutants_of_concern_and_sources_in_stormwater_runoff (Accessed: 7 October 2019).

Vandergraaf, T. T., Ticknor, K. V. and Melnyk, T. W. (1992) *The selection and use of a sorption database for the geosphere model in the Canadian nuclear fuel waste management program*.

Van de Ven, F. H. M. (2016) *Water Management in Urban Areas*.

Van de Ven, F. H. M. (2017) *Lecture Slides CIE4491 Water & Its management in Urban Areas*.

Vlaamse Milieumaatschappij (2019) *Kwaliteit drinkwater per leveringsgebied*. Available at: https://www.vmm.be/data/kwaliteit-drinkwater-per-leveringsgebied/kwaliteit-drinkwater-per-leveringsgebied (Accessed: 5 July 2019).

Volz, C. (2017) *Lecture 13, Retardation of Chemical Movement in Aquifers and Biodegradation of Chemicals in Aquifers and the Unsaturated Zone*.

VROM (2009) *Infiltratiebesluit bodembescherming*.

VROM (2011) *Drinkwaterbesluit*.

Walsh, C. J. *et al.* (2016) 'Principles for urban stormwater management to protect stream ecosystems', *Freshwater Science*, 35(1), pp. 398–411. doi: 10.1086/685284.

Wang, C. *et al.* (2015) 'An invisible soil acidification: Critical role of soil carbonate and its impact on heavy metal bioavailability', *Scientific Reports*. Nature Publishing Group, 5(November 2014), pp. 1–9. doi: 10.1038/srep12735.

WBCSD (2020) *Circular water management*. Available at: https://www.wbcsd.org/Programs/Food-and-Nature/Water/Circular-water-management (Accessed: 24 February 2020).

Weatherbase (2019) *Amsterdam, Netherlands Köppen Climate Classification (Weatherbase)*. Available at: https://www.weatherbase.com/weather/weather-summary.php3?s=4260&cityname=Amsterdam,+Netherlands (Accessed: 2 October 2019).

Whitacre, J. (2014) *Biofiltration Systems for Stormwater Management | Fourth Corner Nurseries*. Available at: http://fourthcornernurseries.com/biofiltration-systems-for-stormwater-management-the-vegetation-component/ (Accessed: 6 March 2020).

Wijesiri, B. *et al.* (2016) 'Assessing uncertainty in stormwater quality modelling', *Water Research*. Elsevier Ltd, 103, pp. 10–20. doi: 10.1016/j.watres.2016.07.011.

Yong, S. T. Y. and Chen, W. (2002) 'Modeling the relationship between land use and surface water quality', *Journal of Environmental Management*, 66(4), pp. 377–393. doi: 10.1006/jema.2002.0593.

Young, T. M. and Weber, W. J. (2018) 'Sorption and Desorption Rates for Neutral Organic Compounds in Soils', in. John Wiley & Sons, Ltd, pp. 519–561. doi: 10.2136/sssabookser8.c11.

Zhang, J. *et al.* (1999) 'Factors influencing changes in rainwater composition from urban versus remote regions of the Yellow Sea', *Journal of Geophysical Research Atmospheres*, 104(D1), pp. 1631–1644. doi: 10.1029/1998JD100019.

Zhang, Y. *et al.* (2010) 'Alternative water resources for rural residential development in Western Australia', *Water Resources Management*, 24(1), pp. 25–36. doi: 10.1007/s11269-009-9435-0.

Zuurbier, K. *et al.* (2019) ‘Preventing pluvial flooding and water shortages by integrating local aquifer storage and recovery in urban areas’, *ISMAR10 Symposium*, pp. 1–9.

Zuurbier, K. and van Dooren, T. (2019) *Urban Waterbuffer Spangen: Resultaten*.

C. APPENDICES

I. DUTCH INFILTRATION STANDARDS

Infiltratiebesluit bodembescherming. Geldend van 22-12-2009 t/m heden

nr.	parameter	unit	protection level (dissolved)[1]
Macro parameters			
1	acidity (pH)	–	– [2]
2	suspended solids	mg/l	0.5 [3]
3	calcium (Ca^{++})	mg/l	– [2]
4	chloride (Cl^-)	mg/l	200 [2 3]
5	bicarbonate (HCO_3^-)	mg/l	– [2]
6	sodium (Na^+)	mg/l	120 [2 3]
7	ammonium (NH_4^+)	mg/l-N	2.5
8	nitrate (NO_3^-)	mg/l-N	5.6 [2 3]
9	total-phosphate (PO_4^2-tot)	mg/l-P	0,4
10	sulphate (SO_4^2-)	mg/l	150 [2]
11	fluoride (F^-)	mg/l	1
12	cyanides total (CN (tot))	µg/l	10
Heavy Metals			
13	arsenic (As)	µg/l	10
14	barium (Ba)	µg/l	200 [3]
15	cadmium (Cd)	µg/l	0.4
l6	cobalt (Co)	µg/l	20
l7	chromium (Cr)	µg/l	2
18	copper(Cu)	µg/l	15
19	mercury (Hg)	µg/l	0.05
20	nickel (Ni)	µg/l	15
2l	lead (Pb)	µg/l	15
22	zinc (Zn)	µg/l	65
Pesticides			
23	sum pesticides	µg/l	0.5 [4]
Organochlorine pesticides			
24	sum (organochlorine pesticides)	µg/l	0.1
25	endosulfan	µg/l	0.05

26	α-HCH	µg/l	0.05
27	-HCH (lindane)	µg/l	0.05
28	DDT (incl. DDD and DDE)	µg/l	0.05
29	dichloropropene	µg/l	0.05
30	aldrin	µg/l	0,05
3l	dieldrin	µg/l	0.05
32	endrin	µg/l	0.05
33	heptachlor	µg/l	0.05
34	heptachlor epoxide	µg/l	0.05
35	hexachlorobutadiene	µg/l	0.05
36	hexachlorobenzene	µg/l	0.05
Organophosphorus pesticides			
37	azinphos-methyl	µg/l	0.1
38	dichlorvos	µg/l	0.1
39	dimethoate	µg/l	0.1
40	mevinphos	µg/l	0.1
41	parathion	µg/l	0.1
Triazines/triazolones/anilids			
42	atrazine	µg/l	0.1
43	simazine	µg/l	0.1
44	metolachlor	µg/l	0.1
Chlorophenoxy herbicides			
45	2-methyl-4-chloorfenoxy-azijnzuur (MCPA)	µg/l	0.1
46	mecoprop	µg/l	0.1
47	2,4-dichloorfenoxy-azijnzuur (2,4 D)	µg/l	0.1
Urea herbicides			
48	chlortoluron	µg/l	0.1
49	isoproturon	µg/l	0.1
50	metoxuron	µg/l	0.1
51	linuron	µg/l	0.1
Chlorophenols			
52	trichlorophenol	µg/l	0.1
53	tetrachlorophenol	µg/l	0.1
54	pentachlorophenol	µg/l	0.1
Miscellaneous			
55	dinoseb	µg/l	0.1

56	2,4 dinitrophenol	µg/l	0.1
57	bentazon	µg/l	0.1
Oil			
58	mineral oil	µg/l	200
Polycyclic Aromatic Carbohydrates (PAH)			
59	naphthalene	µg/l	0.1
60	anthracene	µg/l	0.02
61	phenanthrene	µg/l	0.02
62	chrysene	µg/l	0.02
63	fluoranthene	µg/l	∑ 0.1
64	benzo(a)anthracene	µg/l	
65	benzo(k)fluoranthene	µg/l	
66	benzo(a)pyrene	µg/l	
67	benzo(ghi)perylene	µg/l	
68	indeno(l23cd)pyrene	µg/l	
Halogenated hydrocarbons			
69	trichloroethene	µg/l	0.5
70	tetrachloroethene	µg/l	0.5
71	trihalomethanes (THM's)	µg/l	2 [5]
72	dichlorophenol	µg/l	0.5
73	adsorbable organic halides (AOX)	µg/l	30 [6]

[1] The protection limit for suspended solids does not include the dissolved fraction.

[2] Point of interest for granting permit of local situation.

[3] For the infiltration water a 70 days a year a concentration above the here stated is allowed, as long as the following maximum concentration are not exceeded: suspended solids 2 mg/l; Cl^- 300 mg/l; Na^+ 180 mg/l and NO_3^2-11,2 mgN/l; Ba 300 µg/l.

[4] Sum of the concentrations in this list of pesticides, of which the detected result < detection limit a O is allocated.

[5] THM is determined as sum of concentrations of chloroform, bromodichloromethane, dibromochloromethane and bromoform. If a transport chlorine disinfection is applied, the allowed maximum is 70 µg/l.

[6] If a transport chlorine disinfection is applied, the allowed maximum is 100 µg/l.

II. OPERATION PROTOCOL AARTSELAAR DEMO

This information of this chapter is written in Dutch for the purpose of understanding for Aquafin personnel.

Handleiding operatie Bluebloqs demo Aartselaar

		Handeling	Bijzonderheden
A1		**Opslag tank aanvullen**	
	1	Dakwater vult de opslagtank. De opslagtank dient gevuld te worden tot 4m3 voor iedere run. Open de kraan onder aan de opslagtank.	
	2	Vul de tank bij met kraanwater, zie gelogde data S:CAN. De vlotter geeft aan hoeveel water al in de tank is.	
	3	Vul tot 1400mm om een volume van 4m^3 in de tank te bewerkstelligen	
	4	Draai de tapwater kraan dicht	
A2		**Doorlopen met mix met chemicaliën**	
	1	Controleer of de opslagtank gevuld is tot 4m^3.	
	2	Neem de 1L fles van de opslag met de bijbehorende datum. Draag beschermende handshoenen.	
	3	Schud de fles rustig en plaats een magneet.	
	4	Plaats de fles naast de opslagtank op een mixer en sluit aan op de kleine pomp. Zet de mixer aan en laat een kleine kolk ontstaan.	
	5	Zijn zowel de pomp als de opslagtank aangesloten, kunnen beide pompen aan worden gezet. De grote pomp loopt leeg met 0.5 m3/h en de kleine mix loopt leeg met 0.125 L/h, beide in 8 uur geleegd.	
	6	Controleer of beide pompen lopen. Het water loopt na enige tijd op de biofilter.	
A3		**Afsluiten van het systeem**	
	1	Na 8 uur verloop zullen de opslagtank en de mix met chemicalies zijn leeggepompt. Controleer of de pompen zijn uitgeschakeld.	
	2	De fles met de mix kan worden teruggeplaatst in het lab.	

Handleiding monsters nemen

		Handeling	Bijzonderheden
B1		**Monster van opslagtank (Storage)**	
	1	Roer rustig in het water, zodat het water mengt.	

	Handeling	Bijzonderheden
2	Neem twee 15 mL monsterbuisjes (rode dop). Neem een 180 mL monsterbuisje. Noteer op alle **"monsternummer" (S1-S) + "datum".**	
3	Neem een 50 mL injectiespuit. Creeer **langzaam** een vacuum om het water te laten stromen in de injectiespuit. Plaats een vinger op de spuit. Meet de zuurstofconcentratie met een sonde.	
4	Plaats een 0.45 µm filter op de injectie spuit.	
5	Injecteer deze dosis water in twee monsterbuisjes van 15 mL (rode dop). De ene volledig 15 mL en de andere tot 14 mL (om later aan te zuren). Geef de laatste een rode stip om aan te geven dat deze wordt aangezuurd.	
6	Neem een ongefilterd monster 180 mL en test op DO, pH, EC. DO ter plaatse en pH, EC en alkaliniteit in het lab. Instructies per parameter meting volgt hieronder.	
7	Noteer in het logboek het tijdstip en datum van het nemen van het monster. Noteer ook eventuele aanmerkingen en/of condities van het systeem.	
8	Bewaar de alle 15mL monsters verticaal geplaatst in de koelkast van het laboratorium.	

	Handeling	Bijzonderheden
B2-B6	**Monsters van de biofilter**	
1	Op de buisjes aangegeven welke diepte het is. S2-5 = 5cm diepte. Neem twee monsterbuisjes van 15 mL (rode dop). Neem een monsterbuisje van 180 mL. Noteer op de monsters **"monsternummer (S2-5) + datum".** (Verschilt dus per diepte)	
2	Neem een 50 mL injectiespuit. Creeer **langzaam** een vacuum om het water te laten stromen in de injectiespuit. Zo komt het water van de juiste waterlaag. **Gooi deze eerste dosis weg, omdat het stilstaand water bevat**.	
3	Herhaal bovenstaande en neem een tweede dosis, deze wordt wel gebruikt. Plaats een vinger op de spuit. Meet de zuurstofconcentratie met een sonde.	
4	Plaats een 0.45 µm filter op de injectie spuit.	
5	Injecteer deze dosis water in twee monsterbuisjes van 15 mL (rode dop). De ene volledig 15 mL en de andere tot 14 mL (om later aan te zuren). Geef de laatste een rode stip om aan te geven dat deze wordt aangezuurd.	
6	Neem een ongefilterd monster 180 mL en test op DO, pH, EC. DO ter plaatse en pH, EC en alkaliniteit in het lab. Instructies per parameter meting volgt hieronder.	
7	Noteer in het logboek het tijdstip en datum van het nemen van het monster. Noteer ook eventuele aanmerkingen en/of condities van het systeem.	
8	Herhaal bovenstaande ook voor de andere monsters S3-10 = 10 cm; S4-20 = 20 cm, S5-55 = 55 cm, S6-70 = 70 cm. Herhaal stap 1-8.	
9	Bewaar de alle 15mL monsters verticaal geplaatst in de koelkast van het lab.	

	Handeling	Bijzonderheden
B7	**Monster van de drainage tank (Drainage)**	
18	Neem twee monsterbuisjes van 15 mL. Neem een monsterbuisje van 180 mL. Noteer op de monsters **"monsternummer (S7-D) + datum".**	
19	Roer rustig in het water, zodat het water mengt.	
20	Gebruik een 50 mL injectiespuit en neem een monster in het midden op enige diepte onder het waterniveau. Plaats een vinger op de spuit. Meet de zuurstofconcentratie met een sonde.	
21	Plaats een 0.45 µm filter op de injectie spuit.	
22	Injecteer deze dosis water in twee monsterbuisjes van 15 mL (rode dop). De ene volledig 15 mL en de andere tot 14 mL (om later aan te zuren). Geef de laatste een rode stip om aan te geven dat deze wordt aangezuurd.	
23	Neem een ongefilterd monster 180 mL en test op DO, pH, EC. DO ter plaats en pH, EC en alkaliniteit in het lab. Instructies per parameter meting volgt hieronder.	
24	Noteer in het logboek het tijdstip en datum van het nemen van het monster. Noteer ook eventuele aanmerkingen en/of condities van het systeem.	
25	Bewaar de alle 15mL monsters verticaal geplaatst in de koelkast van het lab.	

	Handeling	Bijzonderheden
B8	**Monster van dakwater (Roof)**	
1	Neem twee monsterbuisjes van 15 mL. Neem een monsterbuisje van 180 mL. Noteer op de monsters **"S8-R + datum"**	
2	Gebruik een 50 mL injectiespuit en neem een monster in het midden op enige diepte onder het waterniveau. Plaats een vinger op de spuit. Meet de zuurstofconcentratie met een sonde.	
3	Plaats een 0.45 µm filter op de injectie spuit	
4	Injecteer deze dosis water in twee monsterbuisjes van 15 mL (rode dop). De ene volledig 15 mL en de andere tot 14 mL (om later aan te zuren). Geef de laatste een rode stip om aan te geven dat deze wordt aangezuurd.	
5	Neem een ongefilterd monster 180 mL en test op DO, pH, EC. DO ter plaatse en pH, EC en alkaliniteit in het lab. Instructies per parameter meting volgt hieronder	
6	Noteer in het logboek het tijdstip en datum van het nemen van het monster. Noteer ook eventuele aanmerkingen en/of condities van het systeem.	
7	Bewaar de alle 15mL monsters verticaal geplaatst in de koelkast van het lab.	

III. APPENDIX : AARTSELAAR DEMO RESULTS

Cycle A

191010. pilot. Aquafin sampling summer/autumn 2019								
	Influent	Effluent	Biofilter 5	Biofilter 10	Biofilter 20	Biofilter 40	Biofilter 55	Biofilter 70
code	080819IN	080819UIT	080819BB5	080819BB10	080819BB20	080819BB40	080819BB55	080819BB70
In situ								
Temperature (EC) (°C)	22.4	23	22.9	23.9	24.3	24.5	24.8	27.7
EC (µS/cm)	592	520	557	562	561	556	556	1555
DO (mg/L)	6.1	3.2	5.3	3.6	4.3	3.3	3	3.5
pH (-)	8.14	7.56	7.97	8.58	7.91	8.63	7.7	7.91
Suspended Solids (mg/L)	<2	23						
Turbidity (NTU)								
Macro								
	Influent	Effluent	Biofilter 5	Biofilter 10	Biofilter 20	Biofilter 40	Biofilter 55	Biofilter 70
Chloride Cl (mg/L)	56.884	54.448	56.382	55.468	55.462	56.842	55.872	55.618
Sodium Na (mg/L)	42.734	39.74	41.666	41.82	41.82	42.096	41.744	41.516
Fluorine F (mg/L)	2.272	2.234	2.26	2.254	2.256	2.26	2.256	2.26
Bromine Br (mg/L)	n.d.	n.d.	n.d.	n.d.	n.d.	n.d.	n.d.	n.d.
Potassium K (mg/L)	5.56	5.024	5.396	5.48	5.698	5.506	5.092	5.756
Calcium Ca (mg/L)	66.62	62.798	67.396	68.178	67.672	68.352	66.956	67.072
	55	50						
Magnesium Mg (mg/L)	7.74	7.206	7.59	7.676	7.574	7.61	7.584	7.4
	7.36	7.57						
Iron Fe (mg/L)	0.052	0.100	3.66E-02	5.96E-02	4.81E-02	5.95E-02	6.07E-02	6.24E-02

Manganese Mn (mg/L)	0.001	0.077	1.67E-02	2.95E-02	3.28E-02	5.77E-02	9.44E-02	2.65E-01
Bicarbonate (HCO3-) (mg/L)								
Ammonium NH4 (mg/L)	n.d.	5.218	n.d.	n.d.	n.d.	n.d.	n.d.	n.d.
Nitrate NO3 (mg/L)	5.392	5.846	5.306	5.216	5.202	5.314	5.116	5.066
Nitrite NO2 (mg/L)	n.d.	n.d.	n.d.	n.d.	n.d.	n.d.	n.d.	n.d.
Total Phosphate PO4 (mg/L)	n.d.	n.d.	n.d.	n.d.	n.d.	n.d.	n.d.	n.d.
Sulphate SO4 (mg/L)	61.87	59.692	61.386	60.482	60.534	62.084	60.818	60.728
Total hardness (meq/L)								
TOC (mg C/L)	2.8	4.9						
Heavy Metals								
	Influent	Effluent	Biofilter 5	Biofilter 10	Biofilter 20	Biofilter 40	Biofilter 55	Biofilter 70
Arsenic As (µg/L)	n.d.	n.d.	n.d.	n.d.	n.d.	n.d.	n.d.	n.d.
Cadmium Cd (µg/L)	0.0462	1.0582	0.1287	0.0407	0.088	1.3893	0.6589	0.0765
Copper Cu (µg/L)	9.603	13.9491	8.3215	8.5679	8.4073	15.0172	8.4821	7.44
Lead Pb (µg/L)	2.7302	41.2016	0.5016	1.1649	1.1264	100.0186	27.8905	2.0235
Nickel Ni (µg/L)	89.4146	53.5117	89.3981	87.7756	88.0429	41.7626	41.4095	54.879
Zinc Zn (µg/L)	7.7792	22.7139	6.8277	6.5241	8.3171	9.0585	8.1004	7.1295
Molybdenum Mo (µg/L)	2.9546	2.9942	3.1383	3.1416	3.4155	3.1482	3.0459	2.805

Cycle B

190829. pilot. Aquafin sampling summer/autumn 2019								
	Influent	Effluent	Biofilter 5	Biofilter 10	Biofilter 20	Biofilter 40	Biofilter 55	Biofilter 70
code	290819IN	290819UIT	290819BB5	290819BB10	290819BB20	290819BB40	290819BB55	290819BB70
In situ								
Temperature (EC) (°C)	21.5	23.5	23.7	23.4	24.5	24.2	24.3	25.6
EC (µS/cm)	512	523	809	573	573	583	566	889
DO (mg/L)	5.8	0.7	5.2	4.1	6.1	4.2	3.9	2.7
pH (-)	7.85	7.85	10.21	7.85	7.46	7.62	7.57	7.71
Suspended Solids (mg/L)	3	10						
Turbidity (NTU)	<0.1	<0.1						
Macro								
	Influent	Effluent	Biofilter 5	Biofilter 10	Biofilter 20	Biofilter 40	Biofilter 55	Biofilter 70
Chloride Cl (mg/L)	49.83	53.294	50.986	49.966	49.316	49.816	49.414	49.504
Sodium Na (mg/L)	32.652	35.324	33.582	33.274	32.854	33.058	33.05	32.916
Fluorine F (mg/L)	1.416	1.418	1.392	1.384	1.398	1.39	1.402	1.432
Bromine Br (mg/L)	2.362	2.366	2.362	2.356	2.362	2.362	2.368	2.366
Potassium K (mg/L)	4.43	4.824	4.434	4.37	4.562	4.592	4.584	5.888
Calcium Ca (mg/L)	46.672	52.198	50.998	50.662	49.774	50.38	50.82	49.816
Magnesium Mg (mg/L)	6.292	6.428	6.634	6.582	6.428	6.54	6.482	6.172
Iron Fe (mg/L)	0.03172	0.04714	0.03035	0.02418	0.01698	0.01583	0.01657	0.99561
Manganese Mn (mg/L)	0.01972	0.127362	0.00601	0.00508	0.00523	0.00824	0.01676	n.d.

Bicarbonate (HCO3-) (mg/L)								
Ammonium NH4 (mg/L)	2.154	0	0.806	0.684	0.908	0.364	0.068	0.33
Nitrate NO3 (mg/L)	9.364	9.98	8.808	8.942	9.3	9.776	9.722	10.768
Nitrite NO2 (mg/L)	n.d.	2.972	3.114	3.042	3016	3.034	3.042	3.124
Total Phosphate PO4 (mg/L)	2.06							
Sulphate SO4 (mg/L)	51.248	57.386	52.358	51.562	51.35	52.166	51.634	51.794
Total hardness (meq/L)								
TOC (mg C/L)	12	12						
Heavy Metals								
	Influent	Effluent	Biofilter 5	Biofilter 10	Biofilter 20	Biofilter 40	Biofilter 55	Biofilter 70
Arsenic As (µg/L)	0.9482	1.13	0.6916	0.6913	0.7621	0.8082	0.8628	0.8587
Cadmium Cd (µg/L)	3.07	0.0768	0.1994	0.0724	0.0566	0.04	0.0354	0.0212
Copper Cu (µg/L)	43.01	5.62	15.04	11.57	10.63	7.81	6.92	3.07
Lead Pb (µg/L)	12.64	0.1942	1.27	0.9438	1.05	0.9662	0.7304	3.56
Nickel Ni (µg/L)	14.88	4.62	5.31	4.28	4.11	3.49	3.5	4.18
Zinc Zn (µg/L)	353.415	9.07	17.02	6.46	5.58	3.44	3.95	11.53
Molybdenum Mo (µg/L)								

Cycle C

190919. pilot. Aquafin sampling summer/autumn 2019								
	Influent	Effluent	Biofilter 5	Biofilter 10	Biofilter 20	Biofilter 40	Biofilter 55	Biofilter 70
code	190919IN	190919UIT	190919BB5	190919BB10	190919BB20	190919BB40	190919BB55	190919BB70
In situ								
Temperature (EC) (°C)	15.7	14.0	16.4	17.5	16.8	16.0	15.9	15.7
EC (µS/cm)	636	385	636	637	600	664	574	557
DO (mg/L)	10.8		2.8	4.1	4.0			
pH (-)	7.6	6.82	6.86	6.94	7.00	6.93	6.79	6.6
Suspended Solids (mg/L)								
Turbidity (NTU)								
Macro								
	Influent	Effluent	Biofilter 5	Biofilter 10	Biofilter 20	Biofilter 40	Biofilter 55	Biofilter 70
Chloride Cl (mg/L)	120.068	90.198	90.37	89.622	87.086	90.738	90.244	86.112
Sodium Na (mg/L)	57.672	57.982	58.518	58.654	57.292	59.114	59.014	56.892
Fluorine F (mg/L)	1.936	1.882	1.898	1.888	1.888	1.884	1.94	n.d.
Bromine Br (mg/L)	0.622	0.654	0.636	0.626	0.638	0.648	0.642	0.656
Potassium K (mg/L)	7.45	6.762	7.07	6.982	6.36	6.928	7.31	8.266
Calcium Ca (mg/L)	70.126	73.952	74.468	74.674	73.448	75.048	74.398	74.784
Magnesium Mg (mg/L)	9.13	9.18	9.262	9.348	9.16	9.146	9.29	9.246
Iron Fe (mg/L)	0.16684	0.17571	0.16488	0.17766	0.18268	0.17994	0.17395	0.18773
Manganese Mn (mg/L)	0.00025	0.01609	0.00087	0.00094	0.00173	0.00386	0.00772	0.01428

Bicarbonate (HCO3-) (mg/L)								
Ammonium NH4 (mg/L)	14.648	0						
Nitrate NO3 (mg/L)	3.884	6.256	5.562	5.798	6.39	5.478	7.614	6.812
Nitrite NO2 (mg/L)	n.d.	n.d.	1.46	1.442	1.532	n.d,.	n.d.	1.336
Total Phosphate PO4 (mg/L)	0	0	0	0	0	0	0	0
Sulphate SO4 (mg/L)	82.528	84.384	82.8	83.576	83.576	81.682	84.208	78.954
Total hardness (meq/L)								
TOC (mg C/L)								
Heavy Metals								
	Influent	Effluent	Biofilter 5	Biofilter 10	Biofilter 20	Biofilter 40	Biofilter 55	Biofilter 70
Arsenic As (µg/L)	0.4935	0.743	0.4128	0.446	0.506	0.5577	0.5446	0.6551
Cadmium Cd (µg/L)	26.96	0.1358	0.5019	0.3789	0.3169	0.1772	0.1357	0.7647
Copper Cu (µg/L)	157.131	3.65	5.93	5.33	4.49	4.11	3.66	5.37
Lead Pb (µg/L)	11.42	0.0878	0.3315	0.5448	0.1845	0.0929	0.0802	0.4831
Nickel Ni (µg/L)	101.38	6.3	8.5	7.99	7.85	6.42	6.19	9.41
Zinc Zn (µg/L)	2596.5	6.02	42.41	21.78	8.81	4.84	2.33	67.66
Molybdenum Mo (µg/L)	3.56	3.04	2.72	2.87	2.80	2.84	3.04	3.36

Cycle D

191010. pilot. Aquafin sampling summer/autumn 2019								
	Influent	Effluent	Biofilter 5	Biofilter 10	Biofilter 20	Biofilter 40	Biofilter 55	Biofilter 70
code	191010IN	191010UIT	191010BB5	191010BB10	191010BB20	191010BB40	191010BB55	191010BB70
In situ								
Temperature (EC) (°C)	15.7	14	16.4	17.5	16.8	16	15.9	15.7
EC (µS/cm)	636	385	636	637	600	664	574	557
DO (mg/L)	10.8		2.8	4.1	4.0			
pH (-)	7.6	6.82	6.86	6.94	7.00	6.93	6.79	6.6
Suspended Solids (mg/L)								
Turbidity (NTU)								
Macro								
	Influent	Effluent	Biofilter 5	Biofilter 10	Biofilter 20	Biofilter 40	Biofilter 55	Biofilter 70
Chloride Cl (mg/L)	65.99	36.488	64.682	64.588	64.868	63.954	65.862	65.77
Sodium Na (mg/L)	47.696	22.82	45.748	41.288	44.686	42.486	41.68	46.378
Fluorine F (mg/L)	2.49	2.49	2.442	2.362	2.362	2.296	2.302	2.316
Bromine Br (mg/L)	0	0	0	0	0	0	0	0
Potassium K (mg/L)	16.15	13.572	15.314	15.314	15.406	15.924	14.582	15.26
Calcium Ca (mg/L)	66.802	38.028	64.026	62.082	61.998	52.772	57.884	55.504
Magnesium Mg (mg/L)	8.764	5.128	8.158	7.592	7.618	6.326	7.06	7.244
Iron Fe (mg/L)	0.07858	0.08718	0.07256	0.06368	0.06345	0.0742	0.04775	0.1165
Manganese Mn (mg/L)	0.00268	0.1230422	0.00402	0.00819	0.02176	0.03436	0.05847	0.05474

Bicarbonate (HCO3-) (mg/L)								
Ammonium NH4 (mg/L)	2.932	3.562	2.412	2.718	3.458	9.042	4.918	5.8
Nitrate NO3 (mg/L)	6.8	9.114	7.202	9.518	8.314	8.884	10.054	9.05
Nitrite NO2 (mg/L)	0	0	0	1.456	0	0	0	0
Total Phosphate PO4 (mg/L)	0	0	0	0	0	0	0	0
Sulphate SO4 (mg/L)	71.808	34.432	70.044	68.696	69.906	66.684	68.846	70.35
Total hardness (meq/L)								
TOC (mg C/L)								
Heavy Metals								
	Influent	Effluent	Biofilter 5	Biofilter 10	Biofilter 20	Biofilter 40	Biofilter 55	Biofilter 70
Arsenic As (µg/L)	0.4935	0.743	0.4128	0.446	0.506	0.5577	0.5446	0.6551
Cadmium Cd (µg/L)	6.64	0.2284	0.7205	0.5125	1.04	0.405	0.5062	0.501
Copper Cu (µg/L)	66.06	2.81	6.63	4.33	4.06	3.26	3.28	2.99
Lead Pb (µg/L)	52.93	0.17	0.67	0.26	0.14	0.14	0.25	0.23
Nickel Ni (µg/L)	27.23	5.78	10.76	8.23	14.62	7.78	7.05	9.2
Zinc Zn (µg/L)	735.11	16.52	134.3707	67.75	129.242	30.16	27.19	19.94
Molybdenum Mo (µg/L)	2.36	1.13	1.54	1.56	1.79	1.91	1.57	1.87

Cycle E

191104. pilot. Aquafin sampling summer/autumn 2019								
	Influent	Effluent	Biofilter 5	Biofilter 10	Biofilter 20	Biofilter 40	Biofilter 55	Biofilter 70
code	191104IN_x	191104UIT_x	191104BB5_x	191104BB10_x	191104BB20_x	191104BB40_x	191104BB55_x	191104BB70_x
In situ								
Temperature (EC) (°C)	11.8	12.5	11.9	12.2	12.1	11.9	12.5	12.8
EC (µS/cm)	403	665	455	427	430	457	468	536
DO (mg/L)								
pH (-)	7.78	7.42	7.67	7.93	7.65	7.48	7.36	7.47
Suspended Solids (mg/L)								
Turbidity (NTU)								
Macro								
	Influent	Effluent	Biofilter 5	Biofilter 10	Biofilter 20	Biofilter 40	Biofilter 55	Biofilter 70
Chloride Cl (mg/L)	39.114	51.518	43.656	36.848	34.616	37.388	36.454	36.022
Sodium Na (mg/L)								
Fluorine F (mg/L)	1.27	1.302	1.358	1.354	1.338	1.36	1.346	1.324
Bromine Br (mg/L)								
Potassium K (mg/L)								
Calcium Ca (mg/L)	14.458	18.732	15.914	15.166	15.338	16.032	15.928	15.868
Magnesium Mg (mg/L)								
Iron Fe (mg/L)	171.15	13.11	58.39	95.68	86.53	42	36.54	31.81

Manganese Mn (mg/L)	100.51	4.59	2.2	6.25	2.01	3.93	43.62	19.84
Bicarbonate (HCO3-) (mg/L)								
Ammonium NH4 (mg/L)								
Nitrate NO3 (mg/L)	3.186	3.756	4.46	3.466	3.332	3.882	3.902	3.106
Nitrite NO2 (mg/L)	0	0	0	0	0	0	0	0
Total Phosphate PO4 (mg/L)	0	0	0	0	0	0	0	0
Sulphate SO4 (mg/L)	39.294	48.684	43.998	37.454	34.816	37.202	36.764	35.576
Total hardness (meq/L)								
TOC (mg C/L)								
Heavy Metals								
	Influent	Effluent	Biofilter 5	Biofilter 10	Biofilter 20	Biofilter 40	Biofilter 55	Biofilter 70
Arsenic As (µg/L)	0.5	0.51	0.37	0.38	0.4	0.39	0.46	0.46
Cadmium Cd (µg/L)	1.98	0.49	0.48	0.37	0.47	0.36	0.45	1.4
Copper Cu (µg/L)	21.54	3.47	8.32	8.39	8.12	5.27	4.56	3.89
Lead Pb (µg/L)	40.73	0.4	5.36	8.66	6.14	1.76	1.38	1.14
Nickel Ni (µg/L)	9.47	5.47	5.47	4.27	5.17	4.57	5.66	10.12
Zinc Zn (µg/L)	201.82	32.71	74.38	53.3	71.15	39.2	35.81	195.34
Molybdenum Mo (µg/L)	2.36	2.57	2.18	2.11	2.15	2.48	2.56	2.85

Cycle F

191121. pilot. Aquafin sampling summer/autumn 2019								
	Influent	Effluent	Biofilter 5	Biofilter 10	Biofilter 20	Biofilter 40	Biofilter 55	Biofilter 70
code	191121IN_x	191121UIT_x	191121BB5_x	191121BB10_x	191121BB20_x	191121BB40_x	191121BB55_x	191121BB70_x
In situ								
Temperature (EC) (°C)	7	9.3	7.1	7.3	7.2	6.8	6.3	6.8
EC (µS/cm)	830	576	822	826	830	827	819	745
DO (mg/L)								
pH (-)	7.73	7.37	7.47	7.47	7.44	7.37	7.33	7.34
Suspended Solids (mg/L)	5	<4						
Turbidity (NTU)	0.7	1.1						
Macro								
	Influent	Effluent	Biofilter 5	Biofilter 10	Biofilter 20	Biofilter 40	Biofilter 55	Biofilter 70
Chloride Cl (mg/L)	72.464	39.608	72.344	70.178	69.104	71.224	71.092	59.446
Sodium Na (mg/L)								
Fluorine F (mg/L)								
Bromine Br (mg/L)								
Potassium K (mg/L)								
Calcium Ca (mg/L)	70.054	18.87	69.012	68.406	20.166	20.002	20.608	19.596
Magnesium Mg (mg/L)								
Iron Fe (mg/L)	0.14657	0.08017	0.09932	0.10219	0.13065	0.10652	0.10827	0.11829

Manganese Mn (mg/L)	0.6117643	0.00891	0.0687	0.07381	0.126779	0.06474	0.00736	0.02374
Bicarbonate (HCO3-) (mg/L)								
Ammoniu m NH4 (mg/L)								
Nitrate NO3 (mg/L)	6.442	4.808	8.008	7.184	6.92	6.906	7.764	8.19
Nitrite NO2 (mg/L)								
Total Phosphat e PO4 (mg/L)								
Sulphate SO4 (mg/L)	53.666	39.594	53.852	52.63	51.896	53.34	50.282	41.568
Total hardness (meq/L)								
TOC (mg C/L)	2.2	2.3						
Heavy Metals								
	Influent	Effluent	Biofilter 5	Biofilter 10	Biofilter 20	Biofilter 40	Biofilter 55	Biofilter 70
Arsenic As (µg/L)	0.23	0.44	0.23	0.24	0.32	0.28	0.33	0.35
Cadmium Cd (µg/L)	10.57	0.49	1.6	0.9	0.93	0.65	0.82	0.85
Copper Cu (µg/L)	28.81	4.25	4.98	4.25	4.37	4	4.355	4.85
Lead Pb (µg/L)	16.07	0.24	0.57	0.48	0.34	0.29	0.63	0.32
Nickel Ni (µg/L)	48.4	5.51	15.8	10.81	11.16	7.59	7.31	9.19
Zinc Zn (µg/L)	13.85	88.78	67.71	69.62	48.52	61.11	128.1582	32.73
Molybden um Mo (µg/L)	3.54	2.74	2.76	3.16	3.37	3.28	2.79	2.28

Cycle G

191212 pilot. Aquafin sampling summer/autumn 2019								
	Influent	Effluent	Biofilter 5	Biofilter 10	Biofilter 20	Biofilter 40	Biofilter 55	Biofilter 70
code	191212IN_x	191212UIT_x	191212BB5_x	191212BB10_x	191212BB20_x	191212BB40_x	191212BB55_x	191212BB70_x
In situ								
Temperature (EC) (°C)	7.6	8.1	6.9	6.9	7	6.5	6.6	7
EC (µS/cm)	576	551	788	772	800	1074	988	812
DO (mg/L)								
pH (-)	7.77	7.16	7.28	7.15	7.09	7.01	7.06	7.09
Suspended Solids (mg/L)	<2	<2						
Turbidity (NTU)								
Macro								
	Influent	Effluent	Biofilter 5	Biofilter 10	Biofilter 20	Biofilter 40	Biofilter 55	Biofilter 70
Chloride Cl (mg/L)	63.15	67.53	99.49	131.02	129.14	197.29	186.30	127.17
Sodium Na (mg/L)	42.23	37.65	39.34	39.41	39.66	43.21	45.47	45.07
Fluorine F (mg/L)	1.16	1.08	1.13	1.10	1.09	1.04	1.03	1.11
Bromine Br (mg/L)								
Potassium K (mg/L)			0.61	2.56	5.15	6.95		
Calcium Ca (mg/L)	60.50	48.95	46.60	54.16	48.20	89.07	32.92	80.69
	57.00	47.70						
Magnesium Mg (mg/L)						39.94	42.93	33.05
	7.28	6.30						
Iron Fe (mg/L)	0.19	0.01	0.01	0.01	0.01	0.01	0.01	0.16

Manganese Mn (mg/L)	0.11	0.02	0.75	0.10	0.12	0.16	0.09	0.58
Bicarbonate (HCO3-) (mg/L)								
Ammonium NH4 (mg/L)	1.02	6.80	26.90	38.03	40.39	35.70	1.03	1.68
Nitrate NO3 (mg/L)	6.24	9.11	10.87	14.89	14.64	24.28	23.07	14.52
Nitrite NO2 (mg/L)								
Total Phosphate PO4 (mg/L)								
Sulphate SO4 (mg/L)	60.48	53.20	62.06	62.61	62.46	62.19	61.02	57.65
Total hardness (meq/L)								
TOC (mg C/L)	2.4	2.1						
Heavy Metals								
	Influent	Effluent	Biofilter 5	Biofilter 10	Biofilter 20	Biofilter 40	Biofilter 55	Biofilter 70
Arsenic As (µg/L)	0.25	0.48	0.50	0.25	0.29	0.32	0.37	0.34
Cadmium Cd (µg/L)	3.29	0.54	6.03	1.22	1.30	1.28	1.37	0.77
Copper Cu (µg/L)	33.02	3.25	11.92	5.25	5.36	4.13	3.49	3.92
Lead Pb (µg/L)	56.70	0.21	1.09	0.49	0.37	0.37	0.30	0.28
Nickel Ni (µg/L)	417.20	3.42	52.12	12.29	13.61	9.60	10.28	10.30
Zinc Zn (µg/L)	13.93	49.34	331.81	126.70	132.99	122.87	115.95	105.57
Molybdenum Mo (µg/L)	3.37	2.29	2.83	1.21	1.18	1.19	1.30	2.12

IV. GENÇ-FUHRMAN (2007) REMOVAL EFFICIENCIES

As				**Cd**			
IOCS		Quartz sand		IOCS		Quartz sand	
Ce	qe	Ce	qe	Ce	qe	Ce	qe
0.79	0.01	0.73	0.00	0.10	0.00	2.26	0.03
0.81	0.11	13.63	0.00	1.09	0.11	7.76	0.13
0.84	0.75	96.71	0.16	3.04	0.38	23.34	0.04
0.86	1.15	317.55	3.41	6.24	1.02	149.91	0.73
0.85	2.89	-	-	89.35	4.74	223.31	0.53
0.88	7.02	-	-	138.33	6.37	738.13	1.90
1.97	21.80	-	-	533.42	12.68	2,786.47	2.87
-	-	-	-	2540.56	10.42	-	-

Cr				**Cu**			
IOCS		Quartz sand		IOCS		Quartz sand	
Ce	qe	Ce	qe	Ce	qe	Ce	qe
0.98	0.13	0.28	0.00	2.93	0.98	1.64	0.30
7.18	0.65	1.73	-0.12	3.71	0.20	1.85	0.03
14.58	1.14	12.33	0.24	4.43	1.68	3.84	1.66
126.43	6.47	34.35	0.00	16.20	12.12	13.04	0.33
309.58	6.07	211.52	0.49	35.07	31.59	14.04	1.09
608.53	17.65	341.58	2.44	117.99	69.05	178.65	3.05
2823.94	27.82	820.12	0.73	-	-	296.38	16.09
-	-	3,076.37	1.71	-	-	694.74	30.74

Ni				**Zn**			
IOCS		Quartz sand		IOCS		Quartz sand	
Ce	qe	Ce	qe	Ce	qe	Ce	qe
11.15	0.06	10.49	0.09	12.41	0.56	14.19	0.36
52.21	0.41	58.06	0.13	23.71	2.33	52.28	0.65
71.21	1.22	87.99	0.27	99.35	25.14	477.65	1.89
151.09	2.00	166.81	0.81	118.54	13.38	1,390.65	1.96
502.74	5.53	2,333.76	3.03	640.94	44.15	3,301.97	8.20
2370.17	11.34	9,380.42	8.76	1676.61	114.48	13,627.73	47.03
9969.67	16.16	-	-	9805.67	275.59	54,180.81	161.03
-	-	-	-	50978.42	446.75	-	-

Data retrieved by https://apps.automeris.io/wpd/

V. CROSS SECTION OF SYNTHETIC FEEDS AARTSELAAR

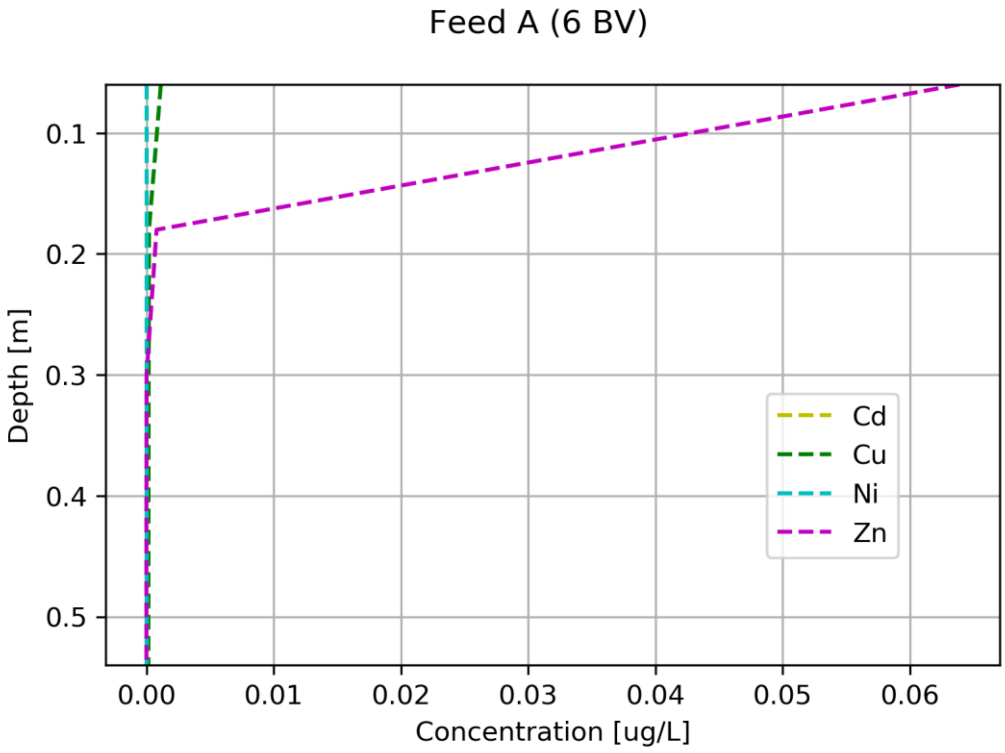

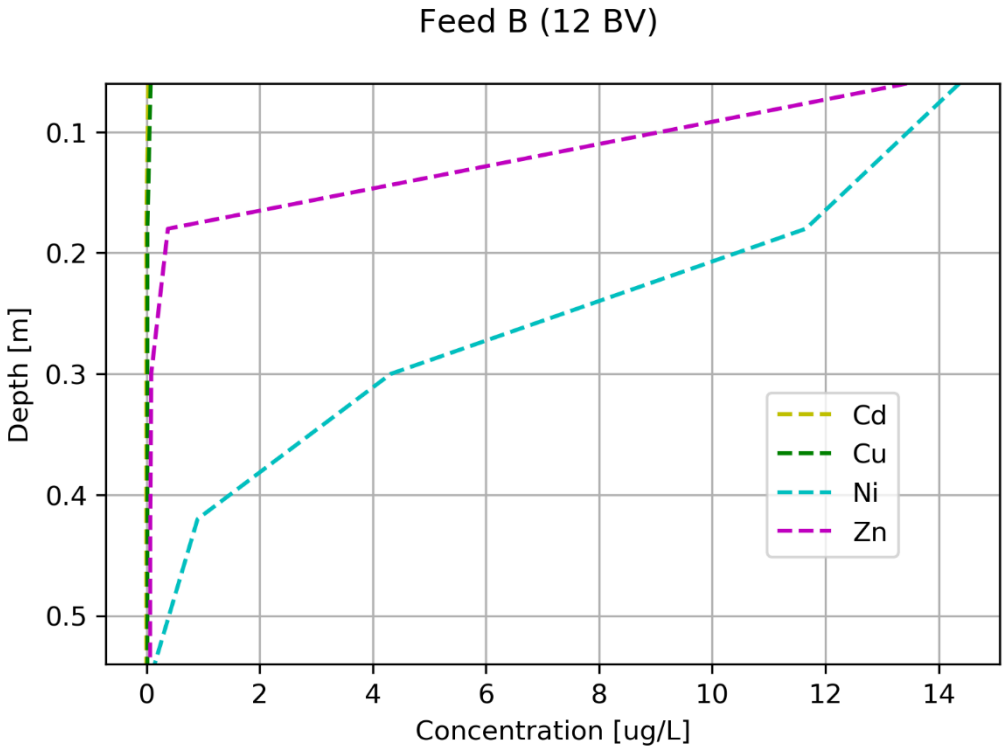

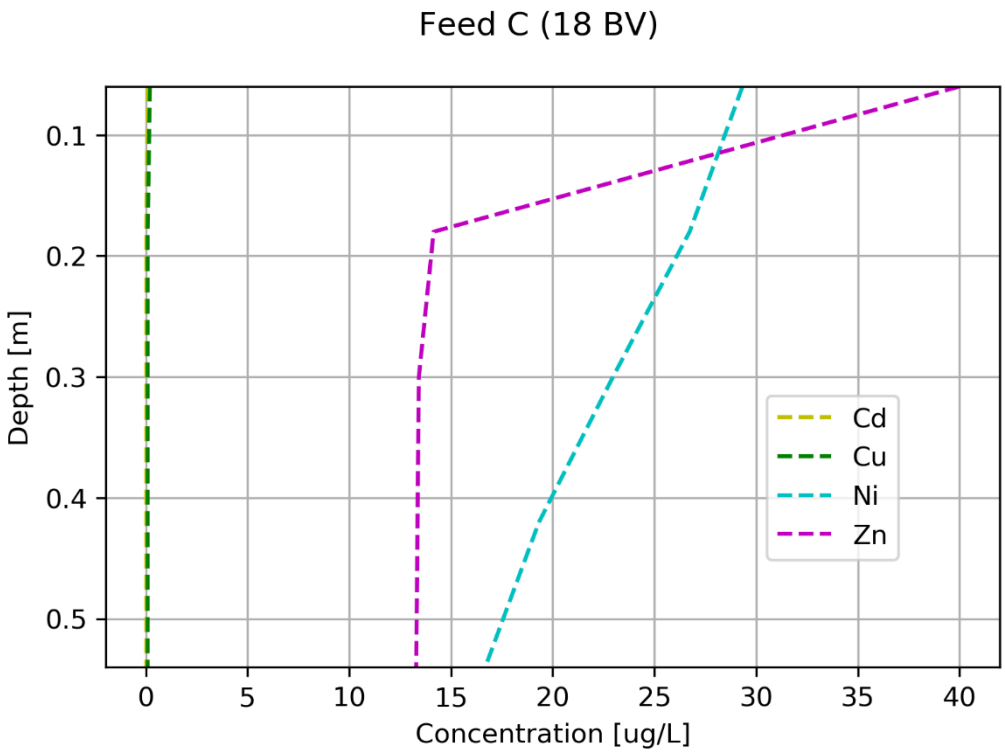
Feed C (18 BV)
Depth [m]
0.1
0.2
0.3
0.4
0.5
0
5
10
15
20
25
30
35
40
Concentration [ug/L]
Cd
Cu
Ni
Zn

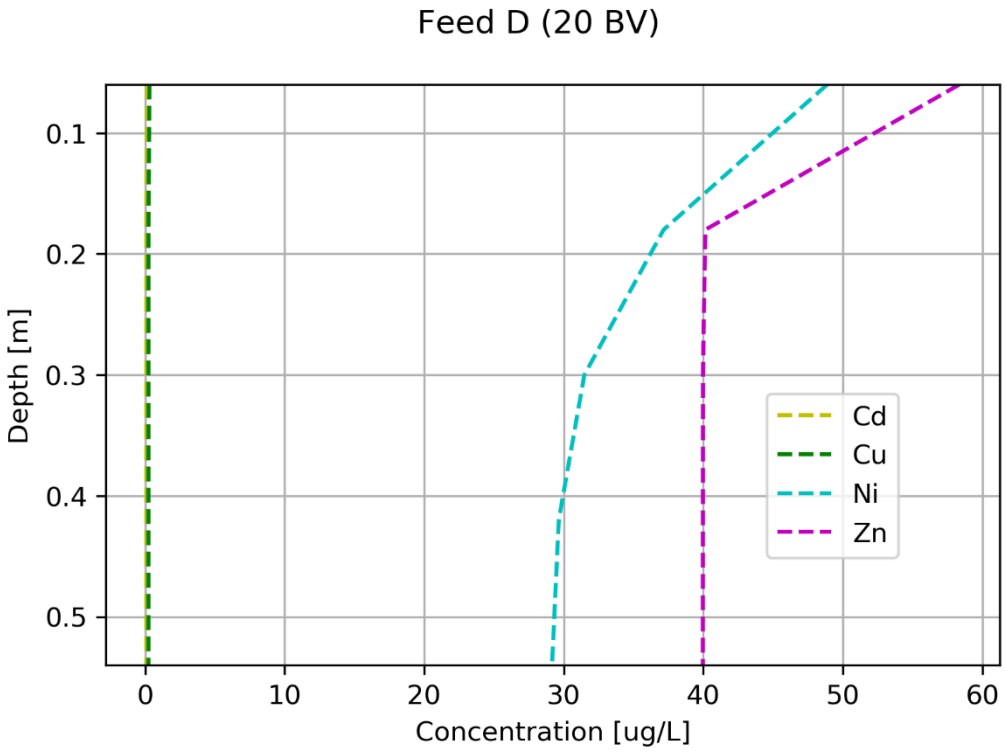
Feed D (20 BV)
Depth [m]
0.1
0.2
0.3
0.4
0.5
0
10
20
30
40
50
60
Concentration [ug/L]
Cd
Cu
Ni
Zn

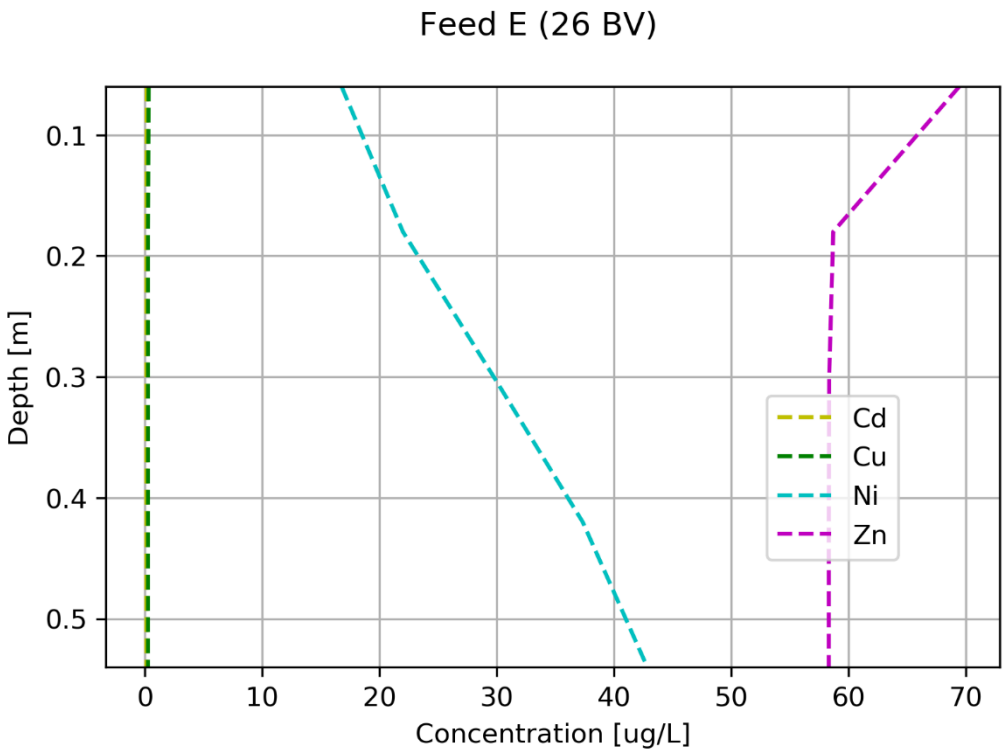
Feed E (26 BV)
Depth [m]
0.1
0.2
0.3
0.4
0.5
0
10
20
30
40
50
60
70
Concentration [ug/L]
Cd
Cu
Ni
Zn

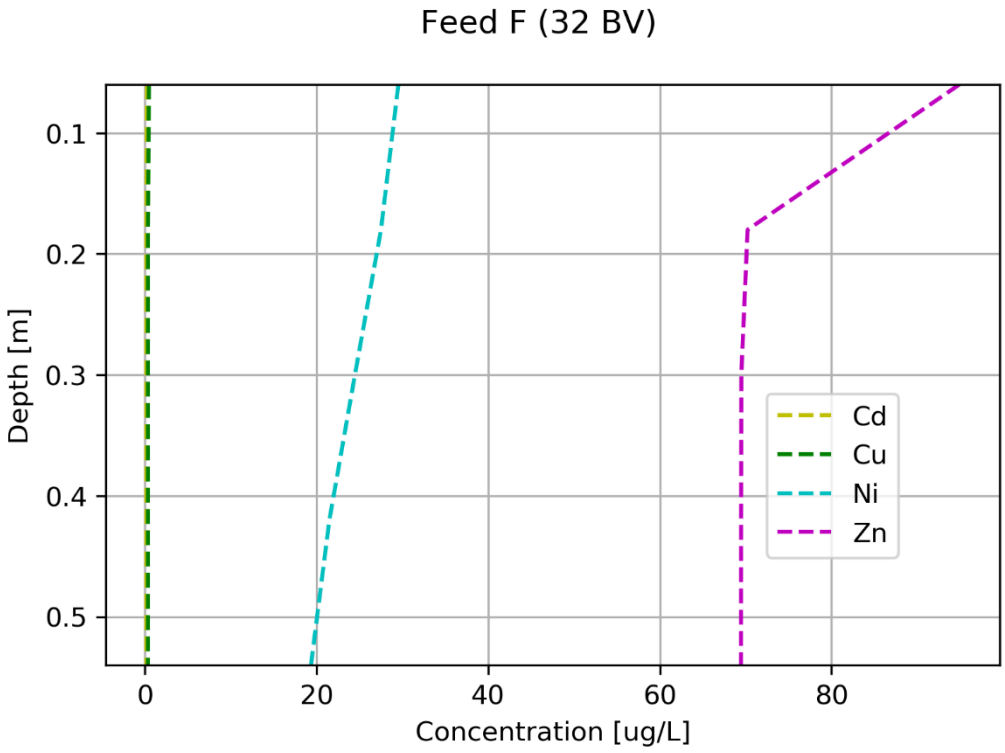
Feed F (32 BV)
Depth [m]
0.1
0.2
0.3
0.4
0.5
0
20
40
60
80
Concentration [ug/L]
Cd
Cu
Ni
Zn